Advances in Instrumentation and Data Analysis Techniques for Increasing Peak Capacity and Peak Capacity Production in One and Two-Dimensional Gas Chromatography

Brian David Fitz

A dissertation
submitted in partial fulfillment of the
requirements for the degree of:

Doctor of Philosophy

University of Washington
2015

Reading Committee:
Robert Synovec, Chair
Matthew Bush
D. Michael Heinekey

Program Authorized to Offer Degree:
Chemistry

University of Washington

Abstract

Advances in Instrumentation and Data Analysis Techniques for Increasing Peak Capacity and Peak Capacity Production in One and Two-Dimensional Gas Chromatography

Brian David Fitz

Chair of the Supervisory Committee:

Professor Robert E. Synovec

Department of Chemistry

Techniques to substantially increase peak capacity (number of peaks per separation window) and peak capacity production (number of peaks produced per unit time) for one and two-dimensional gas chromatography are demonstrated. First, instrumental advances related to sample introduction and column heating rate are discussed. Rapid sample introduction to the chromatographic system was achieved with a thermal injection device to deliver ultra-narrow peaks onto the GC column. When compared to standard sample introduction, thermal injection can provide peaks that are ~10 times narrower which gives rise to peak capacities an order of magnitude larger when compared to traditional GC practice. To further increase peak capacity and peak capacity production, a low thermal mass (LTM) GC system operated at a heating rate of 250 °C/min was applied with thermal injection to produce a separation with a peak capacity of ~300 in 1 minute. Additionally, thermal injection was applied to a comprehensive two-

dimensional gas chromatographic system coupled to time-of-flight mass spectrometry (GC × GC – TOFMS) to produce a separation with a peak capacity of ~6,000 in 6 minutes, affording a peak capacity production rate of ~1,000 peaks/minute.

Second, a novel algorithmic approach for processing GC-TOFMS data is presented which can increase the peak capacity and peak capacity production values even further. The algorithm relies on GC-TOFMS data that is sampled with sufficient data density (> 100 points/peak) to accurately measure analyte peak widths, W, and retention times, t_R. Separation visualization is made possible by transforming the data from a signal versus time format to a peak width versus retention time format. This is achieved by measuring the W and t_R of each *m/z* for each analyte in the separation, followed by plotting of the data (W vs. t_R) in a two-dimensional format. Plotting the data in this fashion allows for the visualization of pure and interfered *m/z* of analytes. Coupled with chemometric analysis allows for the deconvolution of poorly-resolved analytes down to a resolution, $R_s = 0.03$. The peak capacity of a 7 minute GC-TOFMS separation was increased from ~400 to ~10,000 using this technique.

Table of Contents

List of Figures

List of Tables

Chapter 1. Introduction to gas chromatography[1]

1.1 Introduction

Gas chromatography (GC) is a powerful analytical tool commonly used in chemical analysis. The power of GC lies in its ability to physically separate different analytes from one another based on their chemical properties (e.g. boiling point, polarity, functional groups, chirality, or thermodynamic properties). GC is capable of resolving thousands of compounds in a single analysis, and when coupled to an appropriate type of detector, can detect them at very low concentrations. The ability to separate, identify, and quantify thousands of compounds in a single analysis is unparalleled in analytical instrumentation and makes GC useful in many disciplines. The widespread use of GC has permeated the chemical analysis field and is commonly employed in such fields as: metabolomics (small bio-molecules) [1-4], forensics [5, 6], petroleomics & fuels [7-9], food testing [10, 11], flavor & fragrance [12], chemical weapons precursor analysis [13], drug monitoring [14], cancer diagnoses [15], environmental monitoring [16], and more.

Over the past several decades many technological advances have been made to increase the separation and detection capabilities of GC instruments. These improvements include: the development of narrow bore, thin film capillary columns with high chromatographic efficiencies [17]; detectors capable of scanning large mass spectral ranges (~1000 m/z) with rapid spectral collection rates (500 Hz) [18]; column heating rates which can reduce run time from hours to minutes, even seconds [19]; adding a second separation dimension [20, 21]; and novel injection technology allowing for ultra-narrow peaks to be delivered to the chromatographic system.

[1] Some parts of this chapter has been reproduced from B.D. Fitz, R.B. Wilson, B.A. Parsons, J.C. Hoggard, R.E. Synovec, *Journal of Chromatography A* 1266 (2012) 116-123 and B.D. Fitz, B.C. Reaser, D.K. Pinkerton, J.C. Hoggard, K.J. Skogerboe, R.E. Synovec, *Analytical Chemistry* 86 (2014) 3973-3979

Injection mechanisms include thermal injection [20-26], valve based [27-29], fluid logic gates [30, 31], high split ratios [32], and micro-loop systems [33].

1.2 GC Theory

1.2.1 Separation Fundamentals

To sufficiently quantify the improvements made in this dissertation, a brief review of relevant GC theory will be provided. For a more in-depth coverage of GC theory, a review by Reid and Synovec [17] covers sufficient GC theory as it pertains to fast GC. GC relies on the diffusion of analytes between a gaseous mobile phase and a solid stationary phase. The stationary phase is generally a liquid polymer bound to the inner surface of a microbore open tubular fused silica column. Current practice employs capillary columns with lengths between 1 and 100 m and inner diameters (i.d.) between 50 µm (micro-bore) to 530 µm (wide-bore). Most commonly utilized are 10-30 m columns with i.d. between 100-250 µm using stationary phase thicknesses between 0.05-5 µm, however many situations arise such that columns outside these parameters may be required.

The mobile phase, generally hydrogen or helium gas, flows through the column due to a pressure gradient that exists between the head of the column (high pressure) and the column exit (low pressure). After a sample has been introduced to the system, the components will equilibrate between the stationary phase and the mobile phase and as mobile phase flows through the column. The distribution coefficient, K_D, is defined as:

$$K_D = \frac{[Analyte]_{SP}}{[Analyte]_{MP}} \quad (1)$$

Where $[Analyte]_{SP}$ is the concentration of the analyte in the stationary phase and the $[Analyte]_{MP}$ is the concentration of the analyte in the mobile phase. A higher concentration of analyte in the stationary phase will result in a higher distribution coefficient, which in turn will result in more

retention on column. The selective partitioning of different analytes with different K_D is the fundamental separation mechanic of which GC is based upon. The K_D can be tuned by differences in stationary phase composition (to increase or decrease analyte specificity with the stationary phase) as well as temperature.

The dead time, t_o, is the time required for the mobile phase to traverse the length of the column from time of injection to time of detection. The dead time is indicative of an unretained analyte; an analyte that has no interaction with the stationary phase. The retention time, $t_{R,}$ is a measure of the time the analyte spent in the stationary phase combined with the time spent in the mobile phase. The retention time can be used for compound identification. However, the retention time changes with flow rate, so when comparing different chromatographic systems, retention time correction must be applied. The retention factor, *k*, is defined as:

$$k = \frac{moles\ Analyte_{SP}}{moles\ Analyte_{MP}} \quad (2)$$

Which can also be written as:

$$k = \frac{t_R - t_o}{t_o} \quad (3)$$

Which is the ratio of the time the analyte spent in the stationary phase over the time the analyte spend in the mobile phase. Analytes with more time spent in the stationary phase will have higher retention factors than analytes with less time spent in the stationary phase.

1.1.2 Band Broadening in GC

In a GC separation, the ability to resolve analytes is governed by well-defined separation mechanics. One common way to calculate the separation between analytes is the resolution, R_s, defined as:

$$R_s = \frac{t_{R,2} - t_{R,1}}{W_{b,avg}} \quad (4)$$

Which is the difference in retention time between two analytes divided by the average width at the base of the two analytes. The retention time, as mentioned previously, is a measure of the time the analyte spent between the mobile phase and the stationary phase, which is also the time required for the analyte to elute off the column. The peak width (at base), W_b, is the result of two distinct types of contributions: on-column band broadening and off-column band broadening (also referred to as extra-column band broadening).

Band broadening (BB) is way to describe the experimental and physical mechanisms that give rise to separation quality. On-column band broadening are processes that are solely related to the separation mechanism. The three main sources of on-column band broadening are: longitudinal diffusion, mass transfer in the mobile phase, and mass transfer in the stationary phase. The plate height, *H*, is a measure of the on-column band-broadening contributions. The Golay equation relates *H* to these on-column band broadening processes:

$$H = \frac{B}{\bar{u}} + C_M\bar{u} + C_s\bar{u} + H_{ext} \quad (5)$$

Where *B* is the longitudinal diffusion term, C_M is the term describing resistance to mass transfer in the mobile phase, C_S is the resistance to mass transfer in the stationary phase, and $\bar{u}$ is the linear flow velocity of the mobile phase. H_{ext} is extra-column band broadening, which is governed by non-separation processes. This can be addressed by optimizing instrumentation such as injection, detection, and dead-volumes. By increasing the linear flow velocity, the influence of longitudinal diffusion to the plate height can be significantly reduced, however, the mass transfer terms will become significant. Mass transfer refers to the resistance of a molecule (or group of molecules) which currently reside in one phase to migrate to another phase. For example, if portions of an analyte are currently in the stationary phase while the rest are in the mobile phase, the particles in the mobile phase will bypass by the particles in the stationary phase. This process

of diffusion between mobile phase and stationary phase continues until all of the particles have exited the column.

A more rigorous determination of H was developed [34] which related other experimental parameters to plate height:

$$H = \frac{2D_{G,0}jf}{\bar{u}} + \frac{1+6k+11k^2}{96(1+k)^2}\frac{d_c^2\bar{u}f}{D_{G,0}j} + \frac{2kd_f^2\bar{u}}{3(1+k)^2D_L} \quad (6)$$

Where $D_{G,0}$ is the analyte diffusion coefficient in the gas phase, j and f are gas compressibility correction factors, $\bar{u}$ is the average linear flow velocity, k is the analyte retention factor, d_c is the capillary inner diameter, d_f is the stationary phase film thickness, and D_L is the analyte diffusion coefficient in the stationary phase. Equation (6) is frequently used to relate experimentally derived plate height to values derived from theoretical considerations [17]. Minimizing H can be achieved by using high linear flow rates, narrow column diameters, thin stationary phases, and low k values. However, due to the interrelationships between these variables, it is not as simple as it appears. Significant effort has been put forth to theoretically model separations to achieve optimal separation parameters [24, 35].

The separation (column) efficiency N, is related to plate height, H, and column length, L, by the following equation:

$$N = \frac{L}{H} = 16\left(\frac{t_R}{W_b}\right)^2 \quad (7)$$

Large separation efficiencies are directly related to longer columns and smaller plate heights, and consequently, narrower peak widths. By rearranging equation (7), the plate height can be related to peak width (in units of time) by the following:

$$W_b = 4t_R\sqrt{\frac{H}{L}} \quad (8)$$

It can be seen that by reducing *H* from optimizing experimental parameters as shown in (6), as well as by reducing extra-column band broadening contributions can lead to narrower peak widths.

1.2.3 Separation Figures of Merit

There have been many metrics introduced to compare the separation powers of different GC systems. *N*, the number of theoretical plates, is often used to compare different columns with similar experimental parameters. Plate height, *H*, has been used extensively in predicting peak widths from on-column band broadening using the Golay equation. Peak capacity, n_c, is another commonly used metric to define separation power, which is defined as the number of peaks with an average width at base (4σ), $W_{b,avg}$, that can be separated in a given separation window, t_{sep}:

$$n_c = \frac{t_{sep}}{W_{b,avg}} \tag{9}$$

Peak capacity is a useful metric because it is easy to calculate from experimental data. By simply measuring a few of the peaks in a separation can give a good understanding of the peak capacity of the system. Typically n_c is calculated at unit resolution (R_s = 1). For example, a typical 1D separation may produce average peak widths at base of ~2 s. A separation window of 10 minutes (600 seconds) would produce a peak capacity of 300 at unit resolution. In order to increase the peak capacity of the separation either the separation time can be increased or the width of the peaks decreased. However, simply increasing the separation duration is detrimental because peak widths become wider as run time increases and sample throughput suffers. Even with the technological advances of the past few decades there is still a large discrepancy between peak widths obtained from a standard GC instrument and the peak widths predicted by theory.

Peak capacity production, which is the peak capacity per unit time, is defined as:

$$\frac{n_{c,1d}}{t_{sep}} = \frac{1}{w_{b,avg}} \tag{10}$$

Clearly, the most direct route to increasing peak capacity production is to reduce the width of the peaks. Using the same numbers as the peak capacity example above (n_c = 300, t_{sep} = 10 min) the peak capacity production is 30 peaks/min. The ideal GC system would be able to introduce narrow peaks to the GC system and perform a separation in a fraction of the time as a traditional GC instrument. Chapters 2 and 3 deal with strategies to deliver ultra-narrow peaks to the GC systems and other instrumental improvements to produce correspondingly high peak capacities.

1.3 Comprehensive Two-Dimensional Gas Chromatography (GC × GC)

In addition to the factors described previously, one the most powerful ways to increase peak capacity and peak capacity production is through the use of two-dimensional gas chromatography (GC × GC) developed by Phillips and co-workers in 1991 [21]. For GC × GC, two serially coupled separation columns with sufficiently orthogonal stationary phases (different chemical selectivity) are connected by a modulation interface. Effluent from the primary column is collected and injected onto the secondary column by the modulator at regular intervals defined as the modulation period, P_M. The ideal orthogonal peak capacity of a GC × GC instrument, $n_{c,2D}$, is the product of the peak capacities of each separation dimension, ${}^1n_c \times {}^2n_c$. Since the total separation time of a one-dimensional GC analysis or a GC × GC analysis should be similar, the addition of the secondary column with GC × GC provides a significant improvement in peak capacity and peak capacity production relative to 1D-GC. In addition to the greater peak capacity in the 2D separations, the additional selectivity provided by the orthogonal stationary phase of the second dimension helps resolve co-eluting compounds that may otherwise be overlapped in traditional 1D-GC.

However, peak broadening due to modulation, as expressed by metrics like the β-correction presented by Davis et. al. [36] (discussed in Chapter 3), and the manner in which GC

× GC is typically implemented results in effective peak capacity production rates that are far lower (e.g. ~50–150 peaks/min) than what is theoretically possible. The modulation ratio parameter, M_R, first described by Khummueng et. al. [37] and studied by Siegler et. al. [38] is defined as:

$$M_R = \frac{W_b}{P_M} \tag{11}$$

Where W_b is the width at base of the first dimension peak (4σ) and P_M is the modulation period. In GC × GC there is a trade-off of obtaining enough modulations across the first dimension peak while simultaneously trying to maximize the second dimension peak capacity. For example, a modulation period of 2.0 s with peak widths at base (4σ) on the second dimension of ~200 ms produces a second dimension peak capacity of 10. To achieve a modulation ratio between 2 and 4 (commonly applied in GC × GC separations) would require peak widths at base on the primary column of ~4-8 s (average of 6 s). This would provide a two-dimensional peak capacity production of ~100 peaks/min, which is common in standard GC × GC applications, but is much lower than theoretically possible. Chapter 3 explores novel instrumentation and experimental parameters for GC × GC to produce peak capacities closer to theoretical maximum than with conventional instrumentation.

1.4 Data Analysis Techniques to Improve Peak Capacity

The ability to analyze GC data and obtain useful chemical information is paramount to the utility of gas chromatography. The field of chemometrics specializes in mathematically gleaning useful information from chemical measurements [39-43]. Researchers in this field have spent decades developing software approaches to address the many challenges that arise. The various approaches developed, which aim to deconvolute and quantify overlapped peaks, depend upon the dimensionality (or order) of the data. Common instrumental platforms that produce

second order data, inherently two-dimensional (2D) for a single sample run, include comprehensive 2D chromatography (e.g., GC × GC and LC × LC) or chromatography combined with spectral detection (GC-MS, LC-MS, LC-UV/vis absorbance).

For GC-MS the data structure is second order or "bilinear," where each analyte response can be expressed as a matrix produced by taking the outer product of the chromatographic elution peak profile (a vector) with the mass spectrum (a vector). The bilinearity of the data structure makes GC-MS readily amenable to chemometric data analysis. Analytes require deconvolution when their chromatographic elution profiles overlap. The lower the chromatographic resolution, the more severe the overlap. The goal of deconvolution is to mathematically resolve the components and obtain the pure chromatographic elution profiles and pure mass spectra for each analyte. For analyte deconvolution to work successfully, either the mass spectra or chromatographic elution profiles of the overlapped analytes must be known. At significantly low resolution, generally around $R_s = 0.3$, without *a priori* knowledge of the system, deconvolution becomes problematic due to the inability to obtain a pure elution profile or mass spectra of target compounds. Chapters 4 and 5 explore the development of a novel chemometric algorithm aimed at increasing the ability to visualize and successfully deconvolute low resolution analytes, as well as to increase the peak capacity of the system by performing a novel data reduction and visualization method.

1.5 Hypotheses

Four hypotheses for increasing the peak capacity and peak capacity production of one and two-dimensional gas chromatographic systems are presented. Two of them are based upon experimental and instrumental improvements to reduce peak widths and therefore increase peak

capacities. The other two are the result of improved data analysis and data visualization methods. The hypotheses are listed below in the order the subsequent chapters appear.

1.5.1 Chapter 2: Evaluation of injection methods for fast, high peak capacity separations using low thermal mass gas chromatography

To achieve significant peak capacity gains in one-dimensional GC, two instrumental improvements are studied. The first is the use of a thermal injection system to cryogenically trap analytes as they are introduced from the standard instrument inlet to the GC system. The trapped analytes are then ballistically desorbed by a resistive heating device and reinjected to produce narrow GC peaks. The second instrumental system being studied is a low thermal mass (LTM) GC. The LTM GC is operated at 250 °C/min heating rate to produce a rapid temperature programmed separation. The hypothesis is that providing ultra-narrow GC peaks via thermal injection to the LTM-GC will result in a significant gain in peak capacity production in a short amount of time while still maintaining a useful overall peak capacity.

1.5.2 Chapter 3: Fast, high peak capacity separations in comprehensive two-dimensional gas chromatography with time-of-flight mass spectrometry

Comprehensive two dimensional gas chromatography (GC × GC) can provide significant peak capacity gains over its corresponding one-dimensional counterpart. However, the way GC × GC is traditionally practiced (long separation times, wide first dimension peaks, and long modulation periods) limits the peak capacity and peak capacity production. To speed up sample analysis, narrow first dimension peaks and fast modulation periods are required. The hypothesis is that using a cryogenic injection system to provide ultra-narrow peaks to the GC system while simultaneously running at optimal experimental conditions determined by chromatographic modeling will allow for peak capacity production values that are significantly higher than with

standard instrumentation. Also, the amount of useful chemical information, which can be inferred by things such as peak capacity, peak capacity production, chromatographic elution profiles, mass spectra, etc. is hypothesized to be similar to that of traditional GC × GC

1.5.3 Chapter 4: Enhancing gas chromatography time-of-flight mass spectrometry data analysis using two-dimensional mass cluster plots

One of the drawbacks of performing fast GC analyses is the loss in resolution between analytes. In order to obtain comparable chromatographic information from fast GC analyses, new data analysis tools are required. By using a high spectral collection rate (100 points per peak) the peak widths, W, and the retention times, $t_{R,}$ of peaks in the separation can be measured very accurately. The data can then be restructured into a peak width, W, versus retention time, t_R format. The hypothesis is that by reshaping the data and performing novel plotting will allow for easier selection of pure chromatographic elution profiles for low resolution analyte deconvolution. Also, by performing data reduction, the novel visualization method will increase the peak capacity as well.

1.5.4 Chapter 5: Implementation of two-dimensional mass cluster plots in fast, high peak capacity separations utilizing low thermal mass gas chromatography with time-of-flight mass spectrometry

The final chapter takes into account the concepts learned from the previous chapters. Novel instrumentation, specifically low thermal mass (LTM) GC coupled to time-of-flight mass spectrometry is utilized to produce information rich separations in a very short amount of time. The hypothesis is that the combination of LTM-TOFMS with algorithmic improvements to the chemometric developments obtained in Chapter 4 will provide even more peak capacity and analyte resolution gains.

1.5 List of Works Cited

[1] E.M. Humston, K.M. Dombek, J.C. Hoggard, E.T. Young, R.E. Synovec, Time-Dependent Profiling of Metabolites from Snf1 Mutant and Wild Type Yeast Cells, *Analytical Chemistry* 80 (2008) 8002–8011.

[2] E.M. Humston, J.D. Knowles, A. McShea, R.E. Synovec, Quantitative assessment of moisture damage for cacao bean quality using two-dimensional gas chromatography combined with time-of-flight mass spectrometry and chemometrics, *Journal of Chromatography A* 1217 (2010) 1963–1970.

[3] L.C. Marney, S.C. Kolwicz Jr., R. Tian, R.E. Synovec, Sample preparation methodology for mouse heart metabolomics using comprehensive two-dimensional gas chromatography coupled with time-of-flight mass spectrometry, Talanta. 108 (2013) 123–130. doi:10.1016/j.talanta.2013.03.005.

[4] R.E. Mohler, K.M. Dombek, J.C. Hoggard, E.T. Young, R.E. Synovec, Comprehensive Two-Dimensional Gas Chromatography Time-of-Flight Mass Spectrometry Analysis of Metabolites in Fermenting and Respiring Yeast Cells, *Analytical Chemistry* 78 (2006) 2700–2709.

[5] G.L. Burleson, B. Gonzalez, K. Simons, J.C.C. Yu, Forensic analysis of a single particle of partially burnt gunpowder by solid phase micro-extraction–gas chromatography-nitrogen phosphorus detector, *Journal of Chromatography A* 1216 (2009) 4679–4683.

[6] C. Brasseur, J. Dekeirsschieter, E.M.J. Schotsmans, S. de Koning, A.S. Wilson, E. Haubruge, et al., Comprehensive two-dimensional gas chromatography–time-of-flight mass spectrometry for the forensic study of cadaveric volatile organic compounds released in soil by buried decaying pig carcasses, *Journal of Chromatography A* 1255 (2012) 163–170.

[7] J.C. Hoggard, W.C. Siegler, R.E. Synovec, Toward automated peak resolution in complete GC × GC–TOFMS chromatograms by PARAFAC, *Journal of Chemometrics* 23 (2009) 421–431.

[8] L.C. Marney, W. Christopher Siegler, B.A. Parsons, J.C. Hoggard, B.W. Wright, R.E. Synovec, Tile-based Fisher-ratio software for improved feature selection analysis of comprehensive two-dimensional gas chromatography–time-of-flight mass spectrometry data, Talanta. 115 (2013) 887–895. doi:10.1016/j.talanta.2013.06.038.

[9] B.A. Parsons, L.C. Marney, W.C. Siegler, J.C. Hoggard, B.W. Wright, R.E. Synovec, Tile-Based Fisher Ratio Analysis of Comprehensive Two-Dimensional Gas Chromatography Time-of-Flight Mass Spectrometry (GC × GC–TOFMS) Data Using a Null Distribution Approach, Anal. Chem. 87 (2015) 3812–3819. doi:10.1021/ac504472s.

[10] G. Contarini, M. Povolo, Volatile Fraction of Milk: Comparison between Purge and Trap and Solid Phase Microextraction Techniques, J. Agric. Food Chem. 50 (2002) 7350–7355. doi:10.1021/jf025713a.

[11] S. Risticevic, Y. Chen, L. Kudlejova, R. Vatinno, B. Baltensperger, J.R. Stuff, et al., Protocol for the development of automated high-throughput SPME–GC methods for the analysis of volatile and semivolatile constituents in wine samples, Nature Protocols. 5 (2010) 162–176. doi:10.1038/nprot.2009.181.

[12] A. Hoffman, Flavor and fragrance analysis of consumer products – dynamic headspace compared to some traditional analysis approaches, Gerstel Application Note, (2014).

[13] J.C. Hoggard, J.H. Wahl, R.E. Synovec, G.M. Mong, C.G. Fraga, Impurity Profiling of a Chemical Weapon Precursor for Possible Forensic Signatures by Comprehensive Two-Dimensional Gas Chromatography/Mass Spectrometry and Chemometrics, *Analytical Chemistry* 82 (2010) 689–698.
[14] D.F. Chollet, E. Castella, L. Goumaz, G. Anderegg, Gas chromatography–mass spectrometry assay method for the therapeutic drug monitoring of the antiepileptic drug tiagabine, *Journal of Pharmaceutical and Biomedical Analysis* 21 (1999) 641–646.
[15] K.A. Kouremenos, M. Johansson, P.J. Marriott, Advances in gas chromatographic methods for the identification of biomarkers in cancer, *Journal of Cancer* 3 (2012) 404-420
[16] F.J. Santos, M.T. Galceran, Modern developments in gas chromatography–mass spectrometry-based environmental analysis, *Journal of Chromatography A* 1000 (2003) 125–151.
[17] V.R. Reid, R.E. Synovec, High-speed gas chromatography: The importance of instrumentation optimization and the elimination of extra-column band broadening, *Talanta*. 76 (2008) 703–717.
[18] M.M. van Deursen, J. Beens, H.-G. Janssen, P.A. Leclercq, C.A. Cramers, Evaluation of time-of-flight mass spectrometric detection for fast gas chromatography, *Journal of Chromatography A* 878 (2000) 205–213.
[19] J. Luong, R. Gras, R. Mustacich, H. Cortes, Low Thermal Mass Gas Chromatography: Principles and Applications, *Journal of Chromatographic Science* 44 (2006) 253–261.
[20] Z. Liu, J.B. Phillips, High-speed gas chromatography using an on-column thermal desorption modulator, *Journal of Microcolumn Separations* 1 (1989) 249–256.
[21] Z. Liu, J.B. Phillips, Comprehensive Two-Dimensional Gas Chromatography using an On-Column Thermal Modulator Interface, *Journal of Chromatographic Science* 29 (1991) 227–231.
[22] A. Van Es, J. Janssen, C. Cramers, J. Rijks, Sample enrichment in high speed narrow bore capillary gas chromatography, *Journal of High Resolution Chromatography* 11 (1988) 852–857.
[23] A. Peters, M. Klemp, L. Puig, C. Rankin, R. Sacks, Instrumentation and strategies for high-speed gas chromatography, *Analyst* 116 (1991) 1313–1320.
[24] R.B. Wilson, J.C. Hoggard, R.E. Synovec, Fast, High Peak Capacity Separations in Gas Chromatography–Time-of-Flight Mass Spectrometry, *Analytical Chemistry* 84 (2012) 4167–4173.
[25] R.B. Wilson, B.D. Fitz, B.C. Mannion, T. Lai, R.K. Olund, J.C. Hoggard, R.E. Synovec High-speed cryo-focusing injection for gas chromatography: Reduction of injection band broadening with concentration enrichment, *Talanta*. 97 (2012) 9–15.
[26] B.D. Fitz, R.B. Wilson, B.A. Parsons, J.C. Hoggard, R.E. Synovec, Fast, high peak capacity separations in comprehensive two-dimensional gas chromatography with time-of-flight mass spectrometry, *Journal of Chromatography A* 1266 (2012) 116–123.
[27] J.L. Hope, K.J. Johnson, M.A. Cavelti, B.J. Prazen, J.W. Grate, R.E. Synovec, High-speed gas chromatographic separations with diaphragm valve-based injection and chemometric analysis as a gas chromatographic "sensor," *Analytica Chimica Acta* 490 (2003) 223–230.
[28] G.M. Gross, B.J. Prazen, J.W. Grate, R.E. Synovec, High-Speed Gas Chromatography Using Synchronized Dual-Valve Injection, *Analytical Chemistry* 76 (2004) 3517–3524.

[29] R.B. Wilson, W.C. Siegler, J.C. Hoggard, J.S. Nadeau, R.E. Synovec, Achieving high peak capacity production for gas chromatography and comprehensive two-dimensional gas chromatography by minimizing off-column peak broadening, *Journal of Chromatography A* 1218 (2011) 2130-3139.
[30] G. Gaspar, P. Arpino, G. Guiochon, Study in High Speed Gas Chromatography I. Injections of Narrow Sample Plugs, *Journal of Chromatographic Science* 15 (1977) 256–261.
[31] R.L. Wade, S.P. Cram, Fluidic logic sampling and injection system for gas chromatography, *Analytical Chemistry* 44 (1972) 131–139.
[32] H. Wollnik, R. Becker, H. Götz, A. Kraft, H. Jung, C.-C. Chen, et al., A high-speed gas chromatograph coupled to a time-of-flight mass analyzer, *International Journal of Mass Spectrometry and Ion Processes* 130 (1994) L7–L11.
[33] A.J. Borgerding, C.W. Wilkerson, A Comparison of Cryo-focusing Injectors for Gas Sampling and Analysis in Fast GC, *Analytical Chemistry* 68 (1996) 2874–2878.
[34] M.L. Lee, F.J. Yang, K.D. Bartle, Open Tubular Column Gas Chromatography, Wiley, New York, 1984.
[35] H. Snijders, H.-G. Janssen, C. Cramers, Optimization of temperature-programmed gas chromatographic separations I. Prediction of retention times and peak widths from retention indices, *Journal of Chromatography A* 718 (1995) 339–355.
[36] J.M. Davis, D.R. Stoll, P.W. Carr, Effect of First-Dimension Undersampling on Effective Peak Capacity in Comprehensive Two-Dimensional Separations, *Analytical Chemistry* 80 (2008) 461–473.
[37] W. Khummueng, J. Harynuk, P.J. Marriott, Modulation Ratio in Comprehensive Two-dimensional Gas Chromatography, *Analytical Chemistry* 78 (2006) 4578–4587.
[38] W.C. Siegler, B.D. Fitz, J.C. Hoggard, R.E. Synovec, Experimental Study of the Quantitative Precision for Valve-Based Comprehensive Two-Dimensional Gas Chromatography, *Analytical Chemistry* 83 (2011) 5190-5196.
[39] C.G. Fraga, Chemometric approach for the resolution and quantification of unresolved peaks in gas chromatography–selected-ion mass spectrometry data, *Journal of Chromatography A* 1019 (2003) 31–42.
[40] S.E. Stein, An integrated method for spectrum extraction and compound identification from gas chromatography/mass spectrometry data, *Journal of the American Society for Mass Spectrometry* 10 (1999) 770–781.
[41] C.G. Fraga, C.A. Bruckner, R.E. Synovec, Increasing the Number of Analyzable Peaks in Comprehensive Two-Dimensional Separations through Chemometrics, *Analytical Chemistry* 73 (2001) 675–683.
[42] J.B. Callis, "Super Resolution in Chromatography by Numerical Deconvolution", In Ultrahigh Resolution Chromatography. ACS Symposium Series (250), Seattle, WA, 1984.
[43] A.E. Sinha, C.G. Fraga, B.J. Prazen, R.E. Synovec, Trilinear chemometric analysis of two-dimensional comprehensive gas chromatography–time-of-flight mass spectrometry data, *Journal of Chromatography A*. 1027 (2004) 269–277.

Chapter 2. Evaluation of injection methods for fast high peak capacity separations with low thermal mass gas chromatography[2]

2.1 Introduction

Gas chromatography (GC) is a powerful analytical tool used in the separation and identification of analytes in complex mixtures. Typical GC separations utilize 20 – 40 m columns with internal diameters ranging from 100 µm to 320 µm and are commonly temperature programmed at rates ranging from 5 °C/min to 20 °C/min. The temperature programming range for volatile and semi-volatile GC analysis is typically from ~ 50 °C to ~ 300 °C however specific applications exist which require cryogenic or extremely high operating temperatures [1-5]. Typical peak widths at base (4σ) associated with these typical conditions range from 3 s (20 peaks/min) to 6 s (10 peaks/min), with corresponding separation run times of 15 min to 1 hour. Corresponding peak capacities, n_c, at unit resolution therefore range from ~ 300 to ~ 600 peaks for these commonly applied conditions [6].

Fast GC has been an active area of study for reducing analysis time and increasing sample throughput [7-17]. A recent review by Tranchida and Mondello [18] discusses the use of microbore capillary columns for fast GC, and another recent review by Wang, Tolley, and Lee [19] outlines the use of resistive heating for fast GC. Other techniques for rapid column heating, such as thermal gradient chromatography [20-23] have shown promise as novel technologies in the fast GC field. The results we present herein, as well as the results presented in previous references have important implications for two-dimensional gas chromatography (GC × GC or GC-GC) [24-26]. Consideration of separation times, peak widths, flow rates, heating rates, and

[2] This chapter has been reproduced from: B.D. Fitz. B.C. Mannion, K. To, T. Hoac, R.E. Synovec, *Journal of Chromatography A* 1392 (2015) 82-90

other instrumental parameters must be implemented in a way that adequately preserves the two-dimensionality of the data that make GC×GC and GC-GC such powerful techniques.

A fast GC separation should maintain an equivalent (or greater) amount of chemical information compared to a traditional GC analysis but should provide the information in a shorter amount of time. Chemical information, which is inferred from figures-of-merit such as peak capacity, peak capacity production, resolution between analytes of interest, supply of satisfactory elution profiles, sufficiently pure mass spectra, separation efficiency, and quantifiable peak signal, should be competitive with traditional GC. Fast GC is typically defined as GC separations taking between 1 min and 10 min. A typical separation temperature program from ~ 50 °C to 300 °C (i.e., a range of 250 °C) would require temperature programing rates of between 25 °C/min and 250 °C/min to complete the separations in 10 min to 1 min, respectively. In order to maintain a similar peak capacity compared to traditional GC, the peak capacity production for fast GC would have to be increased by an order of magnitude, from 10 to 20 peaks/min, to 100 to 200 peaks/min, in order to compensate for the reduced separation run time. Indeed, a peak capacity production of 100 peaks/min has been achieved using GC-TOFMS by minimizing band broadening due to injection and by reducing on-column band broadening processes by operating at optimal experimental conditions, as dictated by chromatographic modeling [6].

Using in-house GC modeling software based on reports by Snijders et al. [27], and Wilson et al. [6], a separation using a 5 m × 100 µm inner diameter (i.d.) column is predicted, to provide a peak capacity of 250 to 300 in a 60 s separation, thereby affording a peak capacity production of 250 to 300 peaks/min. Also, peak widths at base (4σ) predicted by theory should be between 30 ms and 300 ms. To achieve the peak capacity goal of ~ 300 in 60 s, two

instrumental challenges must be addressed: sample introduction must provide a narrow injected pulse to the GC column so as to obtain the theoretically possible peak capacity provided by the column, and rapid column heating must be provided to obtain a typical temperature program range of 250 °C in 60 s.

To address one of these challenges, a recently developed in-house thermal injection device was applied to provide a narrow sample injection pulse [11, 28]. Referred to as high-speed cryo-focusing injection (HSCFI), a stream of cryogenically chilled nitrogen gas is applied to trap and preconcentrate analytes in a narrow band (700 nl volume) within a metal capillary column. A capacitive discharge device is then activated to resistively heat the metal capillary at rates approaching 6,000 °C/s to desorb preconcentrated analytes in 5 – 10 ms. Analyte peaks produced by the HSCFI approach 10 ms (width at base) which aids in substantially increasing the peak capacity ultimately achieved in the separation.

To address the other challenge of rapidly heating the separation column, we utilized a Generation I LTM (low thermal mass) GC instrument from Agilent to perform the rapid temperature program [29]. The LTM-GC was originally developed by RVM scientific [30, 31]. Recently, Luong et al. [32] published an insightful overview covering LTM-GC fundamentals. Conventional air bath GC is generally limited to a maximum heating rate of ~ 50 °C/min (with 5 to 20 °C/min commonly applied). The LTM design bundles the analytical column, resistive heating wires, and thermocouples together in a small toroid configuration which significantly reduces the thermal mass of the device allowing for faster heating rates and reduced cool down times compared to conventional GC. The LTM column module is held outside of the GC in a case attached to the door. Fans are located under the column assembly that rapidly cools the LTM-GC in less than 1 min, which aids in increasing sample throughput. The LTM-GC is rated

to heat at rates up to 1,800 °C/min which, in theory, could accomplish a typical temperature separation range of 250 °C in just under 10 s. However, we opted to evaluate the LTM-GC at 250 °C/min to span a typical temperature program range 250 °C (50 °C to 300 °C) in 60 s. Based on the theoretical capabilities for separation efficiency, we expect that using HSCFI in conjunction with LTM-GC should produce peak capacities of 250 – 300 in a 60 s separation.

Herein, we describe recent studies in which we have explored the use of a commercially available fast GC platform, namely the Generation I LTM from Agilent, for fast, high peak capacity separations. A 73 component mixture was created as a test sample to evaluate the platform. The mixture contained primarily hydrocarbons and substituted hydrocarbons with boiling points spanning a traditional temperature program, i.e. from 50 °C to 300 °C. The 73 component sample mixture was introduced to the LTM platform in three different modes: neat liquid, headspace solid phase micro-extraction (HS-SPME), and direct vapor headspace. The goal was to test the performance and robustness of the platform with different injection techniques commonly used in GC. The sampling methods were analyzed in two sets of experiments, each with a flame ionization detector (LTM-GC-FID). First, the three sampling methods were evaluated in conjunction with HSCFI. Second, the three sampling methods were evaluated without using HSCFI in order to assess the native on-column focusing ability of the LTM platform alone. A third experiment was performed to demonstrate a suitable range of retention indices that the LTM-GC platform can analyze. Finally, in a fourth experiment the LTM-GC was coupled to a time-of-flight mass spectrometer (TOFMS). The LTM-GC-TOFMS was applied to the fast separation of volatile analytes from the headspace of banana peels.

2.2 Experimental

2.2.1 Samples and Injection Conditions

All chemicals for the 73 component mixture were reagent grade or higher (unless otherwise noted), as listed in Table 2.1. For the direct liquid injection of the 73 component mixture onto the LTM-GC-FID, an auto-injector equipped with a 500 nl (0.5 µl) micro-syringe (Hamilton, Reno, NV) injected 50 nl into the inlet, operated in split-less mode. A calibration curve for the syringe was prepared with volumes ranging from 40 nl to 300 nl and was determined to be linear with an $R^2 = 0.9983$. For the HS-SPME analysis of the 73 component mixture, 50 µl of the mixture was placed into a 4 ml vial and heated to 50 °C. A 65 µm DVB-PDMS (divinylbenzene / polydimethysiloxane) SPME fiber was used (Supelco, St. Louis, MO, USA). Prior to use, the fiber was conditioned at 250 °C for 30 min. The fiber was exposed to the mixture headspace for 1 min then transferred to the inlet and exposed in the inlet for 15 s at 250 °C. It was determined that 15 s was sufficient to desorb all analytes from the fiber during sample injection; when removing the fiber after a single injection and performing another injection using the same fiber, no signal was observed in the subsequent injection. For the direct vapor headspace analysis of the 73 component mixture, 50 µl of the mixture was placed into a 4 ml vial and heated to 50 °C for 5 minutes. 100 µl of the headspace was extracted using a 100 µl gas tight syringe and injected manually into the GC inlet, operated in split-less mode.

For the LTM-GC-TOFMS demonstration with HS-SPME sampling, banana peel vapor was analyzed. Bananas were purchased from a local grocery store. To prepare the banana peels for SPME analysis, 30 g from 3 separate banana peels (90 g total) were homogenized with 150 ml of water and placed in a 250 ml Erlenmeyer flask. A 65 µm DVB-PDMS (divinylbenzene / polydimethysiloxane) fiber was conditioned for 30 min at 250 °C prior to use. The SPME fiber was then exposed to the headspace of the magnetically stirred banana peel solution for 5 min at room temperature. The SPME fiber was desorbed in the inlet for 7 s for injection.

2.2.2 Chromatographic Conditions and Instrumentation

2.2.2.1 LTM-GC-FID

The modified LTM-GC-FID instrumental platform is presented in Figure 2.1, utilizing an Agilent 6890 GC with a Series I LTM module (Agilent Technologies, Palo Alto, CA, USA). The column module was a standard 7 inch cartridge, attached to a modified Agilent GC door, with a 5 m x 100 µm inner diameter (i.d.) × 0.40 µm DB-5 film (5% phenyl / 95% dimethyl polysiloxane) column. The inlet and detector were connected to the column ends extending through the insulated door using 20 cm x 100 µm i.d. segments of deactivated fused silica capillary coupled with zero dead volume unions (Valco Instrument Co., Houston, TX, USA).

For separations utilizing HSCFI (see Figure 2.1) [11, 28], a 10 cm segment of 100 µm i.d. MXT-5 column (stainless steel capillary with 5% phenyl / 95% dimethyl polysiloxane stationary phase), which serves as the heart of the HSCFI, was inserted between the fused-silica capillary coming from the inlet and the fused-silica capillary connecting to the head of the LTM-GC column, thus electrically isolating the resistive heating injection mechanism from the rest of the instrument. The metal capillary was connected to the capacitive discharge device by copper clamps attached to thermally insulated wires. Room temperature nitrogen gas was cryogenically cooled by passing through ¼ inch copper tubing submerged in a Dewar flask filled with liquid nitrogen. The cooled nitrogen gas was directed onto the MXT column with a short segment of PTFE (Teflon) tubing. Samples were injected into the standard GC inlet (manually or via auto-injector), passed through the transfer line, and trapped in the region cooled during HSCFI by nitrogen gas. The duration that the liquid nitrogen was actively trapping analytes after introduction into the inlet prior to desorption is referred to as the cryo-focusing time, which was

60 s. After the cryo-focusing time, the capacitor was discharged at 9 V for 50 ms, providing sufficient thermal energy to completely desorb the trapped analytes from the MXT column.

LTM-GC-FID separations using HSCFI were performed with the carrier gas at a constant column head pressure of 689 kPa (100 psig) after thermal injection. However, in order to ensure efficient trapping on the metal capillary column, samples were introduced to the inlet at 34.5 kPa (5 psig) and ramped to 689 kPa (100 psig) at 1,034 kPa/min (150 psig/min) prior to desorption. The column was held at 30 °C for the duration of the cryo-focusing time (60 s) and immediately heated at 250 °C/min after thermal injection to a final temperature of 300 °C. The same pressure ramp was also used during the separations without HSCFI, which facilitated analyte focusing on the head of the column. For separations without HSCFI, the column was held at 30 °C for 12 s after injection (the calculated dead time with the pressure ramp) then heated at 250 °C/min (same rate as with HSCFI) to a final temperature of 300 °C. Since there was no cryo-focusing hold time without HSCFI, the separation began when the sample was introduced into the inlet, which is reflected in the apparent dead time difference between separations with and without HSCFI.

For separations with and without HSCFI, the inlet was held at 250 °C and the column flowrate was 3 ml/min at the end of the temperature program. The flame ionization detector (FID) was held at 300 °C. Grade 5 ultra-pure hydrogen was used as the carrier gas (PraxAir, Seattle, WA, USA). The GC oven was held isothermally at 300 °C during the analysis to minimize band broadening during the transfer from the inlet to the head of the analytical column and from the column outlet to the detector. Maintaining the high oven temperature keeps the analytes essentially unretained in the capillary transfer lines and minimizes additional band broadening prior to detection, which is important for minimizing peak widths and maximizing peak capacity. The ambient temperature of the laboratory was 20 °C.

Agilent ChemStation software was used to control the GC and the LTM module. The stock FID electrometer board on the GC was replaced with an in-house built electrometer board capable of a faster data acquisition rate, operated at 100 kHz and averaged down to 1 kHz. The electrometer was interfaced to a National Instruments data acquisition board (National Instruments, Austin, TX, USA) and the resulting data was collected using an in-house written LabVIEW program. Post-run data processing was performed in Matlab R2012b (The Mathworks, Inc., Natick, MA, USA).

2.2.2.2 LTM-GC-TOFMS

For the LTM-GC-TOFMS separations, the LTM module was equipped on an Agilent 6890A GC coupled to a LECO Pegasus III TOFMS. The instrumental diagram is similar to that of Figure 2.1, however in this case the detector was the TOFMS and the HSCFI equipment was absent. The column module used was a 10 m × 100 µm i.d. with a 0.40 µm DB-5 stationary phase. The inlet and mass spectrometer transfer lines were connected to the analytical column using 30 cm and 60 cm × 100 µm i.d. fused silica transfer capillary lines, respectively. The inlet was held at 250 °C and operated in split mode with a 5:1 split ratio. The carrier gas was grade 5 ultra-pure helium operated at a head pressure of 1,034 kPa (150 psig, 2 ml/min outlet flow) using an aftermarket electronic pressure controller (EPC). The oven and TOFMS transfer line were held at 250 °C. The column was held at 30 °C for 0.5 min (calculated dead time) then heated at 250 °C/min to a final temperature of 300 °C. The TOFMS collected *m/z* 40-250 at 500 spectra/s. The ion source was 250 °C and the electron impact voltage was -70 V.

2.3 Results and Discussion

We begin by reporting separations of the 73 component test mixture using LTM-GC-FID with HSCFI, to assess the relative performance and merit of the three sample introduction

methods. The test mixture (Table 2.1) was amenable to studying the LTM-GC-FID with the various injection approaches, i.e., liquid, HS-SPME and vapor. Figure 2.2A-C shows a series of separations of the 73 component mixture using the LTM-GC-FID with HSCFI as described in section 2.2.1. The separation shown in Figure 2.2A used 50 nl of the neat liquid test mixture with an LTM heating rate of 250 °C/min for a separation time of ~ 60 s. The peak widths at base (4σ) range from ~ 30 ms to ~ 300 ms, providing a peak capacity of 270 and a peak capacity production of 270 peaks/min. The inset in Figure 2.2A shows that many of the peaks are well resolved from adjacent analytes in a very short time period. The LTM-GC separation of the 73 component mixture via HS-SPME sample introduction coupled with HSCFI is provided in Figure 2.2B. The detected peak widths were similar to those of the liquid sample. The separation using HS-SPME contains similar chromatographic features relative to the neat liquid injection separation shown in Figure 2.2A; however, as expected the less volatile analytes are not sampled as well and the relative concentrations vary for the detected analytes when compared to the neat liquid injection. These two factors are due to three main effects: The low vapor pressure of the heavier analytes (i.e., low concentration in the gas phase), the differing affinities of each analyte toward the SPME fiber, and the sampling time. It is likely that equilibration between the SPME fiber and the sample vapor headspace was not obtained with the short sampling time used (1 min). However, equilibrium was not required to study the chromatographic efficiency of the SPME injection. If samples of interest were to by fully characterized, sampling time optimization would be warranted. Figure 2.2C is the resulting chromatogram using 100 µl of vapor headspace of the 73 component mixture injected onto the LTM-GC-FID with HSCFI. The sample is biased toward the volatile analytes due to their increased concentration in the headspace of the vial compared to the mid- and high-molecular weight compounds, which is not surprising.

A subset of the analyte peaks were quantified between the liquid, HS-SPME, and direct vapor injection methods using the 50 µl split-less injection of the test mixture as the quantification reference. The mass of each analyte for each injection method was calculated from the known analyte mass and the volume injected of the liquid mixture, followed by normalization to peak height. To facilitate analyte identification and quantification, the respective chromatograms (liquid, HS-SPME, vapor) were temporally aligned [33, 34]. Separate LTM-GC-TOFMS data (omitted for brevity) was used for peak identification to match the peaks between the three injection methods. Table 2.2 is the list of analytes that were quantified. The analyte identity, retention time, and mass injected with each injection method is provided. The majority of compounds quantified were in the range of hundreds of nanograms injected on column. The peaks were sufficiently symmetric (i.e., Gaussian) and did not show any significant evidence of overloading the column or detector. Two of the quantified analytes in the mixture, methyl laurate and pristane, were of very low concentration in the SPME analysis and not detected in the vapor analysis. The low intensity or non-detected peaks are due to the analyte vapor pressures being sufficiently low so as to not allow for any significant amount of chemical to be present in the vapor phase (headspace) during sampling.

In order to more rigorously evaluate the three sample introduction methods, as applied to HSCFI and LTM-GC-FID, the retention time and peak width for each resolved analyte peak was measured, analogous to our previous report using GC-TOFMS [35]. The peak width as a function of retention time for a sufficient number of resolved analyte peaks are presented in Figures 2.3A-C. Each point is a location in a given chromatogram where a peak finding algorithm identified a local maximum and calculated the width at base of the peak. Outlying points with inflated widths (i.e., peaks unresolved and overlapped with neighboring peaks) were

removed from the plot with an outlier detection algorithm for the sake of visualizing the peak widths of pure eluting analytes. By processing the data this way, the pattern of peak widths as a function of retention time in each separation can be accurately visualized. Since a primary focus of the current study was to maximize the peak capacity of the separation, and to do so in a ~ 1 min separation, understanding the distributions of the peak widths is essential for understanding how HSCFI and the LTM module work together. HSCFI provides an extremely narrow injection pulse to the LTM module. In the separation of the 50 nl liquid sample, the peak width at base (4σ) of the first detected peak was 33 ms while the last eluting peak was ~ 300 ms, which is consistent with GC theory [6]. In Figure 2.3A the peak width increase is nearly linear for peaks eluting from ~ 3 s to ~ 13 s, and then the peak widths are relatively constant from ~ 13 s and ~ 60 s. To accurately calculate the peak capacity for the separation, rather than use an average peak width for the entire separation (which would provide an incorrect result) a recursive calculation was performed based on the following equation [12],

$$R_s = \frac{t_{R,n} - t_{R,n-1}}{0.5(W_{b,n} + W_{b,n-1})} = 1 \quad (1)$$

where R_s is the resolution between two adjacent analytes, $t_{R,n}$ is the retention time of the nth peak, $t_{R,n-1}$ is the retention time of the n-1th peak, $W_{b,n}$ is the peak width of the nth peak, and $W_{b,n-1}$ is the width of the n-1th peak. To apply Eq. (1), a suitable, best-fit continuous function was determined, which provided the relationship between peak width and retention time in Figure 2.3A. Using the continuous function from Figure 2.3A, the calculation with Eq. (1) was performed such that the resolution between each successive peak and the peak before it was set to unit resolution (R_s = 1). The resulting width and retention time of each successive nth peak can be calculated based on the width and the retention time of the n-1th peak. The resulting application of Eq. (1) produced a "simulated" separation at unit resolution to illustrate and

quantify the peak capacity for the LTM-GC-FID separation, with the first 10 s of this simulated separation shown in Figure 2.4. The dead-time has been subtracted from the figure for clarity. In the first second of the separation, a peak capacity of n_c = 25 was calculated. For the first 10 s the peak capacity was n_c = 90. The total peak capacity experimentally achieved for a 60 s separation in Figures 2.2A and 2.3A was determined to be n_c = 270, which is consistent with the objective of the study. The achieved peak capacity of ~ 300 generally requires 15 to 30 min separation run time using conventional GC practices so the use of HSCFI with LTM-GC provides equivalent chromatographic information in only about 7% of the separation run time.

Peak width as a function of retention time plots for the other two separations, using the HS-SPME and 100 µl vapor sample introduction with HSCFI, are similar to the liquid sample, but have fewer peaks toward the end of each chromatogram. Peak capacity for the SPME sample introduction to LTM-GC-FID with HSCFI in Figures 2.2B and 2.3B was n_c = 200 (40 s time interval), while n_c = 125 was achieved for the 20 s time interval with the vapor sample introduction to LTM-GC-FID with HSCFI, in Figures 2.2C and 2.3C. Figure 2.3D is an overlay of Figures 2.3A-C to directly compare the similarity of the peak widths from the three different injection methods with HSCFI. Indeed the peak widths appear very similar between methods. The boiling point range of analytes that were satisfactorily sampled by the SPME analysis ranged up to a boiling point of ~ 220 °C. The boiling point range of the 100 µl vapor sample only extended up to ~ 150 °C. Note that the peak widths for the detected analytes were essentially identical for all three sample introduction methods using HSCFI, and it is only due to the variation in the range of analytes that are introduced by each sampling method to HSCFI, which impacted the separation time window, that then produced a different peak capacity, n_c, for each sample injection method.

The LTM-GC-FID was further evaluated without the use of HSCFI to study the ability of the LTM to trap analytes by itself and also so the benefit of using HSCFI could be quantified. Since the host GC oven is kept at a high temperature (300 °C), we hypothesize the LTM module (which is held outside the oven) acts as a cold trap for the analytes as they transfer from the GC inlet to the column in the LTM module. The ambient laboratory temperature was ~ 20 °C and the initial LTM column temperature was 30 °C. In addition to the temperature gradient between GC and LTM, the column used (5 m x 100 µm i.d. with a 0.4 µm film) had a low phase-volume ratio, β, of 62.5. Volatile analysis columns traditionally have low phase volume ratios ($\beta < 100$) to aid in trapping volatile analytes on the column prior to temperature programming. Columns with a higher phase volume ratio, such as a 100 µm i.d. column with a 0.1 µm phase ($\beta = 250$) will have lower column capacity, but may provide narrower peak widths. We opted to apply the lower β column (thicker film) for higher column capacity and increased trapping ability.

Figures 2.5A-C are the resulting LTM-GC-FID chromatograms (without HSCFI) of the 50 nl liquid, HS-SPME, and 100 µl vapor injections of the 73 component mixture, respectively. The separations look very similar to their HSCFI-implemented counterpart. While the separation window is still 60 s, the increased dead-time (15 s versus 3 s) is due to the difference in flow rate at the moment of injection. The samples introduced with HSCFI were injected at 689 kPa (100 psig) after cryo-trapping, whereas the non-HSCFI samples were undergoing a pressure ramp as they were injected on column in order to allow for focusing at the head of the column. Figures 2.6A-C are the respective peak width versus retention time plots for the separations in Figures 2.5A-C, with Figure 2.6D as an overlay of 2.6A-C for comparison purposes. The plots show a remarkably different trend than those injected with HSCFI. Without the HSCFI, the peaks are wider at the beginning of the chromatogram (~ 300 ms versus ~ 30 ms), reduce slightly in width

toward the middle of the separation, and then increase to ~ 300 ms at the end. The peak width decrease toward the middle of the chromatogram is likely a combination from two factors. First, the increase in linear flow velocity as a result of the increasing pressure ramp causes peaks to be compressed and narrowed. Second, the higher molecular weight analytes focus at the head of the column more effectively (i.e. in a narrower band) compared to the more volatile compounds.

For the 100 µl vapor samples, preconcentration of injected analytes is provided either with or without HSCFI when using LTM-GC. The preconcentration factor is defined herein as the ratio of the maximum concentration of the detected analyte chromatographic peak relative to the analyte concentration injected with the syringe. Defining the preconcentration factor in this manner actually underestimates the maximum preconcentration prior to the GC separation, but is useful to provide the analyst with the knowledge of both effects, sample preconcentration prior to the separation and dilution due to the chromatographic process [12], so is a better quantitative metric for assessing the combination of the sample introduction, preconcentration, and separation steps. With a flow rate 3 ml/min (50 µl/s) at the outlet, the 100 µl vapor sample (see Figure 2.5C) should produce a "rectangular" sample pulse ~ 2 s wide (at base). However, the subsequent GC peaks observed are only ~ 200 to 300 ms wide (at base). The preconcentration factor for the separation without HSCFI was calculated to be 11 for the earliest eluting peak with a peak width of 300 ms, whereas for the separation with HSCFI, a preconcentration factor of 103 was calculated for the earliest eluting peak (33 ms peak width), a substantial improvement for the earlier eluting peak. The difference in preconcentration factors between the vapor sample with HSCFI and the vapor sample without HSCFI is apparent when comparing Figure 2.3C (vapor sample with HSCFI) to Figure 2.6C (vapor sample without HSCFI). The early eluting peaks in Figure 2.3C are focused more efficiently due to the cryogenic nitrogen stream, which results in

significantly narrower peaks when compared to the early eluting peaks of the 100 µl sample without HSCFI (Figure 2.6C). However, the peaks in Figure 2.6C are still preconcentrated relative to the native sample, i.e. the concentration of analytes delivered by the syringe. The peak width data and preconcentration factors provide evidence that the analytes (including the most volatile analytes, such as pentane, boiling point = 36 °C) are focusing on the head of the LTM-GC column even without HSCFI, which is a consequence of the LTM module being mounted outside of the host GC oven (i.e., on the oven door).

We now provide a comparison of peak capacities produced for the three sample introduction methods with and without HSCFI, using the peak width as a function of retention time data in Figures 2.6A-C, which were also analyzed using Eq. (1). The peak capacity for the direct liquid injection sample to the LTM-GC-FID (without HSCFI) data shown in Figure 2.5A and 2.6A was determined to be n_c = 220. Since n_c = 270 was achieved for the separation with HSCFI for the same time interval of 60 s, therefore HSCFI provided a 23% increase in total peak capacity for direct liquid injection. Similarly, the peak capacity for the SPME sample introduction to LTM-GC-FID (without HSCFI) in Figures 2.5B and 2.6B was n_c = 160 (for a 40 s time interval), which is 25% less than the n_c = 200 when HSCFI was implemented (compare to Figures 2.2B and 2.3B). Finally, at the beginning of the separation where the benefit of using HSCFI is most pronounced, n_c = 80 was achieved for the 20 s time interval observed with the vapor sample introduction to the LTM-GC-FID (without HSCFI), presented in Figures 2.5C and 2.6C, which was 56% lower total peak capacity than the n_c = 125 achieved for the vapor sample introduction with HSCFI (Figures 2.2A and 2.3A). Overall, the use of HSCFI provided a significant improvement in peak capacity, although using LTM-GC without HSCFI still

performed reasonably well due to an on-column focusing effect at the head of the LTM column module.

In order to demonstrate a range of retention indices (RI) an analyst may commonly experience in practice, a mixture of even numbered n-alkanes between hexane (n-C_6H_{14}, boiling point = 69 °C) and tetracosane (n-$C_{24}H_{50}$, boiling point = 391 °C) was analyzed. The compounds were added in roughly equal mass and diluted in acetone (solvent peak not pictured) to achieve a suitable signal-to-noise ratio. The alkane mixture separation used identical conditions as those used in the LTM-GC-FID separations without HSCFI per Figures 2.5 and 2.6. Figure 2.7A is the chromatogram of the alkane mixture. Peak widths as a function of retention time in the 60 s separation window in Figure 2.7A are consistent to the previous LTM-GC-FID chromatograms without HSCFI (Figures 2.5 and 2.6). Figure 2.7B shows a zoom of a portion of Figure 2.7A between 30 s and 45 s. The two peaks, octane and decane, have a remarkable resolution (R_s = 45) with peak widths of ~200 ms at base, hence the peak capacity between the two compounds is 45 in a 9 s window. The RI range, 600 (n-C_6) to 2400 (n-C_{24}), while not comprehensive, demonstrates the ability of LTM-GC to rapidly resolve mixtures with wide ranges of boiling points commonly required for routine GC analyses. There are certainly analytes with much higher RI values that may be desirable to analyze, and LTM-GC is likely capable of doing so in a fast, reproducible manner. Future studies may warrant investigation of higher alkanes (RI > 2500) to provide a more extensive characterization.

To demonstrate the viability of LTM-GC-TOFMS on a complex real-world sample, the LTM module was installed on a GC-TOFMS (Agilent 6890A GC, LECO Pegasus III TOFMS). The TOFMS has a rapid spectral collection rate, up to 500 spectra/s, which is an ideal detector for the narrow peaks produced with LTM-GC. Other mass spectrometers, such as the quadrupole

mass spectrometer (qMS) have slow scanning rates, generally 15 to 20 spectra/s at the most in full scan mode. The peaks from the HSCFI-LTM-GC-FID were ~ 30 ms wide at the beginning of the chromatogram. Therefore, a qMS would be unable to detect at a sufficient rate to obtain enough spectra across the narrow peaks to facilitate appropriate data analysis. For demonstration purposes, the sample analyzed with the LTM-GC-TOFMS was the headspace of ripe banana peels sampled with HS-SPME, with the resulting separation shown in Figure 2.8A and 2.8B. The separation window was again ~ 60 s. The average peak widths at base were ~ 360 ms, providing a peak capacity of n_c = 170 peaks. The compound labeled in Figure 2.8A that gives the characteristic banana smell and flavor, isoamyl acetate, was tentatively identified by its mass spectrum (match value = 914). Figure 2.8B shows a zoom of the complex region from Figure 2.8A. Another peak from the separation was tentatively identified as methyl butanoate (match value = 952), highlighting the use of TOFMS to obtain quality spectra of narrow peak width analytes. Several of the peaks in Figure 2.8B appear to have a poor peak shape, but are actually peaks due to the overlap of more than one compound. Table 2.3 is a list of tentatively identified analytes from the separation in Figure 2.8A. Peak identification and deconvolution was performed with previously reported software [35] which allows the analyst to visually identify chromatographically overlapped analytes and obtain deconvoluted mass spectra, which can then be matched to a database. The database used to match spectra was NIST 2011. A library match value over 800 was deemed sufficient for tentative analyte identification.

The reader may potentially come to the conclusion that the relative retention of methyl butanoate (t_R = 73 s in the 100 s separation (Figure 2.8B) indicates that the LTM-GC-TOFMS is only useful for the separation of low molecular weight compounds. However, the low retention index range in this instance is due to the sample consistency, and is not a shortcoming of the

LTM-GC platform. Indeed, Figures 2.7A and 2.7B indicate that the LTM-GC platform can easily analyze compounds up to tetracosane, C_{24} (boiling point = 391 °C). Also, Fialkov, Morag, and Amirav demonstrated that carbon chains up to C_{40} can be analyzed by LTM-GC [7]. The longer column applied for the LTM-GC-TOFMS analysis (10 m) coupled with helium as the carrier gas and longer transfer lines for the TOFMS contributed to slightly wider peak widths and a longer hold-up time compared to the data presented in Figures 2.2 through 2.7. The LTM-GC-TOFMS chromatograms are not meant to be directly compared to the LTM-GC-FID chromatograms, rather the intent is to show that these two instrumental platforms are complementary. In this regard, it is important to note that LTM-GC-TOFMS is still delivering narrower peaks in a significantly shorter time compared to conventional GC-TOFMS instrumentation.

2.4 Conclusion

We have demonstrated with commercial LTM-GC instrumentation a ~ 1 min separation with a peak capacity of 270 with LTM-GC-FID. Using liquid, HS-SPME, and vapor injections of the same sample, we have demonstrated the ability of the LTM column module to natively focus analytes at the head of the column without the need for external instrumentation. This result is a direct consequence of the LTM column module being located outside of the traditional GC oven. A previously developed injection system, the HSCFI [11, 28], did provide an added benefit of preconcentration of volatile analytes with a concurrent improvement in peak capacity relative to not using HSCFI. There is a significant increase in peak capacity in the beginning of the separations with HSCFI where the calculated peak capacity of the 50 nl liquid sample was 90 peaks in the first 10 s, compared to the same separation window from without HSCFI where there were only 43 theoretical peaks in the first 10 s. The results also have implications for the field of GC-GC, and perhaps GC×GC, using LTM technology. Fast column heating can enable

new types of separations and spurn the grown of new technologies, such as faster modulators, to keep up with the speed of fast LTM-GC analyses. Additionally, we also demonstrated use of the LTM-GC coupled to TOFMS to separate volatile analytes in the headspace of banana peels.

2.5 List of Works Cited

[1] B.R. Toledo, L.W. Hantao, T.D. Ho, F. Augusto, J.L. Anderson, A chemometric approach toward the detection and quantification of coffee adulteration by solid-phase microextraction using polymeric ionic liquid sorbent coatings, *Journal of Chromatography A* 1346 (2014) 1–7.

[2] P.A. Sutton, S.J. Rowland, High temperature gas chromatography–time-of-flight-mass spectrometry (HTGC–ToF-MS) for high-boiling compounds, *Journal of Chromatography A* 1243 (2012) 69-80.

[3] P.A. Sutton, M.J. Wilde, S.J. Martin, J. Cvačka, V. Vrkoslav, S.J. Rowland, Studies of long chain lipids in insects by high temperature gas chromatography and high temperature gas chromatography–mass spectrometry, *Journal of Chromatography A* 1297 (2013) 236–240.

[4] L. Mahé, M. Courtiade, C. Dartiguelongue, J. Ponthus, V. Souchon, D. Thiébaut, Overcoming the high-temperature two-dimensional gas chromatography limits to elute heavy compounds, *Journal of Chromatography A* 1229 (2012) 298–301.

[5] J.A. Giannovario, R.J. Gondek, R.L. Grob, A cryogenic gas chromatograph, *Journal of Chromatography A* 89 (1974) 1-9.

[6] R.B. Wilson, J.C. Hoggard, R.E. Synovec, Fast, High Peak Capacity Separations in Gas Chromatography–Time-of-Flight Mass Spectrometry, *Analytical Chemistry* 84 (2012) 4167-4173.

[7] A.B. Fialkov, M. Morag, A. Amirav, A low thermal mass fast gas chromatograph and its implementation in fast gas chromatography mass spectrometry with supersonic molecular beams, *Journal of Chromatography A* 1218 (2011) 9375-9383.

[8] S.D. Stearns, H. Cai, J.A. Koehn, M. Brisbin, C. Cowles, C. Bishop, S. Puente, D. Ashworth, A direct resistively heated gas chromatography column with heating and sensing on the same nickel element, *Journal of Chromatography A* 1217 (2010) 4629-4638.

[9] K. Maštovská, S.J. Lehotay, Practical approaches to fast gas chromatography–mass spectrometry, *Journal of Chromatography A* 1000 (2003) 153-180.

[10] F. Xu, W. Guan, G. Yao, Y. Guan, Fast temperature programming on a stainless-steel narrow-bore capillary column by direct resistive heating for fast gas chromatography *Journal of Chromatography A* 1186 (2008) 183-188.

[11] B.D. Fitz, R.B. Wilson, B.A. Parsons, J.C. Hoggard, R.E. Synovec, Fast, high peak capacity separations in comprehensive two-dimensional gas chromatography with time-of-flight mass spectrometry, *Journal of Chromatography A* 1266 (2012) 116-123.

[12] R.B. Wilson, J.C. Hoggard, R.E. Synovec, High throughput analysis of atmospheric volatile organic compounds by thermal injection – isothermal gas chromatography – time-of-flight mass spectrometry, *Talanta* 103 (2013) 95-102.

[13] M. Rambla-Alegre, B. Tienport, K. Mitsui, E. Masugi, Y. Yoshimura, H. Nagata, F. David, P. Sandra, Coupling gas chromatography and electronic nose detection for detailed cigarette smoke aroma characterization, *Journal of Chromatography A* 1365 (2014) 191-203.
[14] V. Jain and J.B. Phillips, Fast temperature programming on fused silica open tubular capillary columns by direct resistive heating, *Journal of Chromatographic Science* 33 (1995) 55-59.
[15] D. Ehrmann, H.P. Dharmasena, K. Carney, and E.B. Overton, Novel column heater for fast capillary gas chromatography, *Journal of Chromatographic Science* 34 (1996) 533-539.
[16] E.B. Overton and K. Carney, New horizons in gas chromatography: field applications of microminiaturized gas chromatographic techniques, *Trends in Analytical Chemistry* 13 (1994) 252-257.
[17] X. Yan, K.R. Carney, E.B. Overton. Application of Purge-and-Trap Method to Fast and Convenient Field Analysis of Water and Soil Samples, *Journal of Chromatographic Science* 30 (1992) 491-496.
[18] P.Q. Tranchida, L. Mondello, Current-day employment of the micro-bore open-tubular capillary column in the gas chromatography field, *Journal of Chromatography A* 1261 (2012) 23-36.
[19] A. Wang, H.D. Tolley, M.L. Lee, Gas chromatography using resistive heating technology, *Journal of Chromatography A* 1261 (2012) 46-57.
[20] H.D. Tolley, S.E. Tolley, A. Wang, M.L. Lee, Moving thermal gradients in gas chromatography, *Journal of Chromatography A* 1374 (2014) 189-198.
[21] A. Wang, S. Hynynen, A.R. Hawkins, S.E. Tolley, H.D. Tolley, M.L. Lee, Axial thermal gradients in microchip gas chromatography, *Journal of Chromatography A* 1374 (2014) 216-223.
[22] J.A. Contreras, A. Wang, A.L. Rockrood, H.D. Tolley, M.L. Lee, Dynamic thermal gradient gas chromatography, *Journal of Chromatography A* 1302 (2013) 143-151.
[23] J.A. Contreras, A. Wang, A.L. Rockrood, H.D. Tolley, M.L. Lee, Peak sweeping and gating using thermal gradient gas chromatography, *Journal of Chromatography A* 1278 (2013) 160-165.
[24] J. Luong, R. Gras, M. Hawryluk, R. A. Shellie, H. J. Cortes, Multidimensional gas chromatography using microfluidic switching and low thermal mass gas chromatography for the characterization of targeted volatile organic compounds, *Journal of Chromatography A* 1288 (2013) 105-110.
[25] A. Casilli, E. Decorzant, A. Jaquier, E. Delort, Multidimensional gas chromatography hyphenated to mass spectrometry and olfactometry for the volatile analysis of citrus hybrid peel extract, *Journal of Chromatography A* 1373 (2014) 169-178.
[26] E. Dumont, B. Tienpont, N. Higashi, K. Mitsui, N. Ochiai, H. Kanda, F. David, P. Sandra, Heart-cutting two-dimensional gas chromatography in combination with isotope ratio mass spectrometry for the characterization of the wax fraction in plant material, *Journal of Chromatography A* 1317 (2013) 230-238.
[27] H. Snijders, H.-G. Janssen, C. Cramers, Optimization of temperature-programmed gas chromatographic separations: Prediction of retention times and peak widths from retention indices, *Journal of Chromatography A* 718 (1995) 339-355.

[28] R.B. Wilson, B.D. Fitz, B.C. Mannion, T. Lai, R.K. Olund, J.C. Hoggard, R.E. Synovec, High-speed cryo-focusing injection for gas chromatography: Reduction of injection band broadening with concentration enrichment, *Talanta* 97 (2012) 9-15.
[29] Agilent Low Thermal Mass Module, Agilent Technologies, Palo Alto, CA, http://www.chem.agilent.com
[30] R.V. Mustacich, J.F. Everson, U.S. Patent 6,217,829 (2001).
[31] R.V. Mustacich, J.P. Richards, U.S. Patent 6,209,386 (2001).
[32] J. Luong, R. Gras, R. Mustacich, H. Cortes, Low Thermal Mass Gas Chromatography: Principles and Applications, *Journal of Chromatographic Science* 44 (2006) 253-261.
[33] K.M. Pierce, J.L. Hope, K.J. Johnson, B.W. Wright, R.E. Synovec, Classification of gasoline data obtained by gas chromatography using a piecewise alignment algorithm combined with feature selection and principal component analysis, *Journal of Chromatography A* 1096 (2005) 101-110.
[34] N.E. Watson, M.M. VanWingerden, K.M. Pierce, B.W. Wright, R.E. Synovec, Classification of high-speed gas chromatography–mass spectrometry data by principal component analysis coupled with piecewise alignment and feature selection, *Journal of Chromatography A* 1129 (2006) 111-118.
[35] B.D. Fitz, B.C. Reaser, D.K. Pinkerton, J.C. Hoggard, K.J. Skogerboe, R.E. Synovec, Enhancing Gas Chromatography–Time of Flight Mass Spectrometry Data Analysis Using Two-Dimensional Mass Channel Cluster Plots, *Analytical Chemistry* 86 (2014) 3973-3979.

2.6 Tables

Table 2.1 List of the seventy-three compounds included in the test mixture listed in order of increasing boiling point. The mass listed is the mass used in the bulk mixture. A small aliquot was used for analysis.

Chemical	Mass (mg)	Mass Percent	BP (°C)	Vendor
pentane	131	0.0153	36	J.T. Baker
ethyl formate	151	0.0176	54	Sigma-Aldrich
acetone	180	0.0210	56	Sigma-Aldrich
chloroform	132	0.0154	61	Fischer
n-hexane	151	0.0176	69	Sigma-Aldrich
methylcyclopentane	105	0.0122	72	Fluka
2-butanone	143	0.0167	80	Sigma-Aldrich
benzene	112	0.0131	80	Fischer
cyclohexane	119	0.0139	81	Sigma-Aldrich
1-propanol	118	0.0138	97	Sigma-Aldrich
heptane	138	0.0161	98	Fischer
methylcyclohexane	108	0.0126	101	Sigma-Aldrich
2-pentanone	151	0.0176	102	Sigma-Aldrich
toluene	123	0.0143	111	Sigma-Aldrich
2-butanol	131	0.0153	117	Sigma-Aldrich
octane	124	0.0145	126	Sigma-Aldrich
3-hexanone	135	0.0157	128	Sigma-Aldrich
chlorobenzene	121	0.0141	132	Alfa-Aesar
1-chlorohexane	129	0.0150	135	Sigma-Aldrich
ethylbenzene	113	0.0132	136	Sigma-Aldrich
1-pentanol	120	0.0140	137	Sigma-Aldrich
xylenes (o, m, p)	126	0.0147	139	Mallinckrodt
3-heptanone	116	0.0135	141	Sigma-Aldrich
cyclooctane	113	0.0132	150	Sigma-Aldrich
nonane	125	0.0146	151	Sigma-Aldrich
propylbenzene	125	0.0146	152	Sigma-Aldrich
1-bromohexane	129	0.0150	156	Sigma-Aldrich
bromobenzene	118	0.0138	156	Sigma-Aldrich
1-hexanol	117	0.0136	158	Sigma-Aldrich
2-heptanol	118	0.0138	160	Fluka

mesitylene	132	0.0154	163	Sigma-Aldrich
3-octanone	115	0.0134	167	Sigma-Aldrich
t-butylbenzene	141	0.0164	167	Sigma-Aldrich
methyl hexanoate	135	0.0157	168	Sigma-Aldrich
isobutylbenzene	108	0.0126	170	Sigma-Aldrich
sec-butylbenzene	123	0.0143	173	Sigma-Aldrich
decane	95	0.0111	174	Sigma-Aldrich
1-bromoheptane	135	0.0157	179	Sigma-Aldrich
butylcyclohexane	110	0.0128	181	Sigma-Aldrich
butylbenzene	130	0.0152	183	Sigma-Aldrich
methyl octanoate	116	0.0135	193	Sigma-Aldrich
1-octanol	123	0.0143	194	Sigma-Aldrich
2-nonanone	126	0.0147	194	Sigma-Aldrich
undecane	107	0.0125	196	Sigma-Aldrich
1-bromooctane	127	0.0148	199	Sigma-Aldrich
1,3,5-trichlorobenzene	115	0.0134	208	Sigma-Aldrich
2-decanone	114	0.0133	209	Sigma-Aldrich
1-nonanol	110	0.0128	215	Sigma-Aldrich
dodecane	96	0.0112	216	Sigma-Aldrich
naphthalene	118	0.0138	218	Sigma-Aldrich
1,2,3-trichlorobenzene	133	0.0155	219	Sigma-Aldrich
methyl salicylate	117	0.0136	223	Alfa-Aesar
methyl decanoate	123	0.0143	224	Eastman Chemicals
ethyl salicylate	111	0.0129	227	Alfa-Aesar
bicyclohexyl	111	0.0129	227	Sigma-Aldrich
1-decanol	107	0.0125	229	Sigma-Aldrich
1-geraniol	118	0.0138	230	Sigma-Aldrich
2-undecanone	112	0.0131	231	Sigma-Aldrich
tridecane	99	0.0115	235	Sigma-Aldrich
cyclohexylbenzene	130	0.0152	239	Sigma-Aldrich
2-dodecanone	101	0.0118	245	Sigma-Aldrich
tetradecane	94	0.0110	254	Fluka
1-dodecanol	102	0.0119	256	Acros Organics
methyl laurate	125	0.0146	267	Sigma-Aldrich
pentadecane	117	0.0136	271	Alfa-Aesar
hexadecane	137	0.0160	287	Sigma-Aldrich

1-tetradecanol	111	0.0129	289	Sigma-Aldrich
2-pentadecanone	104	0.0121	294	Sigma-Aldrich
pristane	97	0.0113	296	Sigma-Aldrich
1-hexadecanol	122	0.0142	344	Sigma-Aldrich
adamantane	111	0.0129	sublimes	Sigma-Aldrich

Table 2.2 Quantified analytes in the 73 component mixture using HSCFI-LTM-GC-FID separation with the three injection methods. MV refers to mass spectral match value obtained from a separate LTM-GC-TOFMS analysis (value of 1000 indicates a perfect match). The column titles: Liquid, SPME, Vapor, refer to the three injection methods (50 nl liquid, HS-SPME, 100 µl vapor) as explained in the experimental section. The values are the quantified mass (in µg) of each analyte from their respective injection method.

Name (MV)	Retention Time (s)	Mass Injected, Liquid, µg	Mass Injected, SPME, µg	Mass Injected, Vapor, µg
ethyl formate (942)	17.8	0.70	0.65	2.41
1-propanol (936)	19.6	0.55	0.84	0.56
trichloromethane (972)	22.5	0.62	1.13	0.95
methylcyclopentane (972)	23.1	0.49	0.66	1.08
2-pentanone (960)	25.7	0.70	1.26	0.45
n-heptane (952)	26.5	0.64	1.03	0.73
methyl laurate (959)	58.5	0.58	8.86E-03	- [(a)]
pristane (957)	60.7	0.45	4.55E-03	- [(a)]

(a) Methyl laurate and pristane were not detected using direct vapor injection.

Table 2.3 List of tentatively identified analytes from the HS-SPME-LTM-TOFMS separation of banana peel vapor. Names and match values were obtained from NIST 2011. Peaks that were overlapped with adjacent analytes were deconvoluted using previously reported software [35].

Name	Retention Time (s)	Match Value
ethyl acetate	42.2	976
isobutanol	43.7	969
1-butanol	47.6	916
2-pentanone	50.1	989
2-pentanol	51.4	968
3-methyl-1-butanol	55.2	926
isobutyl ethanoate	58.4	951
hexanal	60.5	850
acetic acid	61.2	948
pentyl ethanoate (amyl acetate)	63.9	938
1-hexanol	65.3	936
3-methylbutyl ethanoate (isoamyl acetate)	65.7	924
1-methoxypentane	66.7	800
2-heptanone	66.8	957
2-heptanol	67.3	981
isobutyl isobutanoate	68.1	922
1,3-dimethylbutyl ethanoate	69.7	850
isobutyl butanoate	70.6	930
methyl butanoate	72.7	952
isobutyl isopentanoate	73.4	920
isopentyl isobutanoate	73.7	915
1-methylbutyl butanoate	74.3	892
1-methylhexyl ethanoate	75.1	870
1,4-dimethyl-4-pentyl ethanoate	75.2	810
butyl-3-methyl butanoate	75.5	890
isopentyl butanoate	76.2	885
pentyl-3-methyl butanoate	76.9	842
3-methylbutyl-3-methyl butanoate	78.5	930
pentyl pentanoate	78.9	800
isobutyl hexanoate	80.5	894
isopentyl pentanoate	80.6	827
n-hexyl butanoate	82.3	916
n-hexyl-3-methyl butanoate	84.5	907
isopentyl hexanoate	84.9	911

2.7 Figures

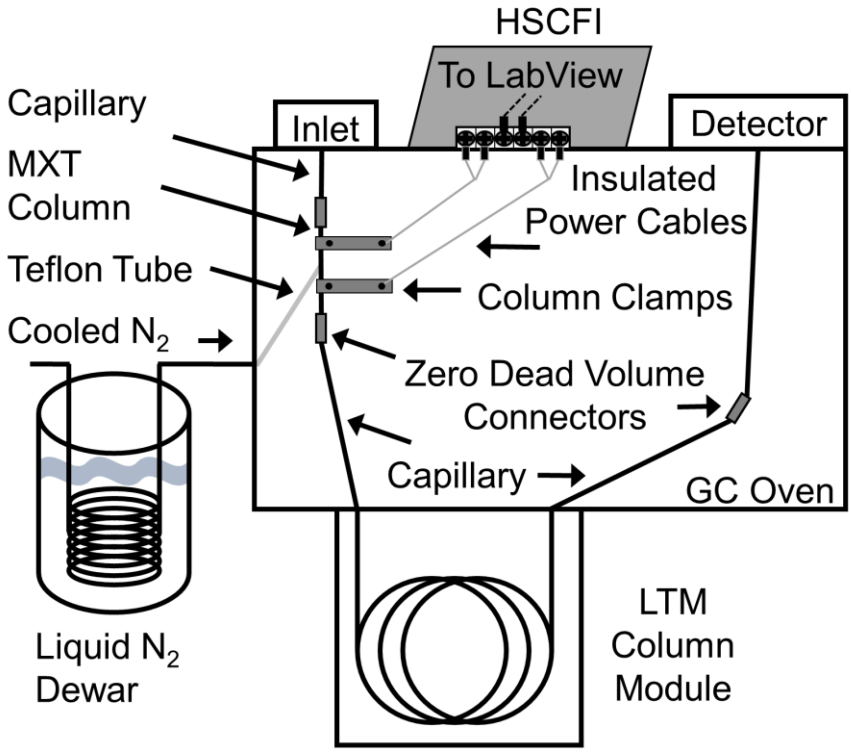

Figure 2.1 Instrument schematic. Diagram of the Agilent 6890 GC, modified for use with high speed cryo-focusing injection (HSCFI) and low thermal mass gas chromatography (LTM-GC). A constant flow of cooled nitrogen is delivered for HSCFI via a liquid nitrogen heat exchanger to trap analytes coming from the inlet. The MXT column component with HSCFI is resistively heated with a capacitive discharge device to re-inject analytes onto the LTM column. The LTM module is external to the main GC oven.

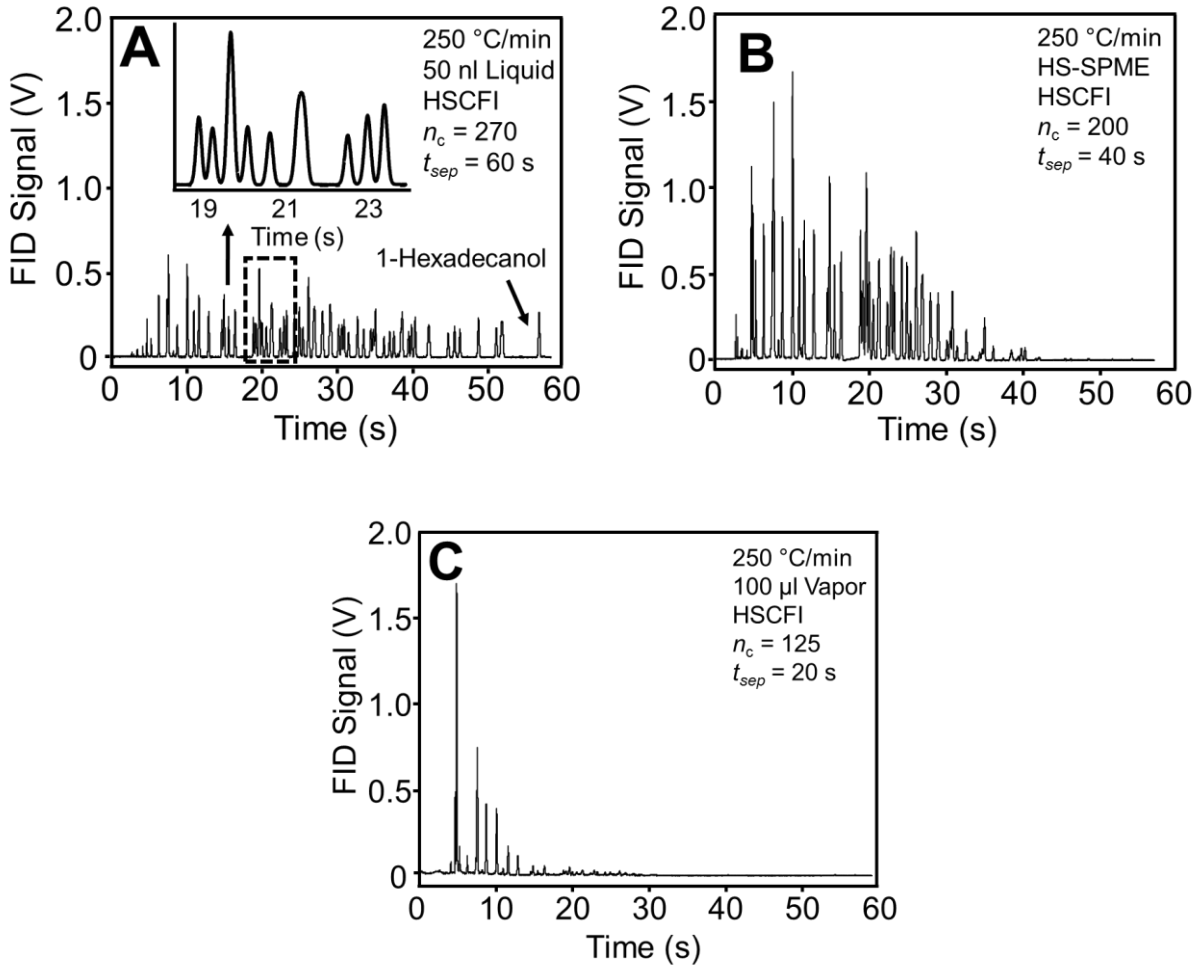

Figure 2.2 HSCFI-LTM-GC-FID separations of the 73 component test mixture using three sample injection methods. An LTM heating rate of 250 °C/min was used. Peak widths (at base) range from 33 ms to ~ 300 ms. (A) 50 nl liquid injection. (B) Headspace solid phase micro-extraction (HS-SPME) injection. (C) 100 µl headspace vapor injection.

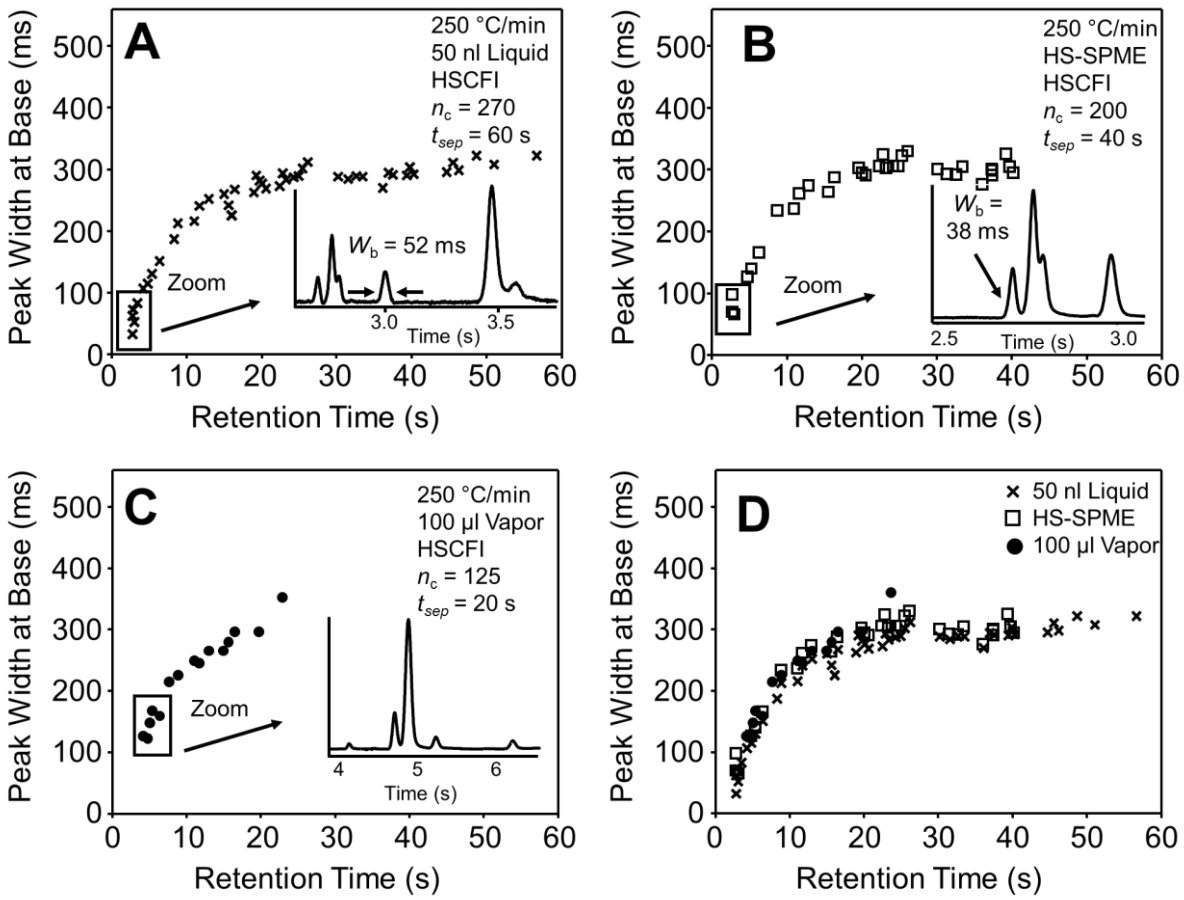

Figure 2.3 Peak width versus retention time plots of representative non-overlapped analyte peaks processed from the HSCFI-LTM-GC-FID separations. Each point represents the measured retention time and peak width for an analyte peak detected in the chromatogram. (A) 50 nl liquid injection. (B) HS-SPME injection. (C) 100 µl headspace vapor injection. (D) Overlay of the three injections methods from A-C.

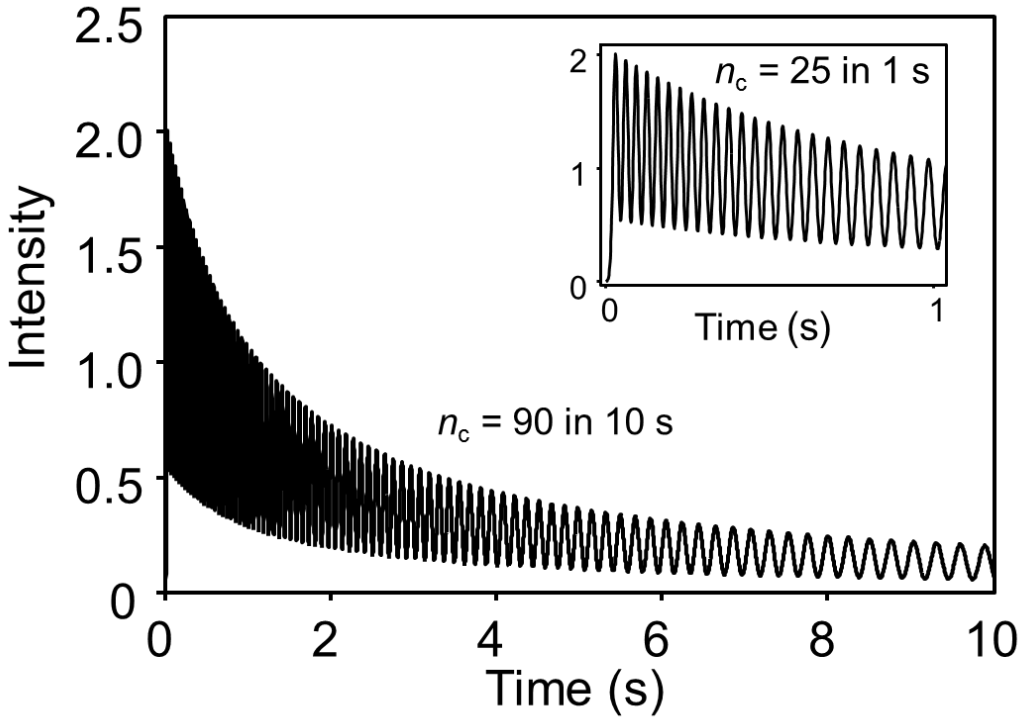

Figure 2.4 Iterative peak capacity calculation based upon the HSCFI-LTM-GC-FID separation using the 50 nl injection of the 73 component mixture. The simulated chromatogram models peaks with increasing peak widths set to a resolution of 1 between adjacent peaks. The function of peak width versus retention time was obtained from the linear portion of Figure 2.3A from 3 s to 13 s. Peak capacity values are provided for the first second and for the first 10 seconds.

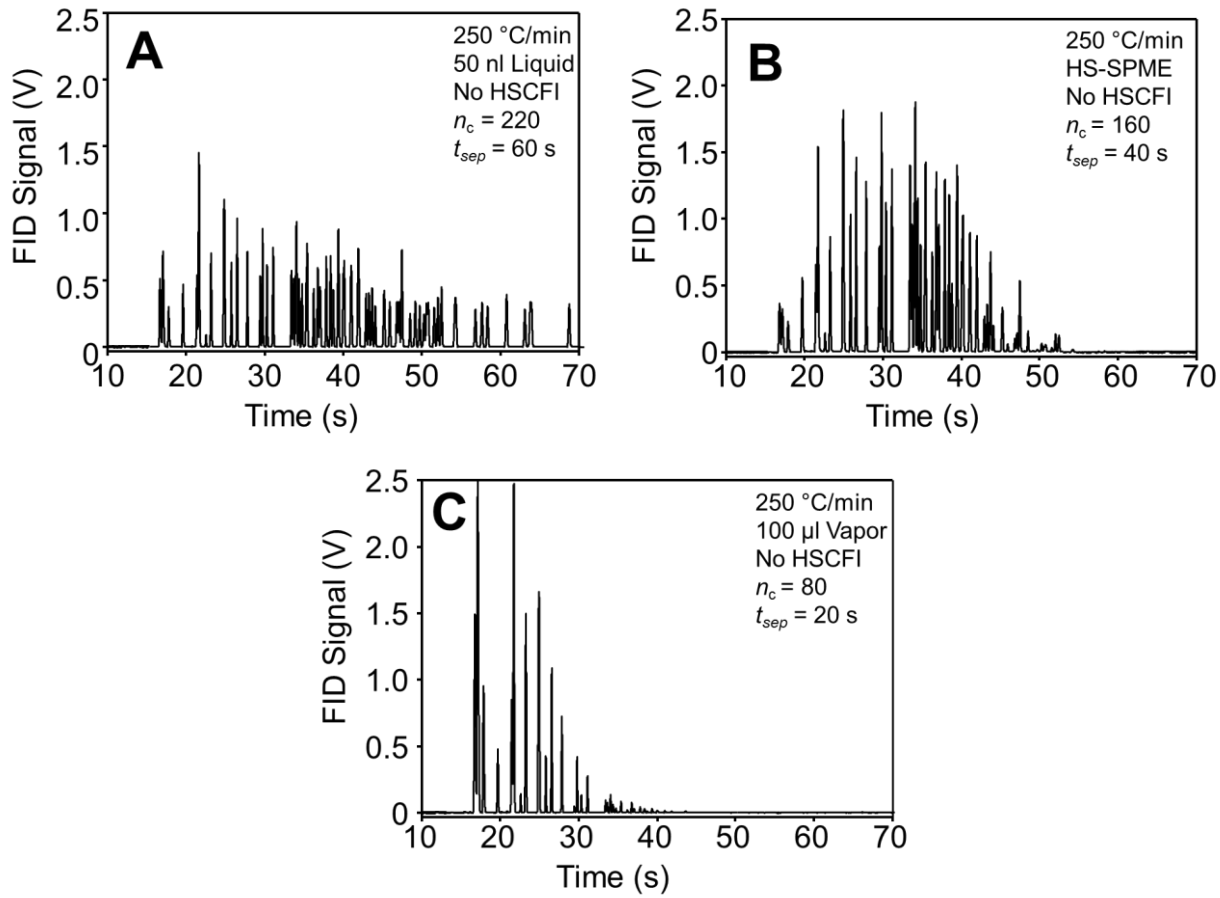

Figure 2.5 LTM-GC-FID chromatograms of the separation of the 73 component mixture without using HSCFI. An LTM heating rate of 250 °C/min was used. (A) 50 nl liquid injection. (B) HS-SPME injection. (C) 100 µl of headspace vapor injection.

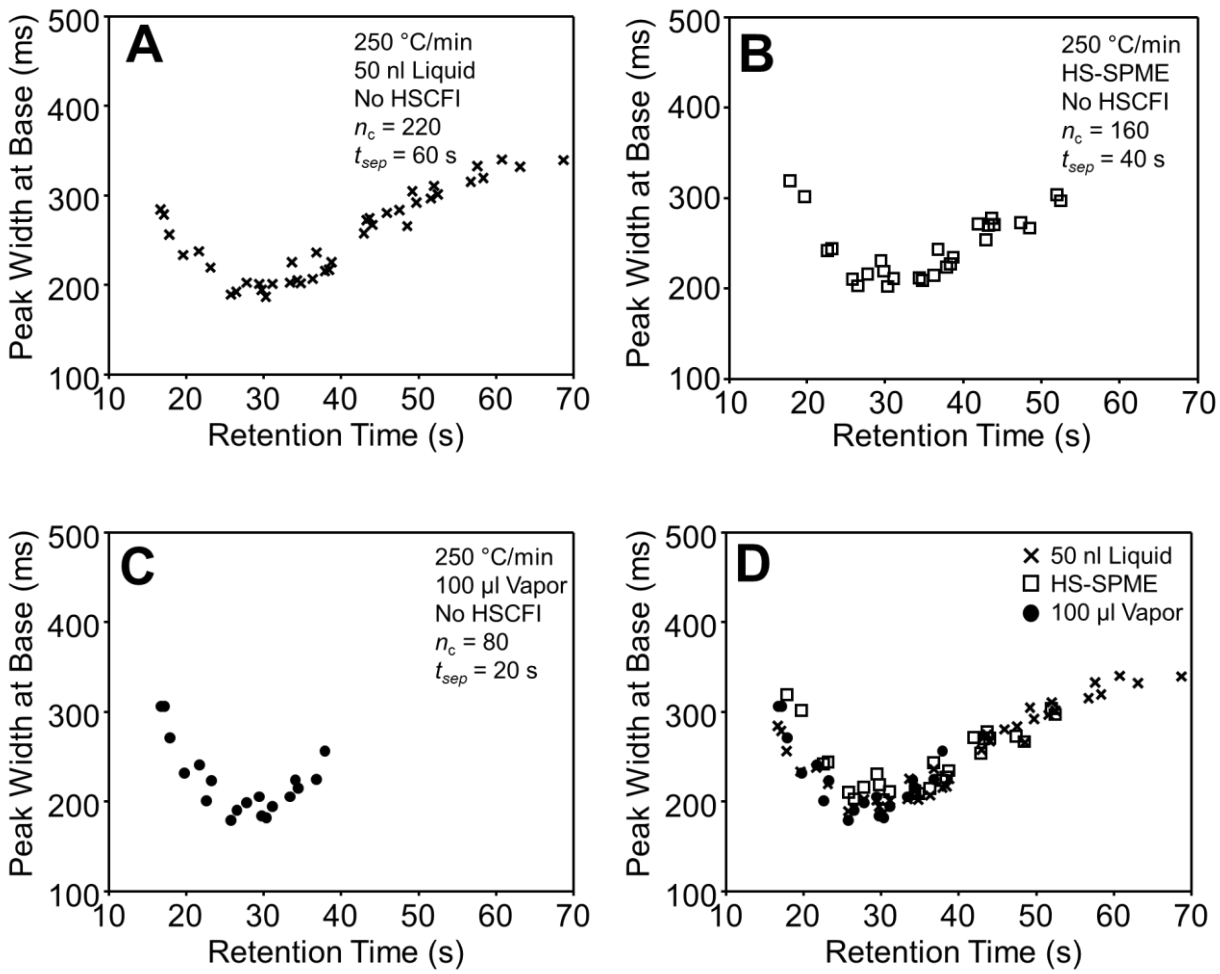

Figure 2.6 Peak width versus retention time plots processed from the LTM-GC-FID separations without HSCFI. Each point represents the measured retention time and peak width for an analyte peak detected in the chromatogram. (A) 50 nl liquid injection. (B) HS-SPME injection. (C) 100 µl vapor injection. (D) Overlay of the three injections methods from A-C.

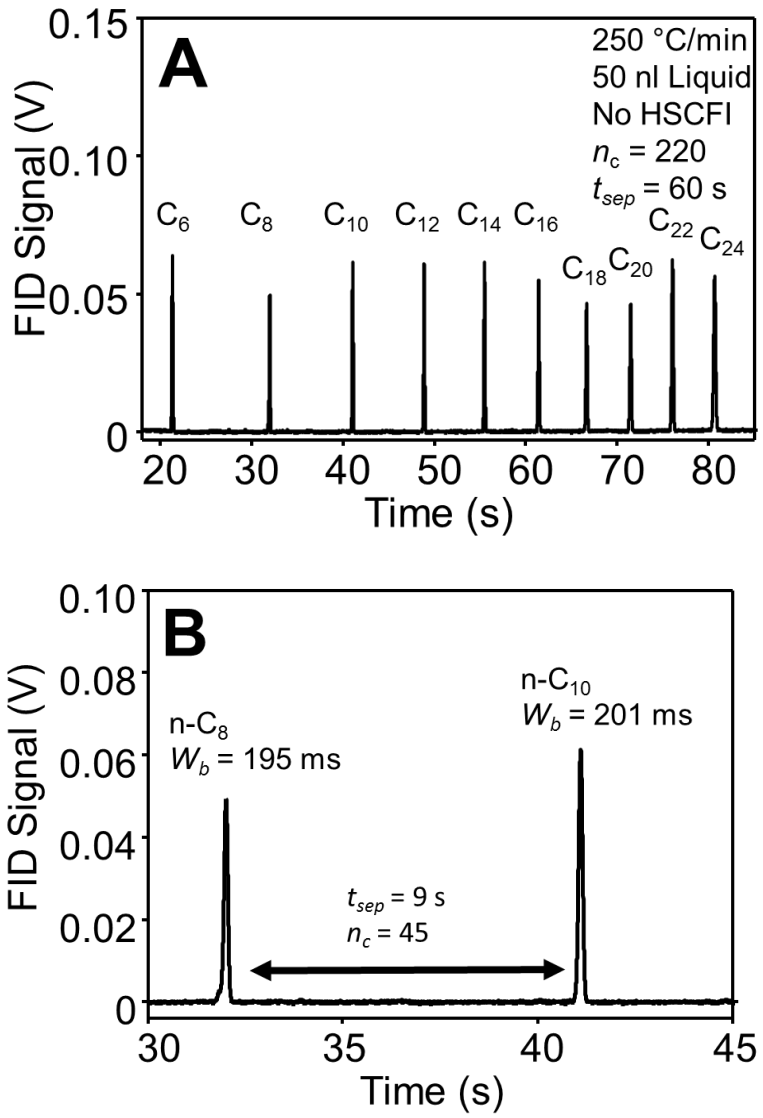

Figure 2.7 (A) Chromatogram of a 10 component mixture of even numbered n-alkanes from hexane (n-C_6) to tetracosane (n-C_{24}). (B) Zoom of a region from (A) containing octane (n-C_8) and decane (n-C_{10}) demonstrating excellent chromatographic resolution between analytes

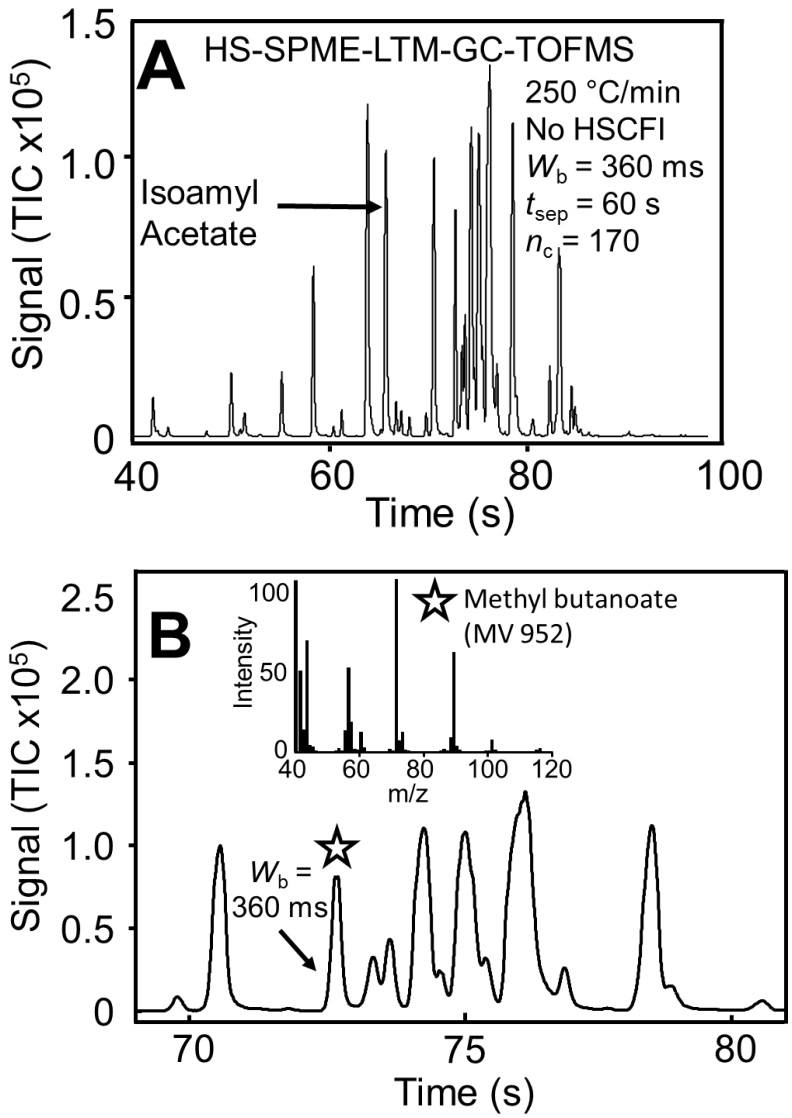

Figure 2.8 (A) Total ion current (TIC) chromatogram of the headspace of ripe banana peels using HS-SPME-LTM-GC-TOFMS. (B) Zoom in of a complex region from (A).

Chapter 3. Fast, high peak capacity separations in comprehensive two-dimensional gas chromatography with time-of-flight mass spectrometry[3]

3.1 Introduction

Comprehensive two-dimensional (2D) gas chromatography, GC × GC, pioneered by Phillips and co-workers in the early 1990s [1], is a popular technique for analyzing complex samples in a wide variety of fields (foods, fuels, metabolomics, etc.) [2–4], providing a powerful approach to increase peak capacity production of a GC instrument [5]. Beyond the pioneering efforts of a few research groups [6–10], relatively little effort has been applied to decrease separation times for thermal modulation based GC × GC, in part because of lengthy sample preparation procedures (i.e. derivatization and extraction) that may make fast separations superfluous and also in part due to the loss of peak capacity and resolution that is often associated with fast separation conditions. Recently, there has been renewed interest in applying fast GC × GC separations of even the most complex samples due to advances in sample preparation technology and automation (mainly automated headspace solid phase microextraction (SPME)) that have reduced sample preparation time [11] to the timeframe of fast GC × GC run times. The process of preparing a sample while the previous sample is being analyzed is critical to the application of fast GC × GC to automated SPME.

For GC × GC, two serially coupled separation columns with sufficiently orthogonal stationary phases are connected by a modulation interface. Effluent from the primary column is collected and injected onto the secondary column by the modulator. The ideal orthogonal peak capacity of a GC × GC instrument, $n_{c,2D}$, is the product of the peak capacities of each separation

[3] This chapter has been reproduced from: B.D. Fitz, R.B. Wilson, B.A. Parsons, J.C. Hoggard, R.E. Synovec, *Journal of Chromatography A* 1266 (2012) 116-123

dimension, ${}^{1}n_c$ x ${}^{2}n_c$. Since the total separation time of a one-dimensional (1D) GC analysis or a GC × GC analysis should be similar, the addition of the secondary column with GC × GC should in principle provide a significant improvement in peak capacity production relative to 1D-GC. However, peak broadening due to modulation (as expressed by metrics like the β-correction presented by Davis et al. [12] and the manner in which GC × GC is typically implemented result in effective peak capacity production rates that are far lower (eg., ~ 50 to 150 peaks/min) than what is theoretically possible, and as we will experimentally demonstrate, is achievable. For example, using a modulation period, P_M, of 2 s, with peak widths at base (4σ) of ~ 200 ms on the secondary column produces a peak capacity on the secondary column of 10. To achieve a modulation ratio, M_R, of ~ 2 to 4 (commonly applied in many GC × GC separations) would require peaks on the primary column of ~ 4 to 8 s (average of 6 s) wide at base (4σ). This would produce a peak capacity of 10 peaks on the primary column and gives a GC × GC peak capacity production of ~ 100 peaks/min [13, 14]. As a benchmark, at this typical GC × GC peak capacity production, for a primary column separation time of 1h, the orthogonal peak capacity will be ~ 6,000 peaks at unit resolution. One of the main obstacles to improving peak capacity production is that thermal modulator technology puts a lower limit on the P_M (generally 1 to 2 s, depending on modulator design [1]), which for a minimum M_R of ~ 2 to 4, in turn dictates a lower limit on the width of the primary column peaks (2 to 6 s) [5]. Simultaneously, the techniques typically utilized for primary injection (split/split-less, on column, headspace SPME, etc.) combined with the column dimensions and separation conditions commonly applied to primary columns produce peaks ~ 4 to 10 s wide, obscuring the potential for improved peak capacity production and analysis throughput even if P_M limitations were absent.

In order to experimentally address the challenges of optimizing GC × GC peak capacity, we must critically evaluate and improve the detected peak widths for both separation dimensions. Detected peak widths are the result of two distinct types of contributions: those due to the separation processes (i.e., longitudinal diffusion, mass transfer, carrier gas flow rate, referred to herein as on-column processes) and those due to non-separation processes (referred to as off-column herein). Off-column peak broadening is generally addressed through improving instrumentation (minimizing broadening due to injection, detection, electronics, dead volumes, etc.), while on-column broadening is minimized by applying band broadening theory to determine optimal pressure and flow conditions for the appropriate column dimensions and oven temperature programming conditions.

To put our research effort into context, we note a small number of recently reported studies of fast GC × GC systems using thermal modulators. First, the work of Junge, et al. [7] which utilized a longitudinal modulation cryogenic system (LMCS) with a 5 m × 100 μm inner diameter (i.d.) primary column and a 0.3 m × 50 μm i.d. secondary column to separate a 25 component mixture in 5 min (4 min separation window). The separation utilized the smallest possible P_M achievable with the LMCS, 1 s, and produced primary column peak widths of 1.2 s and secondary column peak widths of 50 ms (4σ peak widths in each case, equal to 1.7 times the full width at half maximum (FWHM)), for a theoretical orthogonal peak capacity of 2800 and a peak capacity production of 560 peaks/min. Second, the work of Hoggard, et al. [4] which utilized the LECO thermal modulator with a 9.5 m × 250 μm i.d. primary column and a 0.8 m × 180 μm i.d. secondary column to separate a 32 component mixture in 4.5 min (4.2 min separation window). This separation utilized the shortest reported P_M previously reported with the stock LECO thermal modulator, at 250 ms, and produced primary column peak widths of 2 s

and secondary column peak widths of 50 ms, for a theoretical peak capacity of 630 and a peak capacity production of 140 peaks/min. In addition to thermal modulation based GC × GC, the use of valves for modulation emerged in the mid 1990's [17]. Valve based GC × GC typically uses faster modulation periods than thermal modulation due to the fast actuation ability of diaphragm valves. The use of narrow columns, high flows, and fast modulation periods allows for fast, high peak capacity separations [18-20].

Since one common cause of wide peaks (and thus reduced peak capacity and peak capacity production) is off-column broadening due to injection, a wide variety of techniques for producing a narrow injection pulse, ranging from fluid logic gates to single and dual high-speed diaphragm valves have been reported [21-25]. The most easily implemented (and most common) technique for generating narrow injection pulses is the use of high inlet flows and large split ratios in the stock GC inlet. While this approach is capable of producing peaks as narrow as 100 ms [26], it does discard much of the injected sample, thereby raising detection limits and reducing the possible amount of information provided by a given separation. Conversely, thermal injection systems capable of transferring the entire sample to the separation column and producing narrow peaks have been reported previously [27-29]. Recent work in our lab has led to the implementation of high-speed cryo-focusing injection (HSCFI), capable of producing peaks ranging from 7 to 300 ms FWHM in a GC separation [16]. In principle, if HSCFI is applied to the primary column in a GC × GC separation, it should result in narrow peaks and high peak capacity production rates, as we demonstrate in this report.

The secondary column of a GC × GC separation is capable of producing narrow peak widths (~ 30 ms to 200 ms) depending upon the P_M and other separation conditions, placing large demands on the detector design and data acquisition rate. For the analysis of very complex

samples, the added selectivity and dimensionality of mass spectral data is useful (and often necessary) for the application of mathematical deconvolution algorithms and higher order chemometric techniques. Indeed, the non-mass-scanning nature of time-of-flight mass spectrometry (TOFMS) is well-suited for the detection of narrow GC × GC peaks because it is able to collect a complete mass spectrum in as little as 100 μs [26]. Additionally, TOFMS also does not suffer from the skew problems associated with scanning instruments, making post run data analysis less problematic.

In this report, we apply a novel combination of column dimensions, optimized separation conditions [15] and thermal injection via HSCFI onto the primary column [16] with a commercially available Agilent 6890 GC – LECO Pegasus III GC × GC – TOFMS instrument. Thermal injection with the HSCFI provides a state-of-the-art cold trap injection and minimizes off-column band broadening thereby maximizing the peak capacity generated by the primary column. This state-of-the-art GC × GC – TOFMS instrument will provide a total orthogonal peak capacity of ~ 6,000 in ~ 6 min which is a ~ 10-fold improvement in peak capacity production (1000 peaks/min vs. 100 peaks/min produced by traditional GC × GC). This goal will be facilitated by experimentally achieving narrow primary column peak widths (~ 600 ms FWHM), combined with very narrow secondary column peak widths (~20 ms FWHM) with TOFMS detection at 500 spectra/s.

The performance of this GC × GC – TOFMS instrumental design was initially evaluated using a 28 component liquid test mixture to study the interrelationship between M_R, P_M, and both the ideal and β-corrected total orthogonal peak capacities. As P_M increases (and M_R decreases), the effective first dimension peak width increases via β causing a decrease in the theoretical orthogonal primary column separation peak capacity. This is offset by an increase in the peak

capacity in the second dimension due to the increase in P_M. The analyst must carefully balance undersampling on the first dimension, as it will reduce the resolution of adjacent peaks and subsequently reduce peak capacity. If the peaks are not resolved, they may become mass spectrally interfered and quantification may become problematic. A goal for optimization would be to select the P_M to maintain sufficient quantitative precision while still maintaining a large total orthogonal peak capacity in a sufficiently short first dimension separation time for high throughput analysis. Several P_M were studied, with results for 250 ms, 500 ms, and 2 s shown for brevity, as we focus primarily on providing a large total orthogonal peak capacity, since the quantitativeness of GC × GC has been the subject of prior reports [14, 30-32]. Finally, a fast GC × GC – TOFMS separation is provided for two complex gaseous samples, a 65 component volatile organic compound (VOC) mixture and the headspace of a ground coffee sample, to show the necessity and benefit of the separation power and selectivity generated by this instrument.

3.2 Experimental

3.2.1 Chemicals and Samples

All chemicals (unless otherwise noted) were reagent grade or higher and purchased from Sigma-Aldrich (St. Louis, MO, USA). Benzene was purchased from Fischer Scientific (Pittsburgh, PA, USA); methyl decanoate was purchased from Eastman (Kingsport, TN, USA); xylenes were purchased from Mallinckrodt (St. Louis, MO, USA); chlorobenzene was purchased from Alfa (Danvers, MA, USA). The liquid test mixture (consisting of 28 compounds listed in order of elution on the primary column with boiling points in Table 3.1) was made by mixing equal masses (~ 100 mg) of the neat compounds. A standard mixture nominally containing 65 of the 104 VOCs listed in EPA method TO-15 at a concentration of ~ 1 ppm in nitrogen gas (Spectra Gases, Branchburg, NJ) was used as a gaseous test mixture to demonstrate the thermal

injection with the HSCFI [16]. The VOCs contained in this gaseous test mixture are listed, along with their most selective and sensitive mass channels in Table 3.2. The coffee sample obtained locally, was coarsely ground and heated to 60 °C for 20 min prior to headspace sampling. Ultra high purity helium (Grade 5, 99.999%) was used as the carrier gas (Praxair, Seattle, WA, USA).

3.2.2 Instrumentation

All chromatograms were obtained using the modified GC × GC – TOFMS depicted in Figure 3.1A, consisting of an Agilent 6890N GC (Agilent Technologies, Palo Alto, CA, USA), a thermal modulator (4D upgrade, LECO, St. Joseph, MI, USA), a Pegasus III TOFMS (LECO, St. Joseph, MI, USA) and a thermal injection system comprised of the inlet and the HSCFI as described previously [16]. To briefly review, for these studies, the sample is manually injected by a microsyringe (40 nl of a 0.5 µl microsyringe for liquid samples, 500 µl gas tight syringe for vapor samples), flash vaporized in the inlet, and transported via ~ 20 cm of deactivated fused silica transfer capillary line (Restek, Bellefonte, PA, USA) to the MXT trap column of the HSCFI, where it is cryo-focused by a constant flow of nitrogen that has been cooled in a liquid nitrogen heat exchanger. Ideally, all of the sample is trapped in a band significantly narrower than what would have been produced with a manual or auto-injection [16]. Any broadening that occurs prior to the trap is negated by the cryo-trap. A specified time after injection (referred to as the cryo-focusing time) an electrical pulse is applied to the MXT column via an in-house built circuit board, DC power supply, and a LabVIEW program (National Instruments, Austin, TX, USA), causing the sample to be re-vaporized onto the head of the primary separation column. Figure 3.1B schematically depicts the thermal injection with the HSCFI, which consists of a short section of MXT column, (Restek, Bellefonte, PA, USA) ~ 6 cm long, passing perpendicularly through a Teflon tube with an inside diameter of 1 mm. Electrical contact is

achieved by clamping the MXT column between a thick copper lead and a thin flexible sheet of copper; the copper lead is connected to the HCSFI circuit by copper wire. The i.d. of all tubing (both transfer capillary line and MXT) was matched to the i.d. of the primary separation column. Connections between the transfer lines and the HSCFI and the primary separation column were made using zero dead volume internal unions (Valco Instrument Co. Inc. Houston, TX, USA). Post-run data processing (baseline correction, *m/z* selection, etc.) was performed in Matlab R2010b (The Mathworks, Inc., Natick, MA, USA).

3.2.3 Chromatographic Conditions

A GC × GC column arrangement of nonpolar (20 m × 100 µm i.d. × 0.4 µm RTX-5 (Restek, Bellefonte, PA, USA)) to polar (1.8 m × 100 µm i.d. × 0.1 µm RTX-200 (Restek, Bellefonte, PA, USA)) was implemented with the thicker film of the primary column providing sufficient column loading capacity while not appreciably broadening the peaks due to mass transfer in and out of the stationary phase [15]. Compared to the commonly used 250 µm i.d. primary column with a 0.25 µm phase thickness, the use of a 100 µm i.d. primary column with a 0.4 µm film thickness results in only a 36% decrease in column capacity per unit length. A 40 nl injection utilizing a 0.5 µl microsyringe was used to manually introduce the 28 component liquid test mixture to the HSCFI via a split-less inlet. The coffee bean headspace was sampled via two 500 µl aliquots from a 500 µl gas tight syringe and manually injected to the HSCFI through a split-less inlet. The VOC gas sample based on the TO-15 method was injected via four 500 µl aliquots from the gas tight syringe. During cryo-focusing time and thermal injection, the primary column was held at 40 °C and the secondary column at 50 °C. For clarity, HSCFI conditions for each separation are included in the text. The primary and secondary columns were held at 40 °C and 50 °C for the first 30 s after thermal injection to provide an initial hold time approximately

equal to the dead time of this column configuration. Both columns then followed a temperature program that ramped at a rate of 30 °C/min to a final temperature on the primary column of 250 °C (260 °C secondary column). The inlet was maintained at a temperature of 280 °C. The modulator temperature was maintained 70 °C higher than the temperature of the primary column. The transfer line was held at 280 °C and the TOFMS ion source at 250 °C. Mass channels 35 to 334 *m/z* were collected and stored at a rate of 500 spectra/s. An absolute column head pressure of 1,140 kPa (165 psia) was maintained at the column head throughout the run using an upgraded high pressure inlet and pneumatic control module (Agilent Technologies, Palo Alto, CA, USA). As described previously [15], the long, narrow column (20 m × 100 μm i.d.) applied in this report requires high pressure to achieve the desired flow rate. The standard pressure regulator is only capable of controlling the absolute pressure from 100 kPa to 790 kPa and is unable to produce the flow rate desired.

3.3 Results and Discussion

To characterize the performance of the modified GC × GC – TOFMS instrument, a liquid mixture of 28 compounds was utilized with a wide range of boiling points and polarities (see Table 3.1). The test mixture was used to evaluate the retention factor, *k*, range on the secondary column, to calculate the dead time produced by the column configuration in order to determine wrap around, and then ultimately to calculate the 2D peak capacity and peak capacity production. Figure 3.2A is the total ion current (TIC) of the test mixture using a 2 s P_M to evaluate temperature and flow conditions required to take advantage of retention wrap around. At this stage, we were seeking to understand how to fully use the secondary column time window, i.e., the full P_M, concurrent with providing narrow peak widths to achieve a high secondary column peak capacity, ${}^2n_c$. For thermal injection onto the primary column, a cryo-focusing time of 60 s

was used with a 10 V electrical pulse lasting for 75 ms to desorb the sample. The first analyte peak elutes at ~ 0.5 min from the primary column and 0.9 s from the secondary column; both values are consistent with modeling results from LECO's GC × GC Column Calculator software. Under the separation conditions applied, the most retained analytes on the secondary column elute in slightly less than 1.5 s, so the time window of the secondary column eluting peaks is ~ 500 ms. Thus, we achieved a narrow *k* range on the secondary column (~ 0 to 0.7) in a ~ 500 ms window, and concurrently, narrow and nearly constant peak widths as well. Specifically, a slightly higher separation temperature on the secondary column was applied than is typical (concurrent with an appropriate column length and i.d.) to produce a narrow *k* range in a useful time window, which minimized the peak widths and maximized the theoretical peak capacity produced for the second dimension. Indeed, with the column configuration and separation conditions implemented, there is little detriment to wrap around (see Figures 3.2B and C) for the 500 ms and 250 ms, respectively). It should be noted that the y-axis on Figures 3.2B and C is the relative retention time on the secondary column. The apparent position of the analytes shifts when the modulation period is reduced due to wrap around, but is not detrimental to the separation. The shorter P_M improves the use of the 2D separation space and highlights the narrow peaks being generated on the secondary column. Contours for each peak were chosen such that the outer most contour represents peak width at the base (4σ) for the majority of the peaks and shows second dimension peaks are ~ 20 ms on average at FWHM. This choice of initial base contour level does mean some of the less intense peaks eluting between 0.5 min and 2 min are not visible in Figures 3.2B and 3.2C. With regard to the wrap around effect, using a P_M of 500 ms (Figure 3.2B), all of the secondary column eluting peaks fit readily in a single P_M, and have wrapped around about two times, while fully using the P_M time window. It is also worth

mentioning that even though the 2D separation space is not completely utilized for this particular test mixture with the 500 ms P_M, subsequent samples (and their separations) reported herein will demonstrate good usage of the 2D separation space. In contrast, for this particular 28 component liquid test mixture, the GC × GC – TOFMS separation using a 250 ms P_M, presented in Figure 3.2C, shows better use of the entire peak capacity.

For the purpose of ultimately calculating GC × GC peak capacities for the 500 ms and 250 ms P_M, we needed to measure the primary column peak widths in a way that was not impacted by the β undersampling effect, but still representative of other potential extra-column band broadening effects that may be introduced by the thermal modulator during a GC × GC separation. A goal of this experiment was to put an upper limit on the true "fully sampled" primary column peak widths produced when the instrument was run in the GC × GC mode. For this purpose, the 28 component test mixture was run with the same GC × GC column arrangement (20 m × 100 μm i.d. column coupled to a 1.8 m × 100 μm i.d. column), however the modulator was disabled so the separation was a true 1D analysis with a 21.8 m × 100 μm i.d. column. The secondary oven and modulator block were kept at a high temperature (250 °C) throughout the entire run. The high temperature of the secondary oven ensured that no (or very limited) retention occurred on the secondary column so any additional broadening of the peak was minimal and the detected peak width was primarily indicative of the primary column peak width. Figure 3.3A shows the 1D chromatogram of the test mixture run as described. Figure 3.3B shows a detail of the chromatogram near 3.5 min and highlights the narrow, well resolved peaks (~ 600 ms FWHM on average, width indicated for ethylbenzene as example). Hence, the primary column peak widths at base (4σ = 1.7 x FWHM) were taken as ~ 1.0 s; the corresponding

primary column peak capacity, ${}^{1}n_c$, was ~ 400 in the ~ 7 min primary column separation (with a ~ 6.5 min separation time window).

To highlight the performance of the thermal modulator running at P_M of 250 ms and 500 ms, the 2D data was viewed unfolded in a 1D format. Figures 3.4A-D show the unfolded data of a representative region of the 2D separation, containing chlorobenzene, ethylbenzene and p-xylene. Figures 3.4A and B are from the 250 ms P_M separation and Figures 3.4C and D are from the 500 ms P_M. Figure 3.4 A and C highlight the necessity of using a short P_M for adequate sampling of the peaks eluting from the primary column. Even with the fast P_M of 500 ms, the modulator only captures ~ 2 modulations across the peak. For these narrow primary column peaks with a FWHM of only ~ 600 ms (a 4σ peak width at base of ~ 1 s) this corresponds to a M_R of ~ 2. Concurrently, the peaks average ~ 20 ms FWHM (34 ms at base width) on the secondary column in both separations (see Figures 3.4B and D), which yields a theoretical peak capacity, ${}^{2}n_c$, on the secondary column of 15 for a 500 ms P_M, and a ${}^{2}n_c$ of 7.5 for a 250 ms P_M. Note that due to the separation conditions designed and implemented, the peak widths on the secondary column were nearly constant over the small k range applied. According to theory presented by Davis, et. al. [12], a M_R of 2 using a P_M of 500 ms will result in a 36% reduction in the theoretical 2D peak capacity, $n_{c,2D}$ via β-correction for undersampling. None the less and impressively, the ~ 7 min primary column separation (with a ~ 6.5 min separation time window), using a 500 ms P_M has an ideal orthogonal peak capacity $n_{c,2D}$ of ~ 6000 peaks, where $n_{c,2D} = {}^{1}n_c \times {}^{2}n_c$, or 4400 when β-corrected, or $n_{c,2D}/\beta$. On the other hand, the separation utilizing the P_M of 250 ms captures 5 to 6 modulations across the analyte peak which provides a M_R greater than 4. Using a 250 ms P_M, an ideal orthogonal peak capacity of ~ 3000 peaks is achieved (or a β-corrected orthogonal peak capacity of 2600). To summarize, a 1.7-fold increase in $n_{c,2D}$ was

achieved when P_M was doubled from 250 ms to 500 ms; the effective $n_{c,2D}$ was not doubled as one might initially suspect, due to β-correction.

The next study was to evaluate the modified GC × GC – TOFMS instrument for the analysis of gaseous samples. Two gaseous samples were studied: a 65 component VOC mixture and the headspace of ground coffee beans. A mixture of 65 VOCs was chosen as a sample representative of several different chemical classes and to demonstrate the capability of GC × GC to separate a gas phase sample in a single fast analysis. The VOC vapor sample was manually introduced for thermal injection via four successive 500 µl aliquots from a 500 µl gas tight syringe to a split-less inlet. A cryo-focusing time of 60 s was used prior to desorbing sample with an 11 V electrical pulse lasting for 100 ms. Figure 3.5A is the analytical ion chromatogram (AIC) resulting from summing the mass channels for the VOC mixture listed in Table 3.2. The primary column separation window is just over 4.5 min, while the secondary column separation window utilizes the majority of the 500 ms P_M. The separation power of the modified GC × GC – TOFMS instrument is highlighted in Figure 3.5B, which details the separation of dichlorobenzene and trimethylbenzene isomers (enclosed in the box in Figure 3.5A). The mass spectra for each of these analyte peaks in Figure 3.5B are provided in Figure 3.5C, indicating that the chromatographic selectivity is needed for separating the isomers, since the mass spectra are too similar. The spectra for analytes 1, 2, and 3 (trimethylbenzene isomers) are shown on the left of Figure 3.5C and analytes 4, 5, and 6 (dichlorobenzene isomers) are shown on the right. Within the two groups of isomers (analytes 1 – 3, and analytes 3 – 6) the mass spectra are nearly identical. This separation power for the GC × GC is the result of several factors: the narrow injection bandwidth provided by thermal injection (via HSCFI), the application of nearly optimized conditions for the primary column, as detailed in previous reports [15, 16], and

excellent separation conditions on the secondary column providing narrow peak widths. Without the narrow peaks generated on the primary column it is unlikely that the first two isomers in each grouping would have been resolved in this fast analysis as there is little to no difference in retention on the second dimension. Similarly, Figure 3.5A has several regions (in particular the separation window on the primary column from 2 min to 3 min) in which the narrow peaks provided by the primary column (~ 600 ms FWHM) are not adequate to resolve all the analytes but the added second dimension separates them completely. In these situations the stationary phase of the secondary column is crucial to resolving the analytes. The unique position of each analyte in 2D space strongly supports the potential of fast GC × GC - TOFMS for separation and identification of analytes in this example.

To demonstrate the applicability of fast GC × GC - TOFMS to the analysis of a 'real world' complex sample, the technique was applied to the headspace vapor of ground coffee. Separation conditions were the same as those applied to the VOC test mixture, however the separation window was shorter than that of the VOC test mix. The TIC of this separation is shown in Figure 3.6 and demonstrates the large number of analytes present in the sample. Several of the more intense peaks appear to have unusually large peak widths, but this is an artifact of selecting a minimum contour that is lower than ~ 10% of the height of the larger intensity peaks, but is necessary to make the less intense peaks visible in the plot. Peak widths for the coffee vapor head space separation are comparable to those measured in both the liquid and VOC test mixture analysis above. Also note that peak capacity production obtained for the separations in Figures 3.5 and 3.6 for the vapor samples were essentially the same as for the liquid test mixture (Figures 3.2, 3.3, and 3.4).

3.4 Conclusion

In this report, we have demonstrated that thermal injection onto the primary column and using a commercial modulator along with optimized column dimensions and experimental separation conditions for the Agilent 6890 GC – LECO Pegasus III TOFMS leads to a highly efficient instrument for the analysis of complex samples. It is shown that the thermal modulator is capable of producing peaks ~ 20 ms FWHM on a 1.8 m × 100 µm i.d. secondary column even while running at a fast P_M, e.g. 250 ms and 500 ms. The resulting fast GC × GC separations of complex samples contained narrow primary column peaks (~ 600 ms FWHM) giving a peak capacity production of ~ 1000 peaks/min and a total peak capacity production of ~ 6000 peaks for a ~ 6 min run time which is nearly an order of magnitude better than current GC × GC applications (typically ~ 6000 peaks in 60 minutes).

3.5 List of Works Cited

[1] Z. Liu, J.B. Phillips, Comprehensive Two-Dimensional Gas Chromatography using an On-Column Thermal Modulator Interface, *Journal of Chromatographic Science* 29 (1991) 227–231.

[2] E.M. Humston, K.M. Dombek, J.C. Hoggard, E.T. Young, R.E. Synovec, Time-Dependent Profiling of Metabolites from Snf1 Mutant and Wild Type Yeast Cells, *Analytical Chemistry* 80 (2008) 8002–8011.

[3] E.M. Humston, J.D. Knowles, A. McShea, R.E. Synovec, Quantitative assessment of moisture damage for cacao bean quality using two-dimensional gas chromatography combined with time-of-flight mass spectrometry and chemometrics, *Journal of Chromatography A* 1217 (2010) 1963–1970.

[4] J.C. Hoggard, W.C. Siegler, R.E. Synovec, Toward automated peak resolution in complete GC × GC–TOFMS chromatograms by PARAFAC, *Journal of Chemometrics* 23 (2009) 421–431.

[5] L.M. Blumberg, F. David, M.S. Klee, P. Sandra, Comparison of one-dimensional and comprehensive two-dimensional separations by gas chromatography, *Journal of Chromatography A* 1188 (2008) 2–16.

[6] J. Harynuk, P.J. Marriott, Fast GC×GC with Short Primary Columns, *Analytical Chemistry* 78 (2006) 2028–2034.

[7] M. Junge, S. Bieri, H. Huegel, P.J. Marriott, Fast Comprehensive Two-Dimensional Gas Chromatography with Cryogenic Modulation, *Analytical Chemistry* 79 (2007) 4448–4454.

[8] L. Mondello, P.Q. Tranchida, A. Casilli, O. Favoino, P. Dugo, G. Dugo, Fast GC analysis with a 50 μm ID column: theory, practical aspects, and application to a highly complex sample, *Journal of Separation Science* 27 (2004) 1149-1156.
[9] P.Q. Tranchida, G. Purcaro, L. Conte, P. Dugo, G. Dugo, L. Mondello, Enhanced resolution comprehensive two-dimensional gas chromatography applied to the analysis of roasted coffee volatiles, *Journal of Chromatography A* 1216 (2009) 7301–7306.
[10] P.Q. Tranchida, G. Purcaro, C. Fanali, P. Dugo, G. Dugo, L. Mondello, Optimized use of a 50 μm ID secondary column in comprehensive two-dimensional gas chromatography–mass spectrometry, *Journal of Chromatography A* 1217 (2010) 4160–4166.
[11] S. Risticevic, Y. Chen, L. Kudlejova, R. Vatinno, B. Baltensperger, J.R. Stuff, et al., Protocol for the development of automated high-throughput SPME–GC methods for the analysis of volatile and semivolatile constituents in wine samples, *Nature Protocols* 5 (2010) 162–176.
[12] J.M. Davis, D.R. Stoll, P.W. Carr, Effect of First-Dimension Undersampling on Effective Peak Capacity in Comprehensive Two-Dimensional Separations, *Analytical Chemistry* 80 (2008) 461–473.
[13] W. Khummueng, P.J. Marriott, The Nomenclature of Comprehensive Two-Dimensional GasChromatography: Defining the Modulation Ratio (MR), *LC-GC Europe* 22(1) (2009) 38-45
[14] W. Khummueng, J. Harynuk, P.J. Marriott, Modulation Ratio in Comprehensive Two dimensional Gas Chromatography, *Analytical Chemistry* 78 (2006) 4578–4587.
[15] R.B. Wilson, J.C. Hoggard, R.E. Synovec, Fast, High Peak Capacity Separations in Gas Chromatography–Time-of-Flight Mass Spectrometry, *Analytical Chemistry* 84 (2012) 4167–4173.
[16] R.B. Wilson, B.D. Fitz, B.C. Mannion, T. Lai, R.K. Olund, J.C. Hoggard, et al., High-speed cryo-focusing injection for gas chromatography: Reduction of injection band broadening with concentration enrichment, *Talanta* 97 (2012) 9–15.
[17] C.A. Bruckner, B.J. Prazen, R.E. Synovec, Comprehensive Two-Dimensional High-Speed Gas Chromatography with Chemometric Analysis, *Analytical Chemistry* 70 (1998) 2796–2804.
[18] A.E. Sinha, B.J. Prazen, C.G. Fraga, R.E. Synovec, Valve-based comprehensive two-dimensional gas chromatography with time-of-flight mass spectrometric detection: instrumentation and figures-of-merit, *Journal of Chromatography A* 1019 (2003) 79–87.
[19] J.V. Seeley, F. Kramp, C.J. Hicks, Comprehensive Two-Dimensional Gas Chromatography via Differential Flow Modulation, *Analytical Chemistry* 72 (2000) 4346–4352.
[20] R.B. Wilson, W.C. Siegler, J.C. Hoggard, J.S. Nadeau, R.E. Synovec, Achieving high peak capacity production for gas chromatography and comprehensive two-dimensional gas chromatography by minimizing off-column peak broadening, *Journal of Chromatography A* 1218 (2011) 2130-3139.
[21] G. Gaspar, P. Arpino, G. Guiochon, Study in High Speed Gas Chromatography I. Injections of Narrow Sample Plugs, *Journal of Chromatographic Science* 15 (1977) 256–261.
[22] R.L. Wade, S.P. Cram, Fluidic logic sampling and injection system for gas chromatography, *Analytical Chemistry* 44 (1972) 131–139.

[23] G.M. Gross, B.J. Prazen, J.W. Grate, R.E. Synovec, High-Speed Gas Chromatography Using Synchronized Dual-Valve Injection, *Analytical Chemistry* 76 (2004) 3517–3524.
[24] V.R. Reid, A.D. McBrady, R.E. Synovec, Investigation of high-speed gas chromatography using synchronized dual-valve injection and resistively heated temperature programming, *Journal of Chromatography A* 1148 (2007) 236–243.
[25] J.L. Hope, K.J. Johnson, M.A. Cavelti, B.J. Prazen, J.W. Grate, R.E. Synovec, High-speed gas chromatographic separations with diaphragm valve-based injection and chemometric analysis as a gas chromatographic "sensor," *Analytica Chimica Acta* 490 (2003) 223–230.
[26] H. Wollnik, R. Becker, H. Götz, A. Kraft, H. Jung, C.-C. Chen, et al., A high-speed gas chromatograph coupled to a time-of-flight mass analyzer, *International Journal of Mass Spectrometry and Ion Processes* 130 (1994) L7–L11.
[27] A. Van Es, J. Janssen, C. Cramers, J. Rijks, Sample enrichment in high speed narrow bore capillary gas chromatography, *Journal of High Resolution Chromatography* 11 (1988) 852–857.
[28] B.A. Ewels, R.D. Sacks, Electrically-heated cold trap inlet system for high-speed gas chromatography, *Analytical Chemistry* 57 (1985) 2774–2779.
[29] Z. Liu, J.B. Phillips, High-speed gas chromatography using an on-column thermal desorption modulator, *Journal of Microcolumn Separations* 1 (1989) 249–256.
[30] D.F. Thekkudan, S.C. Rutan, P.W. Carr, A study of the precision and accuracy of peak quantification in comprehensive two-dimensional liquid chromatography in time, *Journal of Chromatography A* 1217 (2010) 4313–4327.
[31] J.V. Seeley, Theoretical study of incomplete sampling of the first dimension in comprehensive two-dimensional chromatography, *Journal of Chromatography A* 962 (2002) 21–27.
[32] J.V. Seeley, N.J. Micyus, S.V. Bandurski, S.K. Seeley, J.D. McCurry, Microfluidic Deans Switch for Comprehensive Two-Dimensional Gas Chromatography, *Analytical Chemistry* 79 (2007) 1840–1847.

3.6 Tables

Table 3.1 Twenty-eight compounds included in the liquid test mixture, listed in order of elution on the primary column, with the retention time on the primary and secondary column of the 2.0 s P_M separation (Figure 3.2A).

	Compound	Boiling Point (°C)	Column 1 Retention Time (s)	Column 2 Retention Time (s)
1	ethyl formate†	54	23	1.13
2	n-hexane	69	59	1.04
3	benzene	80	125	1.09
4	2-pentanone	102	133	1.23
5	n-heptane	98	137	1.06
6	1-heptyne	100	149	1.09
7	toluene	111	173	1.14
8	3-hexanone	128	177	1.23
9	octane	126	183	1.10
10	chlorobenzene	152	209	1.18
11	ethylbenzene	136	215	1.17
12	p-xylene	139	219	1.17
13	2-heptanone	151	223	1.28
14	o-xylene, m-xylene	139	229	1.19
15	methyl caproate	168	237	1.23
16	propylbenzene	159	255	1.20
17	3-octanone	167	263	1.28
18	decane	174	267	1.17
19	isobutylbenzene	170	277	1.21
20	butylbenzene	183	297	1.22
21	2-nonanone	194	305	1.32
22	2-decanone	209	341	1.34
23	dodecane	216	341	1.23
24	naphthalene	218	353	1.31
25	2-undecanone	231	375	1.36
26	methyl decanoate	224	383	1.32
27	tetradecane	254	405	1.28
28	2-dodecanone	245	407	1.39

† Denotes analyte too low in intensity to appear in Figure 3.2A.

Table 3.2 Sixty-four compounds identified in VOC test mixture (nominally 65 compounds added) with the most sensitive and selective ion for each compound (used in AIC in Figure 3.5).

	Compound	Mass Channel (*m/z*)	Column 1 Retention Time (s)	Column 2 Retention Time (s)
1	propylene[b]	39	2.5	0.14
2	freon-12[b]	85	3	0.38
3	chloromethane[b]	52	6	0.40
4	freon-114[b]	85	6	0.16
5	vinyl chloride[b]	62	8.5	0.40
6	1,3-butadiene[b]	39	10	0.16
7	bromomethane[b]	94	15	0.40
8	chloroethane[b]	64	16.5	0.43
9	ethanol[b]	45	18	0.49
10	acrolein[b]	56	26	0.09
11	acetone	43	27.5	0.15
12	freon-11	101	25	0.21
13	isopropyl alcohol[b]	45	28.5	0.03
14	1,1-dichloroethene	96	36	0.26
15	freon-113	101	38	0.27
16	methylene chloride	49	41.5	0.02
17	carbon disulfide	76	44	0.47
18	trans-1,2-dichloroethene	61	53.5	0.05
19	methyl tert-butyl ether	73	55	0.07
20	1,1-dichloroethane	63	60	0.12
21	vinyl acetate[b]	86	63.5	0.40
22	methyl ethyl ketone	43	68	0.38
23	hexane	57	68	0.03
24	cis-1,2-dichloroethene	61	74.5	0.10
25	ethyl acetate	43	76.5	0.22
26	chloroform	83	79.5	0.07
27	tetrahydrofuran	42	85.5	0.15
28	1,1,1-trichloroethane	97	94.5	0.08
29	1,2-dichloroethane	62	96.5	0.10
30	benzene	78	104	0.08
31	carbon tetrachloride	117	104	0.03
32	cyclohexane[b]	56	104	0.03
33	1,2-dichloropropane	63	123.5	0.12
34	heptane	43	121	0.03

35	trichloroethylene	95	123.5	0.07
36	bromodichloromethane	83	127.5	0.06
37	1,4-dioxane	88	128	0.16
38	methyl methacrylate	69	128.5	0.14
39	methyl isobutyl ketone	43	144	0.25
40	cis-1,3-dichloropropene	75	145	0.11
41	trans-1,3-dichloropropene	75	145	0.11
42	toluene	91	161	0.11
43	1,1,2-trichloroethane	97	162	0.13
44	methyl butyl ketone	43	169.5	0.23
45	dibromochloromethane	129	177	0.15
46	1,2-dibromoethane	107	183.5	0.28
47	tetrachloroethylene	166	185	0.27
48	chlorobenzene	112	210.5	0.25
49	ethylbenzene	91	217.5	0.34
50	p-xylene	91	222	0.44
51	styrene[b]	104	231	0.31
52	bromoform	173	239	0.28
53	m-xylene	91	241.5	0.37
54	o-xylene[b]	91	241.5	0.37
55	1,1,2,2-tetrachloroethane	83	257.5	0.10
56	4-ethyltoluene	105	282	0.17
57	1,3,5-trimethylbenzene	105	283.5	0.17
58	1,2,4-trimethylbenzene	105	292.5	0.17
59	benzyl chloride	not found	not found	not found
60	1,3-dichlorobenzene	146	299	0.22
61	1,4-dichlorobenzene	146	301	0.22
62	1,2-dichlorobenzene	146	310	0.22
63[a]	1,2,4-trichlorobenzene	180	356	0.24
64[a]	naphthalene	128	360.5	0.26
65[a]	hexachloro-1,3-butadiene	225	367	0.22

[a] Analytes not included in the figure for clarity.
[b] Analytes too low in intensity to appear on Figure 3.5A but are visible when viewed using their respective selective mass channel. Retention times for the secondary column are the apparent retention times, since wrap around is occurring.

3.7 Figures

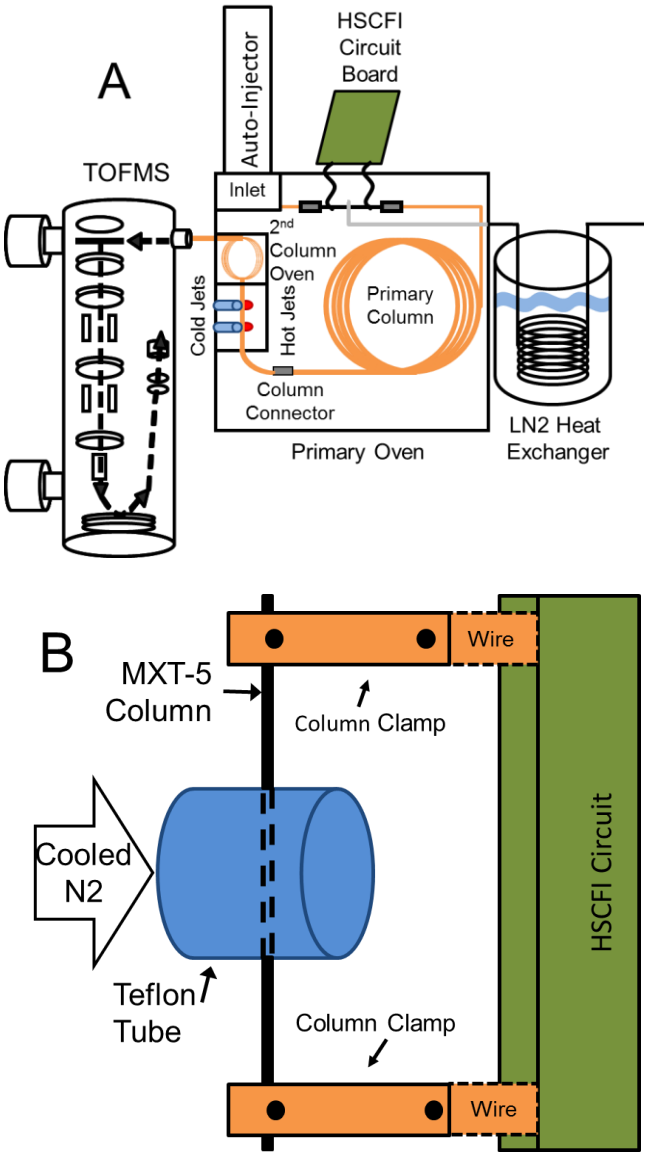

Figure 3.1 (A) Diagram of the modified GC × GC – TOFMS instrument with HSCFI for thermal injection (LECO GC × GC – TOFMS instrument with the commercially available thermal modulator). Cryofocusing of analytes in the MXT column of the HSCFI is achieved with a constant flow of cooled nitrogen delivered from a liquid nitrogen heat exchanger via sections of copper and Teflon tubing. Cryofocused analytes are reinjected by resistively heating the section of MXT column with a controlled capacitive discharge. The head of the separation column is attached to the HSCFI via a low dead volume internal union. (B) Diagram of the HSCFI, illustrating the orientation of the Teflon tube, MXT column and the HSCFI circuit. The MXT column and the Teflon tube are perpendicular to each other. Electrical contact between the circuit and MXT column is maintained by clamping the MXT column between a thin sheet of copper and a solid copper post. The post is connected to the circuit by thick, low resistance copper wires which are longer than depicted in (B), passing through the oven wall to the circuit located outside the oven as shown in (A).

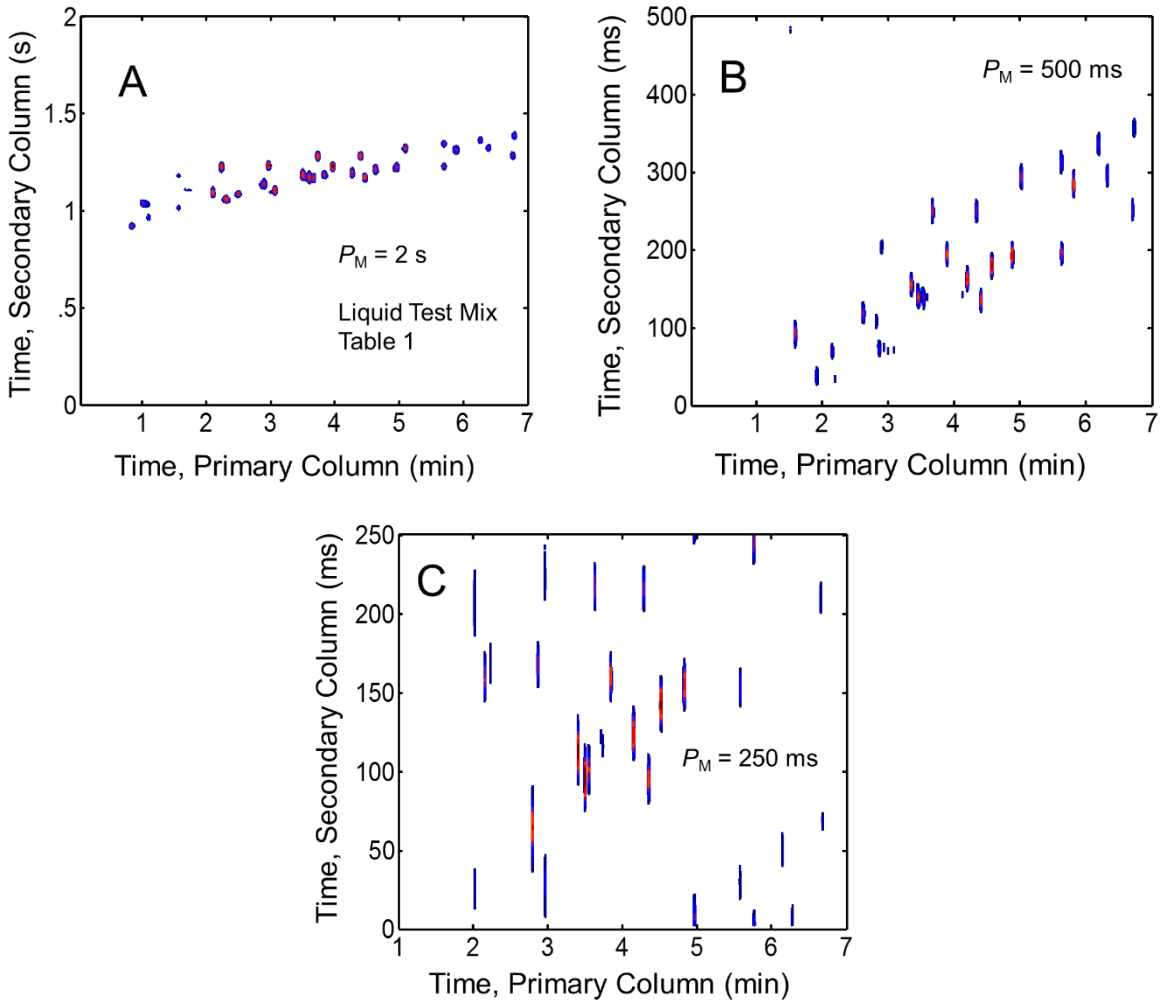

Figure 3.2 (A) GC × GC – TOFMS separation of the 28 component liquid test mixture using a 2 s P_M to determine the dead time and *k* range utilized on the secondary column. The separation window is ~6 min. The first analyte peak elutes from the primary column near 30 s, and ~0.9 s on the secondary column. The last analyte peak elutes from the primary column near 7 min, and slightly before 1.5 s on the secondary column. (B) Same separation conditions as in (A), but with a 500 ms P_M. (C) Same separation conditions as in (A), but with a 250 ms P_M. The P_M of 250 ms more fully utilized the 2D peak capacity for this sample.

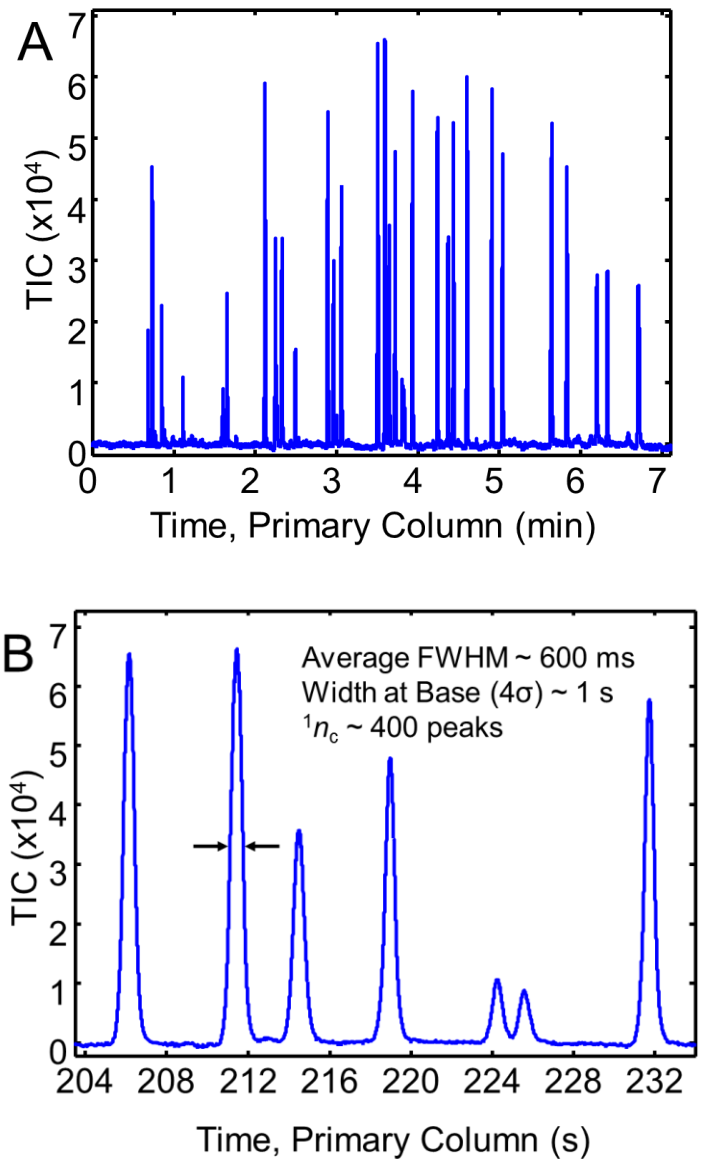

Figure 3.3 (A) One dimensional GC – TOFMS separation of the 28 component liquid test mixture using the same GC × GC – TOFMS instrumental platform as in Figure 3.2, but keeping the secondary oven and modulator block hot (250 °C) throughout the separation. The modulator was shut off as to not modulate the analyte peaks eluting from the primary column. This separation places an 'upper bound' on the primary dimension peak widths of ~600 ms FWHM. (B) Zoom in of a region of (A) near 3.5 minutes. The seven peaks are chlorobenzene, ethylbenzene, p-xylene, 2-heptanone, o-xylene/m-xylene, and methyl caproate. Peaks averaged ~600 ms FWHM.

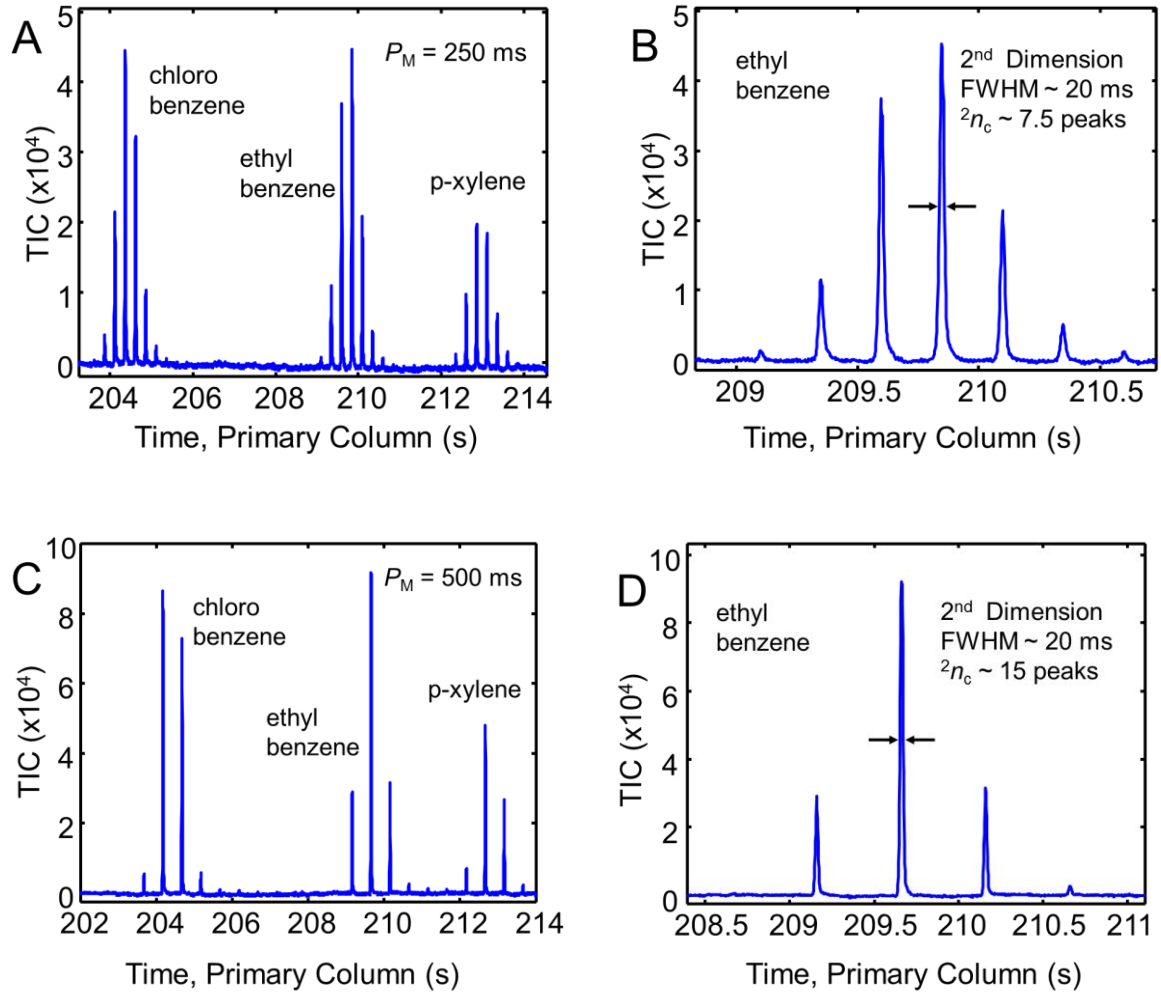

Figure 3.4 (A) Unfolded 2D data from a representative section of the GC × GC – TOFMS separation of the 28 component mixture shown in Figure 3.2(C), collected with a 250 ms P_M. The analyte peaks shown are chlorobenzene, ethylbenzene, and p-xylene. The secondary column peak widths are ~20 ms FWHM. The peaks are ~1s wide at the base on the primary column giving a M_R of ~4. (B) Zoom in of the second analyte, ethylbenzene in (A) highlighting the narrow peak widths produced on the second dimension (~20 ms FWHM). (C) Unfolded GC × GC data from the 2D separation of the 28 component mixture shown in Figure 3.2(B) with a 500 ms P_M. The longer P_M samples the peak fewer times, but overall provides an increased secondary column peak capacity compared to the 250 ms P_M. (D) Zoom in of the second analyte, ethylbenzene, in (C). The secondary column peaks for ethylbenzene are ~20 ms wide at FWHM. The peak is sampled essentially in-phase providing a M_R of ~ 2.

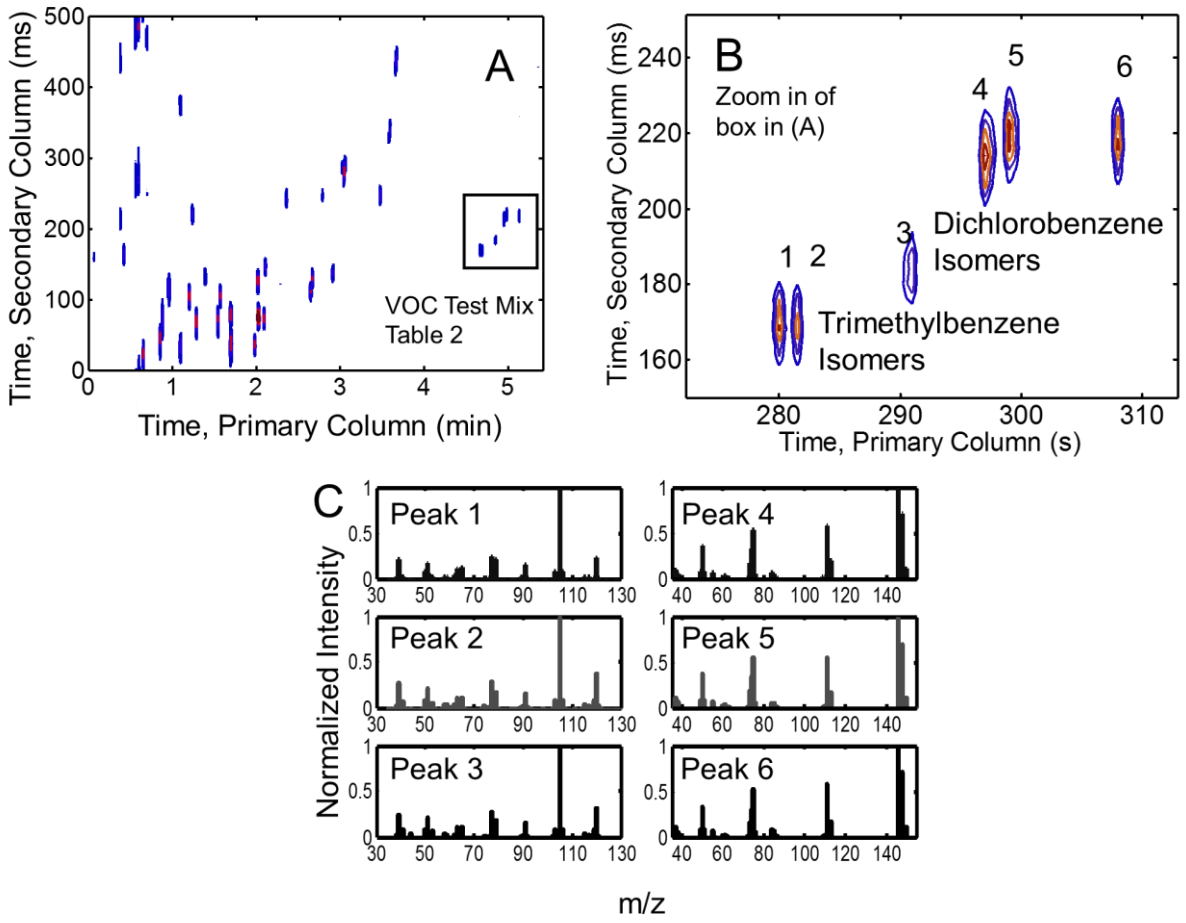

Figure 3.5 (A) GC × GC – TOFMS separation of the VOC text mixture (nominally 65 compounds) using the same separation conditions as in Figure 3.2 and a 500 ms P_M. Sample was introduced for HSCFI via four successive 500 µl aliquots from a 500 µl gas tight syringe to a split-less inlet. A cryo-focusing time of 60 s was used prior to desorbing sample with a 11 V electrical pulse lasting for 100 ms. Plot of analytical ion chromatogram (AIC is the sum of mass channels for each compound listed in Table 3.2) gives an overview of the separation. Some peaks may not be visible due to low relative concentration, but are visible when their selective *m/z* are plotted. (B) Detail view of the boxed area in (A), highlighting the separation of trimethylbenzene isomers and dichlorobenzene isomers. (C) Mass spectral data for each analyte peak in (B). The similarity of the mass spectra for each group of isomers demonstrates the need for chromatographic efficiency and selectivity to separate the isomers.

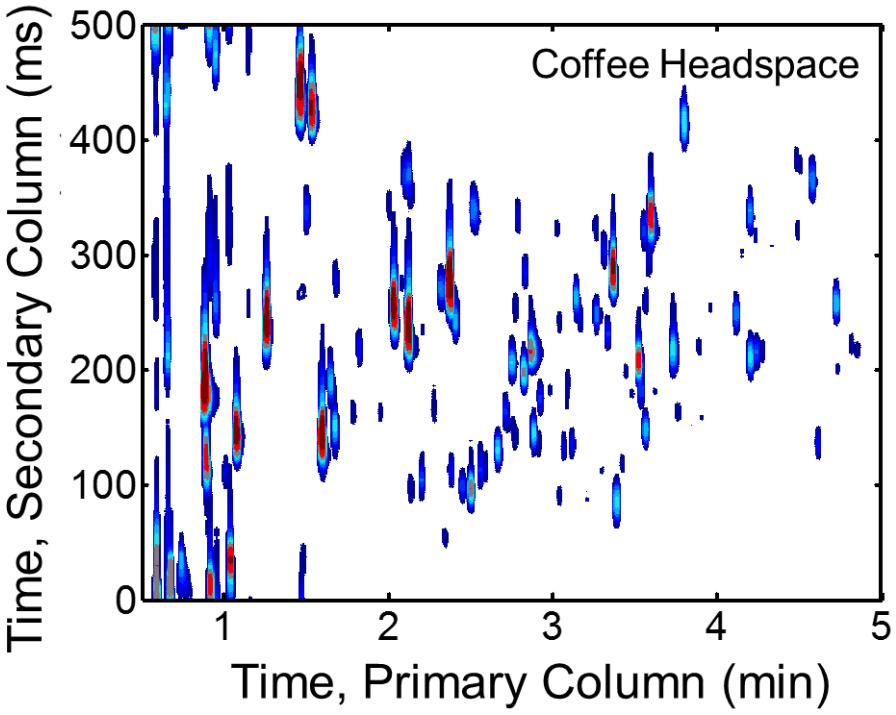

Figure 3.6 GC × GC – TOFMS separation of the headspace of ground coffee beans sampled via a gas tight syringe. The TIC signal plotted is for mass channels 50 to 335 *m/z*.

Chapter 4. Enhancing gas chromatography time-of-flight mass spectrometry data analysis using two-dimensional mass channel cluster plots[4]

4.1 Introduction

Gas chromatography - mass spectrometry (GC-MS) is a widely used instrumental platform for chemical analysis. GC is practiced in a wide range of fields, including metabolomics, food, petrochemical, environmental, and chemical weapon precursor analysis [1-4]. Many researchers have focused on increasing the resolving power of GC systems in order to separate as many compounds as possible in a given sample [5-10]. However, many samples are sufficiently complex that peak overlap inevitably occurs even with state-of-the-art instrumentation. When peak overlap becomes more severe, the ability to confidently identify and quantify the analytes of interest becomes increasingly more challenging.

The field of chemometrics specializes in the process of mathematically gleaning useful information from data collected from chemical measurements [11-13]. Researchers in this field have spent decades developing software approaches to address the many challenges that arise. The various approaches developed, which aim to deconvolute and quantify overlapped peaks, depend upon the dimensionality (or order) of the data. Common instrumental platforms that produce second order data, inherently two-dimensional (2D) for a single sample run, include comprehensive 2D chromatography (e.g. GC × GC and LC × LC), chromatography combined with spectral detection (GC-MS, LC-MS, LC-UV/vis absorbance), and so on. For GC-MS the data structure is second order or "bilinear," where each analyte response can be expressed as a matrix produced by taking the outer product of the chromatographic elution peak profile (a

[4] This chapter has been reproduced from: B.D. Fitz, B.C. Reaser, D.K. Pinkerton, J.C. Hoggard, K.J. Skogerboe, R.E. Synovec, *Analytical Chemistry* 86 (2014) 3973-3979

vector) with the mass spectrum (a vector). The bilinearity of the data structure makes GC-MS readily amenable to chemometric data analysis [14-16].

Time-of-flight mass spectrometry (TOFMS) is an excellent detector for GC, providing sensitive detection, a dynamic range spanning 4-6 orders of magnitude, and most importantly for the method introduced herein, an extremely high mass spectral collection rate [17]. The LECO Pegasus III TOFMS implemented in the method introduced herein can collect a wide mass channel range (*m/z* from 5 to 1000) at a frequency up to 500 Hz (although it is implemented herein at 100 Hz to provide a suitable data density). A fast scan rate can provide hundreds of spectra across a GC peak. Although collecting such a large number of spectra across a peak is not commonly practiced, we shall demonstrate a distinct advantage in doing so.

Often, GC-MS data is oversampled and then mathematically reduced (binned) to facilitate complex mathematical processing (retention time alignment, principal component analysis (PCA), or parallel factor analysis (PARAFAC)) [18, 19]. A rapid collection rate (and thus high data density) can produce data sets that are considered too large for an analyst to sift through manually, but provide the potential for vastly increased chemical information compared to more slowly sampled data. Herein, we report a novel algorithmic method that takes advantage of applying a rapid scan rate with GC-TOFMS to significantly facilitate separation visualization and analyte peak deconvolution. Chromatographic peak maxima (serving as the retention time, t_R) and the chromatographic peak width, *W*, are determined on a per *m/z* basis for each analyte peak. The peak *W* (per *m/z*) is then plotted against its respective t_R in a 2D format, producing a cluster of points, i.e., one point per peak *W* versus t_R per *m/z*. Analysis of GC-TOFMS data by this method produces what is referred to as a "2D *m/z* cluster plot." The method takes advantage of adjacent eluting (even co-eluting) peaks in a temperature programmed separation exhibiting

sufficient variation in peak *W* to provide chemical selectivity in the *W* dimension of the 2D *m/z* cluster plot. The goals of this novel approach are to improve the visualization of overlapped chromatographic peaks for GC-TOFMS, to aid in peak deconvolution at ultra-low chromatographic resolution, R_s, as well as to increase the effective peak capacity of GC-TOFMS separations. The method is evaluated using the LECO (Pegasus III) GC-TOFMS instrument. We demonstrate remarkable resolution of otherwise severely overlapped peaks in the original one-dimensional GC-TOFMS format. While the method is demonstrated using a TOFMS with unit mass resolution, in principle the method should be readily implemented with the emerging high resolution TOFMS.

4.2 Method Fundamentals

The rapid scan rate of the TOFMS provides a means to accurately measure t_R and *W* by collecting many data points across chromatographic peaks, so there is minimal peak variance due to undersampling [20]. A peak finding algorithm based on a moving window moves through the GC-TOFMS chromatograms (preprocessed as described in the Experimental section) and locates local peak maxima above a user specified signal threshold for each *m/z* collected. When a peak maximum is found, this location is taken as the t_R and is determined to the nearest 10 ms (using a spectral collection rate of 100 Hz). The peak *W* (width-at-half-height) at that t_R is then calculated. The algorithm applied interpolates between data points using a linear fit if there is no data point present for the exact value of half of the peak maximum signal. The *W* is then rounded to the nearest 10 ms, to provide the same precision as the t_R. For the remainder of this report, the term '*m/z*' refers to a peak of any mass channel (at unit mass resolution) that was initially detected by the peak finding algorithm, and then has passed the signal threshold, unless further clarification is provided. The processing of the data in this fashion converts the signal at each *m/z*

associated with a chromatographic peak to a single data point consisting of a t_R and *W*. All of the *m/z* are then plotted (*W* versus t_R) to produce a 2D *m/z* cluster plot (with chemical selectivity in both dimensions), since the points (one per each *m/z*) tend to produce a 2D cluster for a purely eluting analyte, since all *m/z* are selective. At a given *m/z*, the *W* of an analyte peak overlapped with an interfering analyte peak will be elevated and readily discernible relative to selective *m/z*. The method was further demonstrated to be readily coupled to chemometric analysis, with classical least squares (CLS) applied to demonstrate the basic principles involved.

4.3 Experimental

All chemicals used were reagent grade or higher. A liquid hydrocarbon mixture containing 73 analytes was created by mixing ~100 mg of the neat compounds. The mixture was a suitably complex sample requiring a typical GC temperature program for separation, producing naturally occurring overlapped peak situations. An aliquot of the mixture was diluted 1:100 with acetone prior to GC-TOFMS analysis. Table 4.1.S1 in the Supporting Information lists the chemicals, mass of compound added to the mixture, vendors, and boiling points of the analytes used in the mixture. Ultra high purity helium (Grade 5, 99.999%) was used as the carrier gas (Praxair, Seattle, WA, USA). GC-TOFMS data was collected using an Agilent 6890N GC (Agilent Technologies, Palo Alto, CA) with a LECO Pegasus III TOFMS (LECO, St. Joseph, MI). A 30 m x 250 µm inner diameter (i.d.) column with a 0.5 µm RTX-5 film was used (5% phenyl / 95% dimethyl polysiloxane, Restek, Bellefonte, PA). The column flow rate was 2.0 ml/min. The oven temperature began at 35 °C and held for 1.0 min. A temperature ramp of 33 °C/min was applied for a final temperature of 280 °C and held for 1.0 min. 0.1 µl of the diluted sample was injected to a split/split-less inlet operated with a 200:1 split ratio at 280 °C. The

TOFMS collected *m/z* 40-230 at 100 spectra/s, with a 100 s solvent delay and an ion source temperature of 250 °C.

Matlab R2012b (The Mathworks, Inc., Natick, MA, USA) was used to preprocess the raw GC-TOFMS data and to create the algorithm and GUI (Graphical User Interface) used in the 2D *m/z* cluster plot method. Preprocessing involved two steps to produce 2D *m/z* clusters with relatively narrow distributions in the two dimensions, W and t_R. First, raw GC-TOFMS chromatograms (signal versus time vector for each *m/z*) were independently baseline corrected. Next, a moving boxcar average was applied to each *m/z* signal vector (performed without a loss in the original number of data points) to smooth the data to reduce the distortion of the apices of each peak from the detected noise. A 31 point moving boxcar window was used, resulting in a ~ 5% decrease in peak height, and a ~ 5% increase in W. The ~ 5% increase in peak broadening was deemed acceptable, since smoothing facilitated a significant reduction in cluster size in the 2D *m/z* cluster plot, translating into a significant increase in the resolving power of the method. We note that other signal filters (such as Savitsky-Golay) could be implemented, and may warrant future investigation. For the separation studied, the algorithm (baseline correction, smoothing, peak finding, plotting) is completed in ~ 45 s with minimal user input.

PLS Toolbox version 7.3.1 (Eigenvector Research, Inc., Wenatchee, WA, USA) was used for performing classical least squares (CLS) deconvolution. A fast non-negative least squares ('fnnls') algorithm was applied, imposing a non-negativity constraint in both the modeled elution peak profiles and mass spectra based on an algorithm by Bro and de Jong [21]. All *m/z*, including those under the signal threshold, were included in the CLS deconvolution. An in-house written function to import the data from the instrumental '.peg' file to the Matlab workspace was used [22].

4.4 Results and Discussion

The 73-component mixture analyzed by GC-TOFMS created a data set amenable to the study of the 2D *m/z* cluster plot method. Figure 4.1A is the total ion current (TIC) chromatogram. The *W* range from ~ 0.6 s to 0.7 s. The arrow in Figure 4.1A indicates the region provided in detail in Figure 4.1B, a plot of five well-resolved analyte peaks selected to demonstrate the basic principles of the method: methyl hexanoate (MH), cyclooctane (CYO), 1-bromohexane (BH), bromobenzene (BB), and propylbenzene (PB), with superimposed peak signals per *m/z*. To help put the 2D *m/z* cluster plot method into perspective, the traditional 2D approach to plot the GC-TOFMS data is provided in Figure 4.1C, with the signal plotted at the corresponding *m/z* and separation run time. The data format in Figure 4.1C provides information about which *m/z* are present for a particular analyte and provides insight into how many analytes may be present in a particular region of a chromatogram. However, the traditional 2D plotting approach does not easily provide detailed information regarding which analyte peaks may be overlapped, or the extent of peak overlap, as we shall see is more readily provided using 2D *m/z* cluster plots.

The 2D *m/z* cluster plot method is illustrated in Figure 4.2A, for two *m/z* peaks of MH. Following baseline correction and boxcar smoothing described previously, for each analyte peak per *m/z*, the t_R (x-axis) and *W* (y-axis) are measured with 10 ms precision. The resulting t_R and *W* per *m/z* are plotted as a single point that occupies a 10 ms x 10 ms 2D square, with the center of the point indicated by a black circle. A signal threshold of 200 was applied, i.e., a signal-to-noise ratio (S/N) of ~ 30. At significantly lower S/N, the measured t_R and *W* become progressively erratic. Additionally, Figure 4.2B shows sections of stacked baseline noise at four representative *m/z*, adjusted vertically for clarity. The noise characteristics of the baseline signal at each *m/z* are

not correlated, giving rise to the potential for slightly different t_R and W per *m/z*, as observed in Figure 4.2A, resulting in *m/z* clusters in the t_R and W dimensions for peaks exhibiting sufficient *m/z* above the signal threshold. For this data set, a S/N ~ 30 provided narrow cluster distributions in the W versus t_R dimensions, with a sufficient number of *m/z* represented.

Figure 4.2C is the resulting 2D *m/z* cluster plot from processing the data in Figure 4.1B using the method illustrated in Figure 4.2A. Since all of the analytes in this section of the chromatogram are well-resolved, each analyte produces a well-defined cluster of points (i.e., 10 ms x 10 ms 2D squares) as indicated in the figure. The zoom-in (Figure 4.2C) indicates the cluster for propylbenzene (PB) is comprised of *m/z* locations spanning 4 data points in the t_R dimension (40 ms), and 3 data points in the W dimension (30 ms). The points have been color coded to the number of *m/z* at each 2D location. Based on the color coded point distribution, the majority of *m/z* for each peak are centered relatively tightly in each cluster, generally with only a few outliers. In addition to each cluster having distributions in the t_R and W dimensions, they also have different locations in the 2D plane. The difference in locations of each cluster in the W dimension provides added chemical selectivity (resolving power). Based on the oven heating rate applied (33 °C /min) the difference in elution temperature between MH and CYO is only 2.7 °C (from the t_R difference of ~ 5 s) but their W differ by ~ 60 ms (~ 10% of their W values). Achieving suitably different W at nearly the same t_R is consistent with GC modeling described in Figure 4.S1 in Supporting Information [23-28]. Hence, the 2D *m/z* cluster plot in Figure 4.2C clearly indicates that chemical selectivity is simultaneously generated in both dimensions.

To study and apply the 2D *m/z* cluster plot method, the distribution of pure clusters must be determined. A pure cluster is defined as a cluster resulting from a chromatographically resolved analyte with no interfering compounds. From the separation in Figure 4.1A, 16

representative, purely eluting analytes (with four injection replicates) were analyzed to create 64 2D *m/z* cluster plots (grid illustrated in Figure 4.2A), containing a total of 1068 sufficiently independent *m/z* responses. The 16 analytes used to make the distributions are noted in Table 4.1.S1 in the Supporting Information. The 64 cluster plots were manually aligned such that the most populated index (the t_R with the largest number of *m/z*) was aligned between each cluster. The 64 aligned cluster plots were then summed, creating the t_R distribution provided on the left in Figure 4.3A. Similarly, the 64 pure clusters were aligned to view the distribution in the *W* dimension. The clusters were aligned such that the most populated peak width index (the aligned *W* with the largest number of *m/z*) were aligned within each cluster and then summed to create the *W* distribution provided on the right in Figure 4.3A. For the t_R dimension, 92.4% of the *m/z* are contained within a 3 data point interval, corresponding to a 30 ms distribution width. Similarly, for the *W* dimension, 96.1% of the *m/z* were also contained within a 30 ms distribution width. Using these distributions, a box of 30 ms x 30 ms in both dimensions was used to determine the sufficiently selective *m/z* from the 2D *m/z* cluster plots, and is referred to herein as a "cluster box." Although the distributions in Figure 4.3A are not strictly Gaussian, since the cluster box encloses ~ 95% of the *m/z* in each dimension, the cluster box dimensions are taken as the 2D "peak width" in the context of a 2D *m/z* cluster plot. The cluster box dimensions may need to be recalculated depending upon the instrumental and separation conditions.

The issue of undersampling with this method should be raised. For example, by taking the GC – TOMFS data measured at 100 Hz and binning it down to 20 Hz, the *m/z* no longer form a distribution in the t_R dimension. Each *m/z* "cluster" is reduced to essentially a single bin, which in the case of 20 Hz data, is 50 ms wide (versus sufficiently sampled and 30 ms wide). Hence, the t_R dimension becomes undersampled. Also, the accuracy of the *W* measurement suffers, and

the clusters all appear to have nearly the same *W*. Overall, the use of a 20 Hz sampling rate results in a reduction in resolving power in both dimensions in the 2D *m/z* cluster plot.

The cluster box may be readily applied to determine the selective *m/z* for a given analyte. To do so, the box is initially centered on the single most populated "indexed" 2D location in a cluster. For this purpose, we elected to require three or more *m/z* at a single location (green or red point per Figure 4.2C) to define a cluster. By manual inspection, it often is readily possible to visually determine a cluster without the location of a green or red point. However, a minimum of three *m/z* at one location was applied for this study. Next, the cluster box is positioned such that the maximum number of nearby *m/z* are included within the box, while also containing the most populated location within the box. The most populated location was not required to be in the center of the cluster box. The chromatographic peaks corresponding to the *m/z* within the box are then summed and averaged, creating an average elution profile for the analyte. Peaks above the signal threshold from *m/z* falling outside this box are not included in the average. Figure 4.3B is an overlay of the TIC from Figure 4.1B and the initial 2D *m/z* cluster plot from Figure 4.2C that has been processed using the cluster box. The method was readily applied in an automated fashion to the entire chromatogram from Figure 4.1A (see Figure 4.3C). In the construction of the 2D *m/z* cluster plot for the entire separation, it is possible that two closely eluting analyte clusters may be combined into one cluster box. Indeed, there is always a limit to how well two closely eluting analytes can be resolved. We note the format of the entire 2D *m/z* cluster plot resembles the 2D separation provided by GC × GC [29]. The width of the clusters in each dimension (30 ms) provides a profound increase in the potential peak capacity of the original GC-TOFMS data (30 ms cluster width versus ~1.1 s peak 4σ width-at-base). The *W* values differ by as much as ~ 90 ms for closely eluting analytes in Figure 4.3C, thus the effective peak

capacity (number of resolved cluster boxes) in the *W* dimension is ~ 3. Since the original GC peaks have a width of ~1.1 s, and the clusters have a width of 30 ms, the effective peak capacity production of the GC-TOFMS data increased nearly 40-fold from ~ 55 peaks/min to ~ 2,000 peaks/min. By taking into account the peak capacity in the *W* dimension, the total peak capacity is potentially ~ 6,000 peaks/min using both dimensions of the 2D *m/z* cluster plot (~ 100-fold improvement). State-of-the-art GC × GC – TOMFS produces a peak capacity production of ~ 1,000 peaks/min [10] thus we are also achieving a significant increase in the apparent peak capacity production over GC × GC.

To demonstrate the benefit of applying the method at relatively low chromatographic resolution, we consider two peaks at a R_s of 0.3 in the original GC-TOFMS format, with a t_R difference of 340 ms and an average peak 4σ width-at-base of 1.1 s. The two analytes, methyl hexanoate (MH, actual t_R = 248 s) and 1, 2, 3-trichlorobenzene (TCB, actual t_R = 350 s) were originally baseline resolved from all analyte peaks in the 73 component mixture. The GC-TOFMS data for these analytes were cut from the chromatogram and mathematically combined in Matlab at R_s = 0.3. These two analytes were chosen for study because they exhibit similar peak intensities, their peak *W* are realistically different, and they provide an adequate number of selective and overlapped *m/z*. The difference in *W* between the MH and TCB (~ 8%) is consistent with the range predicted by the modeling provided in the Supporting Information [24, 25]. Figure 4.4A shows the mathematically convoluted peaks. The TIC is shown in the inset. The TIC peak appears symmetrical which would not suggest this peak as containing overlapped analytes. The tall, black peak is *m/z* 74, a common, high intensity fragment shared between the two analytes. The time dimension is an arbitrary scale since the peaks were removed from their original location in the chromatogram. Figure 4.4B shows the 2D *m/z* cluster plot from the

processed data from Figure 4.4A, prior to applying the cluster box. While the selective *m/z* for each analyte are located in or near the boxes, the *m/z* with W elevated relative to the boxes are *m/z* shared between the two analytes. The horseshoe shape of the overlapped *m/z*, as illustrated by the dashed trace in Figure 4.4B, is a result of both analytes contributing significantly to a resultant net peak profile with the W and t_R altered as compared to peaks from selective *m/z*. A horseshoe shaped pattern is typical for 2D *m/z* cluster plots of poorly resolved peaks ($R_s < 0.4$). Overlapped peaks with R_s between ~ 0.4 and 1.5 (omitted for brevity) still indicate overlapped *m/z*, but they appear directly over selective *m/z* (in the 2D *m/z* cluster plots), indicating using the method would still be beneficial.

For better visualization of the separation of TCB and MH in the 2D *m/z* cluster plot in Figure 4.4C, all *m/z* outside the cluster boxes have been removed (demonstrated in Figure 4.3B). The combination of the W and t_R dimensions benefits identification of overlapped *m/z*, while also providing additional resolution between the selective *m/z* of the two analytes. The selective *m/z* for TCB have a W of ~ 680 ms whereas the selective *m/z* for MH have a W of ~ 630 ms. The two clusters are also separated in the t_R dimension by 340 ms. The 2D resolution, $R_{s,2D}$, between the two clusters is 11.6, where $R_{s,2D}$ is defined as the distance of separation between two clusters divided by the average width of the clusters, where width is generally defined by 4σ, which is 95% of a normal distribution [30]. Recall the 30 ms x 30 ms cluster box defines the 2D cluster width, encompassing ~ 95% of the *m/z* in the W and t_R dimensions. By reducing the data to the 2D *m/z* cluster plot, which contains in essence, the same chemical information as the original GC-TOFMS chromatogram, the effective chromatographic resolution between the two analytes has increased nearly 40-fold, from 0.3 (separation of peaks) to 11.6 (separation of clusters).

The signals at the selective *m/z*, defined as all *m/z* within the cluster boxes in Figure 4.4C, provide the pure elution profile for the analytes TCB and MH. The multiple selective *m/z* within a cluster box are used to more confidently provide the pure elution profile for each analyte. Figure 4.4D shows the resulting peak profiles when the selective *m/z* for TCB and MH are averaged by the number of *m/z* in each cluster box. By creating the average peak profile for each analyte, a constraint to the solution to the CLS deconvolution is imposed. The peak profile at each *m/z* must fit one of the two average chromatographic peak profiles, or if interfered, the peak profile must be a linear combination of the two pure profiles [21, 31]. CLS provides the correct proportion per *m/z* between the two analytes. Hence, CLS analysis provides their deconvoluted peak signal profile and mass spectrum. The deconvoluted peak signal profiles are essentially identical to the average peak profiles by application of the cluster box to the selective *m/z*, in every way except in their relative peak height. For this example at $R_s = 0.3$, the CLS analysis captured 99.98% of the variance with a R^2 of 0.9999 for both analytes. The inset in Figure 4.4D provides the deconvoluted spectra for TCB and MH. The CLS determined mass spectra were matched to the pure spectra (known a priori). Resulting match values (average with standard deviation from four replicates) were 985±3 for TCB and 983±1 for MH, indicating excellent matches to the library spectra and a reproducible analysis.

On the basis of the results presented in Figure 4.4, it is evident the 2D *m/z* cluster plot method has the potential to resolve GC peaks separated by only a small fraction of their width [32]. The W and t_R dimensions work synergistically to facilitate resolution. To explore these ideas further, the study of TCB and MH was extended in Figure 4.S2 to $R_s = 0.03$ in the traditional GC-TOFMS data format (see details in Supporting Information). Figure 4.S2A provides the resulting 2D *m/z* cluster plot with the cluster box applied, where the initial R_s of

0.03 (separation of GC peaks) has been dramatically enhanced to a $R_{s,2D}$ of 1.73 (separation of clusters), a nearly 60-fold increase. Figure 4.S2B provides the CLS deconvoluted pure elution profiles and mass spectra in the inset. The match values were 954±8 for TCB and 920±18 for MH (average with standard deviations from four replicates). Even at this challenging level of low R_s, the 2D *m/z* cluster plot method provides accurate and precise analytical information.

In the separation of the 73 component mixture, two analytes naturally overlapped with R_s ~ 0.04. The 2D *m/z* cluster plot method, with CLS, was used to deconvolute and identify the two analytes. Figure 4.5A provides the 2D *m/z* cluster plot of the section of the chromatogram in question. The TIC is in the inset. From the TIC the peak appears pure. The *W* is not noticeably inflated and the peak shape appears symmetrical. The TIC peak has a *W* of 690 ms and an asymmetry value of 1.05 [33]. The two clusters have a $R_{s,2D}$ of ~ 1.5, which is slightly smaller than the simulated example in Figure 4.2SA, and is primarily due to a smaller difference in *W*. Figure 4.5B provides the CLS modeled peak profiles for each analyte with the deconvoluted mass spectra in the inset. The deconvoluted spectra were matched to library spectra for identification. The two clusters were identified as benzene (match value of 986±2) and cyclohexane (match value of 935±9). These results were validated using individual standards for these analytes. Unless an additional separation dimension is applied, such as in GC × GC, these two analytes are often not well resolved in one-dimensional GC. However, since the analytes display a slight R_s ~ 0.04, and exhibit sufficiently different W, they were readily analyzed by the method presented.

4.5 Supporting Information

The supporting information contains Table 4.1.S1, which is a list of compounds used to make the test mixture. The chromatographic modeling is described in some detail. Finally, an

extra example applying the 2D *m/z* cluster method at a R_s of 0.03 is provided. We previously implemented chromatographic theory to study peak broadening in high-speed isothermal GC separations [23]. Building from that effort, as well as prior research by Snijders, Janssen, and Cramers [24], we recently developed and applied modeling software for high-speed temperature programmed GC separations [25]. In the current report, we implemented our GC modeling software in order to assess the plausibility that the peak *W* for a representative retained analyte, while eluting with a constant t_R, is dependent upon the analyte gas phase diffusion coefficient in the carrier gas mobile phase, D_g. As described by Fuller, Schettler, and Giddings, D_g is dependent on its molecular weight and diffusion volume [26] and is an important variable in the Golay equation, which shows that the peak width is not solely dependent on retention time, but also on analyte specific properties, such as D_g.

The column modeled had dimensions of 30 m x 250 µm i.d. with helium as the carrier gas at a flow rate of 2.0 ml/min. The outlet pressure was ambient pressure, taken as 101.3 kPa (14.7 psi). A chromatographic run time of 500 s was modeled (with a time increment in the temperature program model of 0.01 s). The temperature program began at 35 °C and was held for 1 min, and the temperature was increased at 33°C/min until 280 °C and held for 1 min.

Retention data were also measured as described in the Experimental section for suitable test analytes and converted to retention factors, *k*, to obtain thermodynamic information from Van't Hoff plots used in the modeling. Separations were performed at seven temperatures run isothermally from 100 °C to 250 °C at a 25 °C interval for 3-octanone, dodecane, cyclohexane, and t-butylbenzene. Although Van't Hoff plots for four test analytes were prepared, for the purpose of modeling the D_g influence on the detected peak *W* at a constant t_R, only a single set of representative thermodynamic data was required. We selected 3-octanone, with a Van't Hoff plot

slope of 4,560 (-ΔH/R) and y-intercept of -10.7 (ΔS/R). 3-octanone was chosen as the representative test analyte since it eluted in roughly in the middle of the modeled separation, with a t_R of 340 s, at an elution temperature of 189 °C, with a local k of 0.44 at the moment of elution. For the modeled GC separations, the D_g was varied while keeping all other parameters constant, and the W was determined at each D_g.

Figure 4.S1 is a plot of the modeling results with W versus $D_{g,o}$, the diffusion coefficient at the outlet, which is larger than D_g at the column inlet [27]. Peak widths predicted by the modeling range from 0.70 s to 0.82 s for W. For a typical analyte eluting at a constant t_R, the W can theoretically differ by as much as ~ 100 ms (~ 10 % to 15% of W) which provides a basis for one form of chemical selectivity in the W dimension in the 2D *m/z* cluster plot method. While the modeling presented herein describes one plausible way to account for a change in W (at ~ constant t_R), there are other approaches to consider in future studies, such as an analyte dependent difference in k at moment of elution from the column outlet that relate to differences in analyte thermodynamic properties [28], but the method described utilizes analyte dependent differences in peak W, regardless of how the difference is produced.

Figure 4.S2A provides the resulting 2D *m/z* cluster plot with the cluster box applied, where the initial R_s of 0.03 (separation of GC peaks) has been dramatically enhanced to a $R_{s,2D}$ of 1.73 (separation of clusters), nearly a 60-fold increase. The TIC of the combined signals for the two analytes, provided in the inset, does not provide any evidence of two analytes being present. If the two clusters had no separation in the W dimension the $R_{s,2D}$ would still be ~ 1. Due to the W dimension, the two clusters have an additional dimension to gain resolution. Figure 4.S2B provides the CLS deconvoluted pure elution profiles and mass spectra in the inset. The match

values were 954±8 for TCB and 920±18 for MH (average with standard deviations from four replicates).

4.6 Conclusions

We have introduced a novel way of processing and visualizing GC-TOFMS data. By viewing the processed chromatograms in a 2D *m/z* cluster plot, peaks with $R_s \sim 0.03$ in the traditional signal versus time format can be visually identified as separated, and deconvoluted using chemometrics. The method should in principle be readily applicable to data from a high-resolution TOFMS to gain a significantly higher data point density per cluster, i.e. more *m/z* values. Additionally, this method should be applicable using a modern qMS, but may not provide as much selectivity and resolution in the 2D *m/z* cluster plot due to a lower sampling rate. Studying the effect of tuning the *W* dimension for added selectivity and enhanced resolving power should be investigated. It is quite possible measurements of peak overlap other than *W* as demonstrated herein, would be fruitful. Analyte pairs with $R_s \sim 0$ on the t_R dimension could, in principle, be separated on the *W* dimension, however, a more involved chemometric procedure would likely be required to complete the analysis. The method holds promise as a new approach in chemical separation science similar to the gains generated by GC × GC.

4.7 List of Works Cited

[1] E.M. Humston, K.M. Dombek, J.C. Hoggard, E.T. Young, R.E. Synovec, Time-Dependent Profiling of Metabolites from Snf1 Mutant and Wild Type Yeast Cells, *Analytical Chemistry* 80 (2008) 8002–8011.

[2] E.M. Humston, J.D. Knowles, A. McShea, R.E. Synovec, Quantitative assessment of moisture damage for cacao bean quality using two-dimensional gas chromatography combined with time-of-flight mass spectrometry and chemometrics, *Journal of Chromatography A* 1217 (2010) 1963–1970.

[3] F.J. Santos, M.T. Galceran, Modern developments in gas chromatography–mass spectrometry-based environmental analysis, *Journal of Chromatography A* 1000 (2003) 125–151.

[4] J.C. Hoggard, J.H. Wahl, R.E. Synovec, G.M. Mong, C.G. Fraga, Impurity Profiling of a Chemical Weapon Precursor for Possible Forensic Signatures by Comprehensive Two-

Dimensional Gas Chromatography/Mass Spectrometry and Chemometrics, *Analytical Chemistry* 82 (2010) 689–698.
[5] R.B. Wilson, B.D. Fitz, B.C. Mannion, T. Lai, R.K. Olund, J.C. Hoggard, et al., High-speed cryo-focusing injection for gas chromatography: Reduction of injection band broadening with concentration enrichment, *Talanta*. 97 (2012) 9–15.
[6] R.B. Wilson, W.C. Siegler, J.C. Hoggard, J.S. Nadeau, R.E. Synovec, Achieving high peak capacity production for gas chromatography and comprehensive two-dimensional gas chromatography by minimizing off-column peak broadening, *Journal of Chromatography A* 1218 (2011) 2130-3139.
[7] G. Gaspar, R. Annino, C. Vidal-Madjar, G. Guiochon, Influence of instrumental contributions on the apparent column efficiency in high speed gas chromatography, *Analytical Chemistry* 50 (1978) 1512–1518.
[8] A.J. Borgerding, C.W. Wilkerson, A Comparison of Cryofocusing Injectors for Gas Sampling and Analysis in Fast GC, *Analytical Chemistry* 68 (1996) 2874–2878.
[9] G.M. Gross, B.J. Prazen, J.W. Grate, R.E. Synovec, High-Speed Gas Chromatography Using Synchronized Dual-Valve Injection, *Analytical Chemistry* 76 (2004) 3517–3524.
[10] B.D. Fitz, R.B. Wilson, B.A. Parsons, J.C. Hoggard, R.E. Synovec, Fast, high peak capacity separations in comprehensive two-dimensional gas chromatography with time-of-flight mass spectrometry, *Journal of Chromatography A* 1266 (2012) 116–123.
[11] R. Bro, PARAFAC. Tutorial and applications, *Chemometrics and Intelligent Laboratory Systems* 38 (1997) 149–171.
[12] J.C. Hoggard, W.C. Siegler, R.E. Synovec, Toward automated peak resolution in complete GC × GC–TOFMS chromatograms by PARAFAC, *Journal of Chemometrics* 23 (2009) 421–431.
[13] K.R. Beebe, B.R. Kowalski, An Introduction to Multivariate Calibration and Analysis, *Analytical Chemistry* 59 (1987) 1007A–1017A.
[14] B.J. Prazen, R.E. Synovec, B.R. Kowalski, Standardization of Second-Order Chromatographic/Spectroscopic Data for Optimum Chemical Analysis, *Analytical Chemistry* 70 (1998) 218–225.
[15] R.G. Dromey, M.J. Stefik, T.C. Rindfleisch, A.M. Duffield, Extraction of mass spectra free of background and neighboring component contributions from gas chromatography/mass spectrometry data, *Analytical Chemistry* 48 (1976) 1368–1375.
[16] A. Lorber, L.E. Wangen, B.R. Kowalski, A theoretical foundation for the PLS algorithm, *Journal of Chemometrics* 1 (1987) 19–31.
[17] M.M. van Deursen, J. Beens, H.-G. Janssen, P.A. Leclercq, C.A. Cramers, Evaluation of time-of-flight mass spectrometric detection for fast gas chromatography, *Journal of Chromatography A* 878 (2000) 205–213.
[18] L.C. Marney, W. Christopher Siegler, B.A. Parsons, J.C. Hoggard, B.W. Wright, R.E. Synovec, Tile-based Fisher-ratio software for improved feature selection analysis of comprehensive two-dimensional gas chromatography–time-of-flight mass spectrometry data, *Talanta*. 115 (2013) 887–895.
[19] J.S. Nadeau, R.B. Wilson, J.C. Hoggard, B.W. Wright, R.E. Synovec, Study of the interdependency of the data sampling ratio with retention time alignment and principal component analysis for gas chromatography, *Journal of Chromatography A* 1218 (2011) 9091–9101.

[20] J.M. Davis, D.R. Stoll, P.W. Carr, Effect of First-Dimension Undersampling on Effective Peak Capacity in Comprehensive Two-Dimensional Separations, *Analytical Chemistry* 80 (2008) 461–473.
[21] R. Bro, S. de Jong, A Fast non-negativity constrained least squares algorithm, *Journal of Chemometrics* 11 (1997) 393–401.
[22] K.M. Pierce, J.C. Hoggard, Chromatographic data analysis. Part 3.3.4: handling hyphenated data in chromatography, *Analytical Methods* 6 (2014) 645–653.
[23] V.R. Reid, R.E. Synovec, High-speed gas chromatography: The importance of instrumentation optimization and the elimination of extra-column band broadening, *Talanta*. 76 (2008) 703–717.
[24] H. Snijders, H.-G. Janssen, C. Cramers, Optimization of temperature-programmed gas chromatographic separations I. Prediction of retention times and peak widths from retention indices, *Journal of Chromatography A* 718 (1995) 339–355.
[25] R.B. Wilson, J.C. Hoggard, R.E. Synovec, High throughput analysis of atmospheric volatile organic compounds by thermal injection – isothermal gas chromatography – time-of-flight mass spectrometry, *Talanta*. 103 (2013) 95–102.
[26] E. Fuller, P. Schettler, J.C. Giddings, A new Method for prediction of binary gas-phase diffusion coefficients, *Industrial & Engineering Chemistry* 58 (1966) 18–27.
[27] N. H. Chen, D. F. Othmer, New generalized equation for gas diffusion coefficient, *Journal of Chemical and Engineering Data* 7 (1962) 37-41.
[28] J.M. Davis, M. Pompe, C. Samuel, Justification of Statistical Overlap Theory in Programmed Temperature Gas Chromatography: Thermodynamic Origin of Random Distribution of Retention Times, *Analytical Chemistry* 72 (2000) 5700–5713.
[29] Z. Liu, J.B. Phillips, Comprehensive Two-Dimensional Gas Chromatography using an On-Column Thermal Modulator Interface, *Journal of Chromatographic Science* 29 (1991) 227–231.
[30] R.E. Murphy, M.R. Schure, J.P. Foley, Effect of Sampling Rate on Resolution in Comprehensive Two-Dimensional Liquid Chromatography, *Analytical Chemistry* 70 (1998) 1585–1594.
[31] K. R. Beebe, R.J. Pell, M.B. Seasholtz, *Chemometrics: A Practical Guide*; John Wiley & Sons, Inc., 1998.
[32] J.B. Callis, "Super Resolution in Chromatography by Numerical Deconvolution", In Ultrahigh Resolution Chromatography. ACS Symposium Series (250), Seattle, WA, 1984.
[33] J.P. Foley, J.G. Dorsey, Equations for calculation of chromatographic figures of merit for ideal and skewed peaks, *Analytical Chemistry* 55 (1983) 730–737.

4.8 Tables

Table 4.1.S1. List of compounds with mass, boiling point (BP), and vendor used in the 73 component mixture. An aliquot of the mixture was diluted 1:100 in acetone prior to analysis. * Indicates analyte was used in creating *m/z* distributions in Figure 4.3A.

Chemical	Mass (mg)	BP (°C)	Vendor
pentane	131	36	J.T. Baker
ethyl formate	151	54	Sigma-Aldrich
acetone	180	56	Sigma-Aldrich
chloroform	132	61	Fischer
n-hexane	151	69	Sigma-Aldrich
methylcyclopentane	105	72	Fluka
2-butanone	143	80	Sigma-Aldrich
benzene	112	80	Fischer
cyclohexane	119	81	Sigma-Aldrich
1-propanol	118	97	Sigma-Aldrich
heptane	138	98	Fischer
methylcyclohexane	108	101	Sigma-Aldrich
2-pentanone	151	102	Sigma-Aldrich
toluene	123	111	Sigma-Aldrich
2-butanol	131	117	Sigma-Aldrich
octane	124	126	Sigma-Aldrich
3-hexanone	135	128	Sigma-Aldrich
chlorobenzene	121	132	Alfa-Aesar
1-chlorohexane	129	135	Sigma-Aldrich
ethylbenzene	113	136	Sigma-Aldrich
1-pentanol	120	137	Sigma-Aldrich
xylenes (o, m, p)	126	139	Mallinckrodt
3-heptanone	116	141	Sigma-Aldrich
*cyclooctane	113	150	Sigma-Aldrich
nonane	125	151	Sigma-Aldrich
*propylbenzene	125	152	Sigma-Aldrich
*1-bromohexane	129	156	Sigma-Aldrich
*bromobenzene	118	156	Sigma-Aldrich
1-hexanol	117	158	Sigma-Aldrich
2-heptanol	118	160	Fluka
*mesitylene	132	163	Sigma-Aldrich
*3-octanone	115	167	Sigma-Aldrich
*t-butylbenzene	141	167	Sigma-Aldrich
*methyl hexanoate	135	168	Sigma-Aldrich

isobutylbenzene	108	170	Sigma-Aldrich
sec-butylbenzene	123	173	Sigma-Aldrich
*decane	95	174	Sigma-Aldrich
1-bromoheptane	135	179	Sigma-Aldrich
butylcyclohexane	110	181	Sigma-Aldrich
butylbenzene	130	183	Sigma-Aldrich
*methyl octanoate	116	193	Sigma-Aldrich
1-octanol	123	194	Sigma-Aldrich
*2-nonanone	126	194	Sigma-Aldrich
undecane	107	196	Sigma-Aldrich
*1-bromooctane	127	199	Sigma-Aldrich
*1,3,5-trichlorobenzene	115	208	Sigma-Aldrich
2-decanone	114	209	Sigma-Aldrich
*1-nonanol	110	215	Sigma-Aldrich
dodecane	96	216	Sigma-Aldrich
naphthalene	118	218	Sigma-Aldrich
*1,2,3-trichlorobenzene	133	219	Sigma-Aldrich
methyl salicylate	117	223	Alfa-Aesar
methyl decanoate	123	224	Eastman Chemicals
ethyl salicylate	111	227	Alfa-Aesar
bicyclohexyl	111	227	Sigma-Aldrich
1-decanol	107	229	Sigma-Aldrich
1-geraniol	118	230	Sigma-Aldrich
2-undecanone	112	231	Sigma-Aldrich
tridecane	99	235	Sigma-Aldrich
cyclohexylbenzene	130	239	Sigma-Aldrich
2-dodecanone	101	245	Sigma-Aldrich
tetradecane	94	254	Fluka
1-dodecanol	102	256	Acros Organics
methyl laurate	125	267	Sigma-Aldrich
pentadecane	117	271	Alfa-Aesar
hexadecane	137	287	Sigma-Aldrich
1-tetradecanol	111	289	Sigma-Aldrich
2-pentadecanone	104	294	Sigma-Aldrich
pristane	97	296	Sigma-Aldrich
1-hexadecanol	122	344	Sigma-Aldrich
*adamantane	111	sublimes	Sigma-Aldrich

4.9 Figures

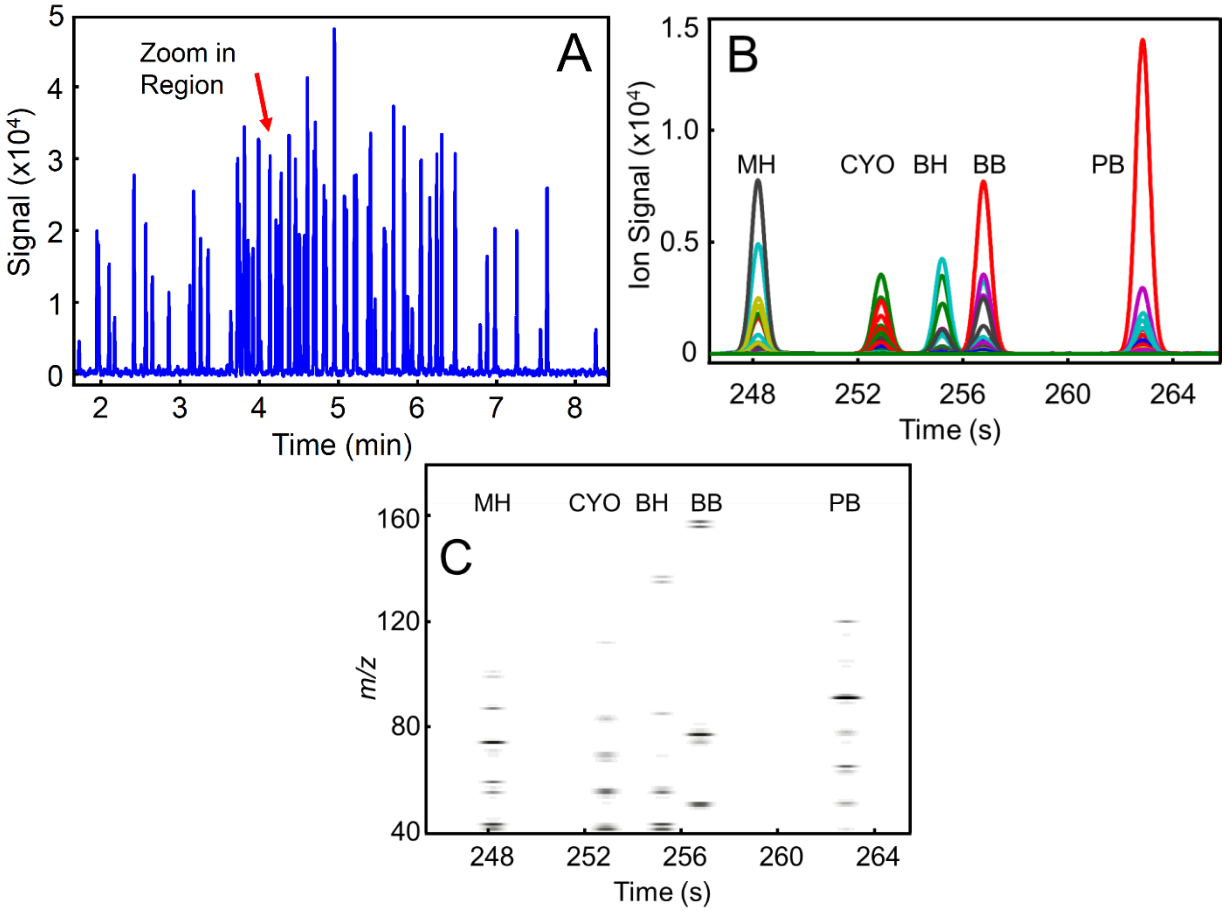

Figure 4.1 (A) TIC chromatogram of the 73-component mixture. Peak widths, *W*, were in the range of ~ 0.6 to 0.7 s. (B) Region of chromatogram from (A) with all *m/z* overlaid. The five analytes are methyl hexanoate (MH), cyclooctane (CYO), 1-bromohexane (BH), bromobenzene (BB), and propylbenzene (PB). (C) Traditional 2D GC-MS image plot of the region from (B).

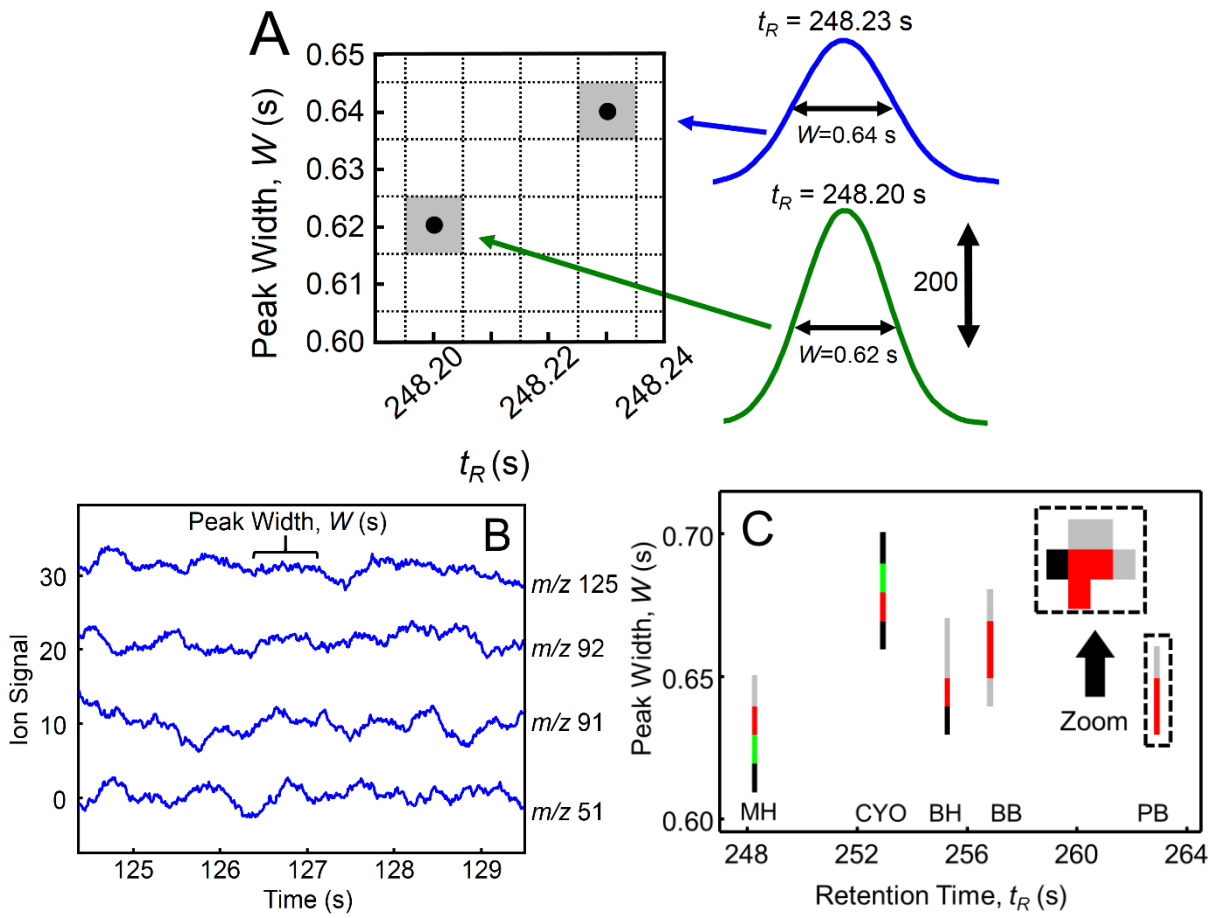

Figure 4.2 (A) Illustration of the 2D *m/z* cluster plot method. Two *m/z* from MH (*m/z* 70, blue and *m/z* 101, green) with slightly different t_R and *W*. The *W* is plotted versus t_R for every peak above the user defined signal threshold. (B) Stacked plot of a noise region for four *m/z*. The noise characteristics differences per *m/z* may result in slightly different t_R and *W* per analyte. (C) 2D *m/z* cluster plot of the region from Figure 4.1B. Each point is the *W* of the GC peak plotted against the t_R per *m/z*. Points in the cluster plot with the same t_R and *W* are color coded based upon the frequency of their occurrence: 1 *m/z*: gray; 2 *m/z*: black; 3 *m/z*: green; 4+ *m/z*: red.

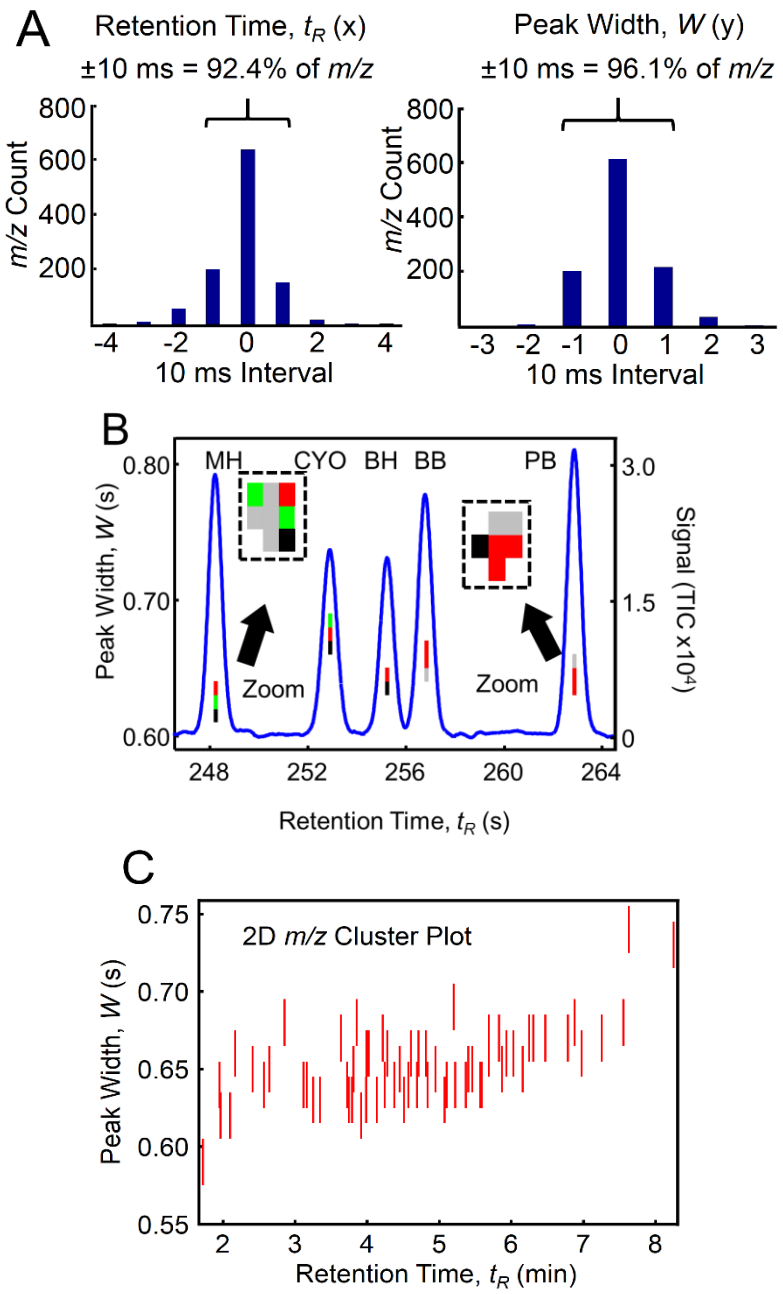

Figure 4.3 (A) Cumulative distributions for 64 pure 2D *m/z* cluster plots (16 analytes with 4 injection replicates). Left: Distribution in the t_R dimension. Right: Distribution in the *W* dimension. See text for description of cluster alignment. A 30 ms x 30 ms window defines a "cluster box," and determines the selective *m/z*. (B) TIC of Figure 4.1B overlaid with the 2D *m/z* cluster plot of the respective region. Each cluster has been processed with the cluster box to remove outlying *m/z*, using the legend in Figure 4.2. (C) Display of the 2D *m/z* cluster plot of the entire separation after applying the cluster box. On this time scale, each cluster box appears as a red vertical line 30 ms tall, centered on the middle of the cluster. The apparent peak capacity in the *W* dimension is ~ 3 for the separation time window from 2 to 7 min.

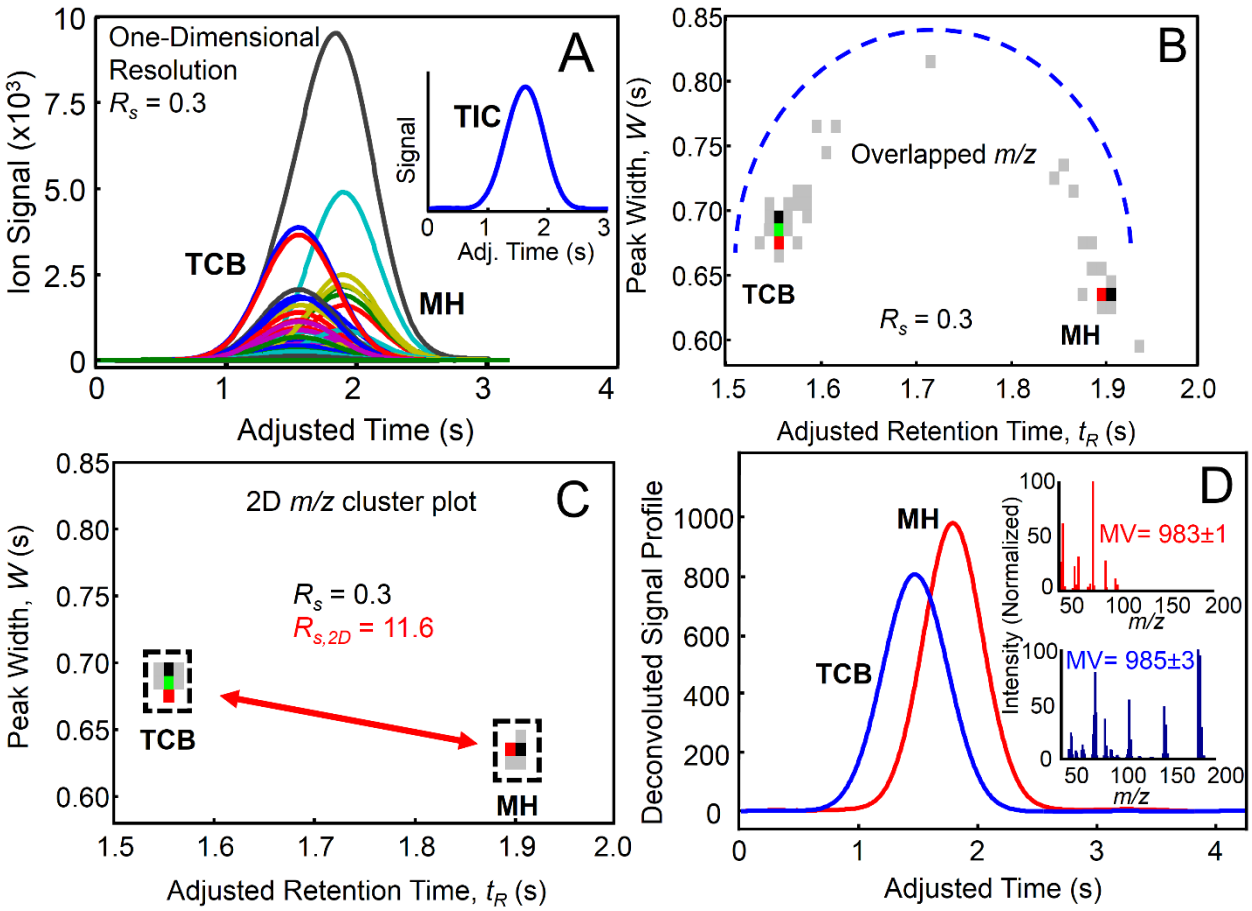

Figure 4.4 (A) Superimposed GC peak signals for two analytes at a R_s of 0.3, right: methyl hexanoate (MH), left: 1, 2, 3-trichlorobenzene (TCB). The most intense black trace is *m/z* 74, a prominent fragment in both analytes. The TIC is provided in the inset. (B) 2D *m/z* cluster plot of the data from (A) prior to applying the cluster box, using the legend in Figure 4.2. The chromatographically overlapped peaks per *m/z* have elevated *W* and intermediate t_R. Blue dashed trace indicates the horseshoe-like shape of overlapped *m/z*. (C) After applying the cluster box, only selective *m/z* (16 for TCB, 9 for MH) remain. The 2D resolution, $R_{s,2D}$, of the clusters for this pair of analytes is 11.6. (D) Deconvoluted peak signal of each analyte obtained from the CLS deconvolution. Inset provides the deconvoluted mass spectra for each analyte (red – MH, blue – TCB) with match values (MV average and standard deviation from four replicates).

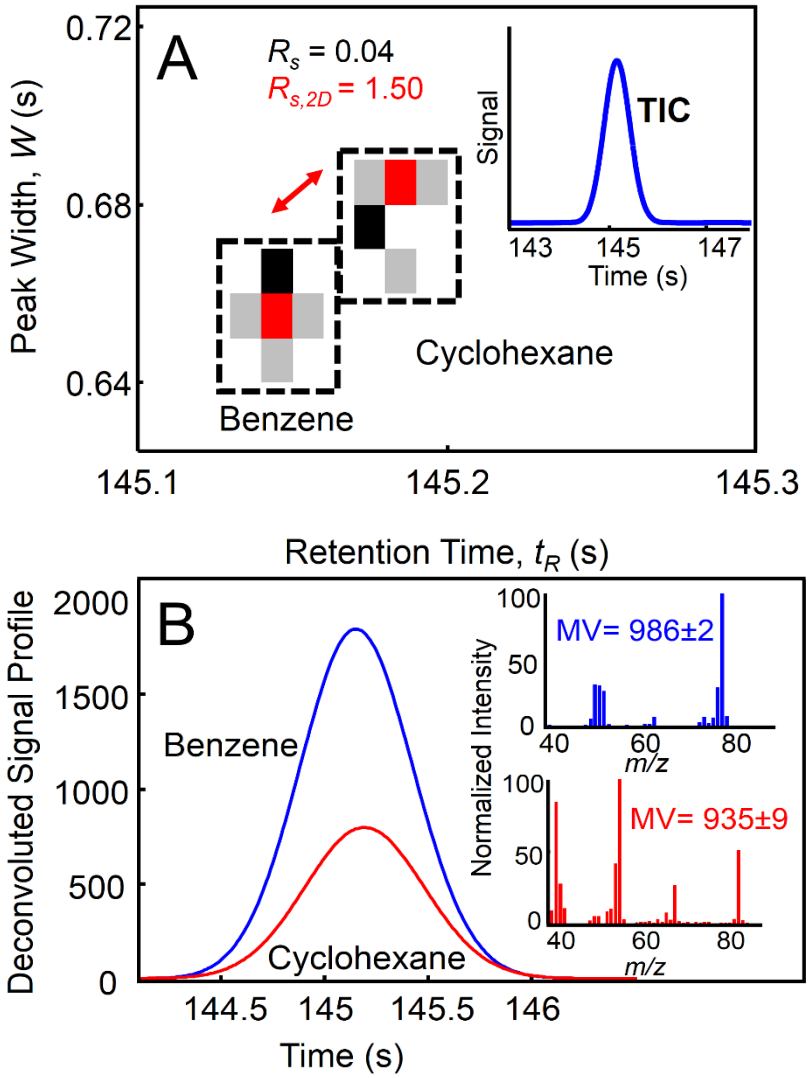

Figure 4.5 (A) 2D *m/z* cluster plot of an unresolved analyte pair from the separation of the 73-component mixture in Figure 4.1A, using legend in Figure 4.2. The analyte pair has a R_s of ~ 0.04. The cluster box has been placed around each cluster to show their selective *m/z*. The TIC is provided in the inset. (B) Deconvoluted signal profiles and mass spectra. Matching the deconvoluted spectra to standard spectra collected in-house determined the two analytes to be benzene and cyclohexane.

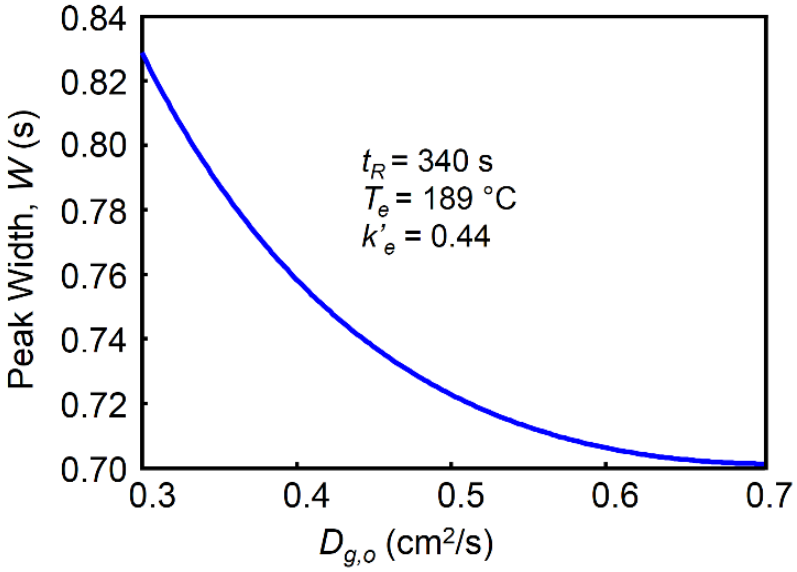

Figure 4.S1 Plot of peak width, *W*, versus the binary gas diffusion coefficient in the mobile phase at the column outlet, $D_{g,o}$, for modeled GC data. The constant retention time, t_R, elution temperature, T_e, and retention factor at elution, k'_e, were 340 s, 189 °C, and 0.44 respectively, for each modeled $D_{g,o}$ value.

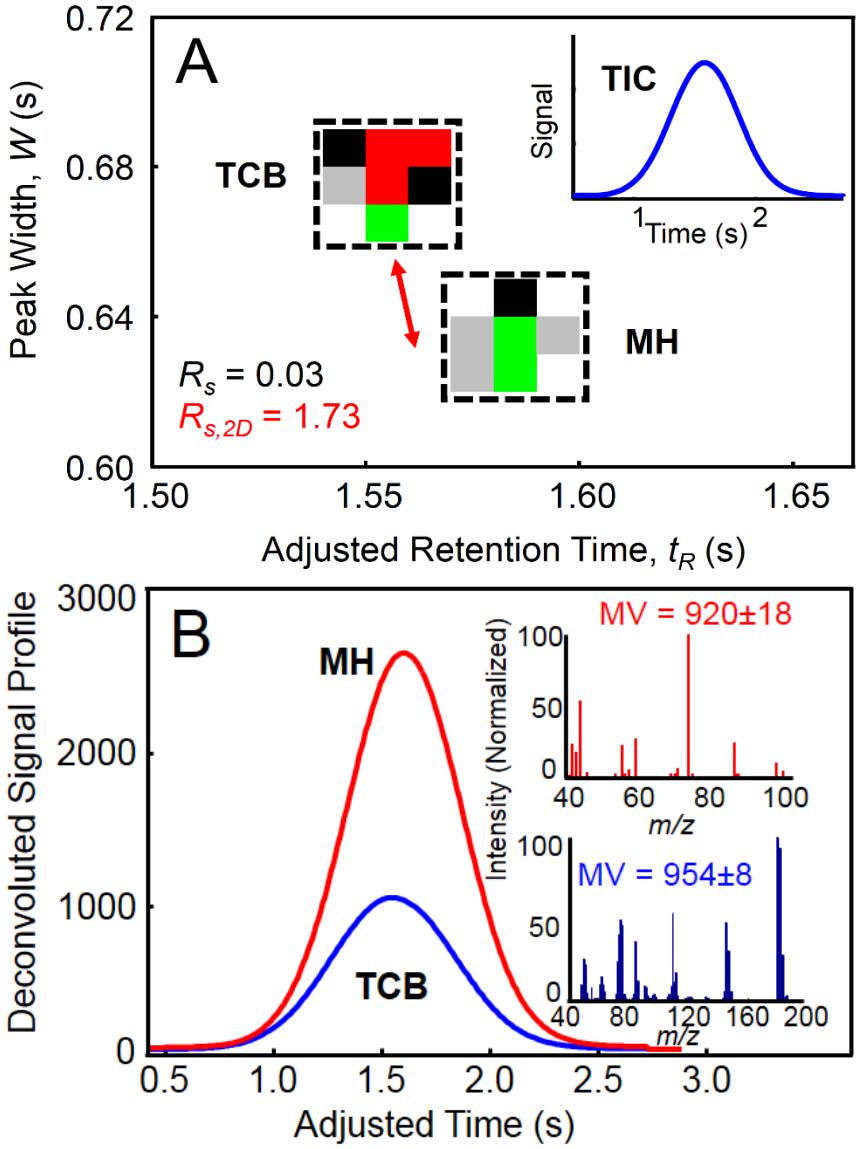

Figure 4.S2 (A) 2D *m/z* cluster plot of the same analyte pair from Figure 4.4 (MH and TCB) set to a R_s of 0.03, using the legend provided in the Figure 4.2 caption. The TIC is provided in the inset. The centers of each analyte cluster and their selective *m/z* are indicated by the two cluster boxes. (B) Deconvoluted peak profiles and mass spectra of the two analytes with match values given (MV average and standard deviation from four replicates).

Chapter 5. Extension of the two-dimensional mass cluster plot method to fast, high peak capacity separations utilizing low thermal mass gas chromatography with time-of-flight mass spectrometry[5]

5.1. Introduction

Gas chromatography mass spectrometry (GC-MS) is a powerful and widely used analytical technique for the separation, identification, and quantification of volatile and semi-volatile compounds in complex mixtures. GC is capable of resolving hundreds, if not thousands of compounds in a single analysis. Many researchers have dedicated significant effort into reducing analysis time while maintaining the separation efficiency. These efforts are due largely to major technological advances in microbore capillary column implementation [1, 2], column heating technology [3-22], flow control [23], injection methods [24-34], and detectors [35]. One of the most promising avenues of advancing the fast GC field is based on resistive heating technology. Two main categories of resistive heating have been developed over the years: Direct resistive heating, which resistively heats a metal separation column directly; and indirect resistive heating, which heats a metal column (or tube) in close proximity to a fused silica separation column. One example of the latter category, the low thermal mass gas chromatograph (LTM-GC) commercialized by Agilent, uses a coiled toroid consisting of a resistive heating element, thermocouple, and fused silica capillary column wrapped in foil to minimize heat loss [7]. The system is capable of heating at rates up to 1800 °C/min (30 °C/s) which in principle can perform a traditional temperature programmed GC separation (~50 °C to 300 °C) in ~ 8 s. A traditional oven bath GC operating at the maximum heating rate capable, 30-50 °C/min, would take several minutes to accomplish the same temperature program.

[5] This chapter is currently under revision in preparation for submission to *Analytica Chimica Acta (2015)*

However, reducing the run time of a GC separation via use of a fast temperature program may inadvertently compromise chromatographic resolution between analytes, which is also manifested as a loss in separation peak capacity, n_c. Resolution, R_s, is a metric of separation and efficiency between adjacent analytes, defined as the difference in retention time, t_R, between analytes, divided by the average peak width at base (4σ), W_b, of the two analytes. If resolution is compromised, this may compromise the ability to obtain information from the data from the overlapped analyte peaks. Mass spectral matching, which is ubiquitously used for analyte identification [36], can be significantly compromised by chromatographic overlap. Spectral matching relies on pure target and library spectra and uses an algorithm to match the ratios of spectral fragment intensities of target vs. library spectra [37, 38]. In order to obtain pure spectra from chromatographically overlapped peaks, mathematical deconvolution is often required. GC-TOFMS provides a bilinear data structure which is amenable to multivariate data analysis techniques to elucidate pure spectra from overlapped analytes [39-41].

We recently reported a study involving LTM-GC with flame ionization detection (FID) for fast, high peak capacity separations involving different sample injection methodologies [42]. The peak capacity, n_c, is a metric of the number of peaks that can be adequately resolved in a given time, defined as the separation window, t_{sep}, divided by the average peak width at base, W_b. The n_c is generally reported at unit resolution, $R_s = 1$. However, if the benefits of analyte peak deconvolution are also considered, the effective n_c is further normalized by dividing n_c initially calculated at unit resolution, by the new R_s limit. For example, common peak finding algorithms that simply count peak maxima, can do so at a R_s limit of 0.5 [43], thus the n_c for such a peak counting algorithm would be doubled relative to n_c at unit resolution. At unit resolution, we previously achieved an n_c of nearly 300 in a 60 s separation using LTM-GC-FID [42]. The large

n_c was fortuitously benefited by on-column focusing, since by manufacturers design the LTM column is located held outside of the GC oven, so the head of the LTM column naturally serves as a cold trap prior to starting the temperature program. The rapid column heating rate, 250 °C/min, kept peaks narrow as they began to separate within the column. The W_b produced by LTM-GC were extremely narrow, reaching ~30 ms on a 5 m x 100 µm inner diameter (i.d.) column for the least retained analyte. Also demonstrated was the remarkable resolution between two adjacent analyte peaks, octane and decane. The two peaks, while separated by only 9 s with W_b = 200 ms, provided R_s = 45 between them. These factors (analyte focusing, rapid column heating, and narrow peak widths) facilitated the demonstration for fast GC analyses to offer similar chemical information in a fraction of the time compared to traditional time-scale GC.

Previously we reported a novel data reduction and visualization method for GC-TOFMS data using two-dimensional mass channel (*m/z*) cluster plots, referred to herein as the "2D *m/z* cluster method" [44]. To summarize, the chromatographic data is first preprocessed by an appropriate smoothing and baseline correction step. Next, the chromatogram is subjected to a peak finding algorithm used to detect peak maxima for all collected *m/z* above a user specified signal threshold (not just the TIC). The peak width, *W*, is then calculated (either at base, W_b, or half-height, W_{hh}) for each peak maxima detected for each *m/z*. Processing the data in this fashion converts the signal at each *m/z* associated with a chromatographic peak into a single data point consisting of a retention time, t_R, and width, *W*, with the coordinate (t_R, *W*). All of the *m/z* are then plotted (*W* versus t_R) to produce a 2D *m/z* cluster plot. Each pure analyte peak produces a cluster of points (one point per *m/z*) in the 2D space, since points at a given coordinate accumulate, providing chemical selectivity in both dimensions, *W* and t_R. Peak signals per *m/z* of overlapped analytes produce points in the cluster plot with inflated *W*, at intermediate t_R relative

to the corresponding t_R of peak signals of pure analyte *m/z*, with the linear combination of the multiple peak signal vectors for the interfered *m/z* producing wider peaks. Thus, both dimensions of a cluster plot provide useful chemical information as well as a novel way to visualize GC-TOFMS data. Additionally, the clusters of *m/z* for each analyte are significantly narrower than the corresponding chromatographic peak, thus significantly increasing the resolution between adjacent analytes. The method can be used to accurately and confidently deconvolute analytes at $R_s \sim 0.03$. Hence, the method can be used to accurately determine the number of analytes in overlapped peaks (i.e. the rank), can provide an accurate determination of the number of analytes in a sample, as well as provide a significant increase in the overall peak capacity of the system.

Herein we implement new algorithmic parameters, methods, and instrumentation with the 2D *m/z* cluster method. The primary focus is the use of an Agilent Low Thermal Mass (LTM) GC system coupled to a LECO Pegasus III TOFMS (LTM-GC-TOFMS) with the 2D *m/z* cluster method. A relatively fast heating rate was applied (250 °C/min) and short column used (10 m x 100 µm i.d.), compared to previous work (33 °C/min heating rate, 30 m x 250 µm i.d. column) [44], to produce a much faster separation with significantly narrower peaks. A rapid spectral collection rate of 500 Hz is implemented (5-fold faster than previously applied) with additional key preprocessing in order to optimally apply the 2D *m/z* cluster method. The peak width-at-base, W_b, is used as the metric of peak purity since it is more selective for interfered *m/z* compared to W_{hh} previously applied. Due to its various benefits for analyte deconvolution, Multivariate curve resolution alternating least squares (MCR-ALS) was evaluated. MCR-ALS has been used extensively in data mining methods in multivariate data sets for deconvolution, calibration, and quantification [45–49]. A key parameter in using MCR-ALS is knowing the rank of the data input for deconvolution. The 2D *m/z* cluster method provides a novel approach to

objectively obtain the rank of the matrix for MCR-ALS, thus improving the deconvolution. Based on previous implementation of the method combined with algorithmic improvements to the method and use of the LTM technology, a 30-fold increase in effective peak capacity is hypothesized (i.e. effective n_c of 10,000 in 120 s).

2. Experimental

All chemicals used were reagent grade or higher unless otherwise noted. A liquid hydrocarbon mixture containing 115 components was created by adding ~100 mg each of the neat compounds (Table 1). For unambiguous peak identification, 9 separate mixtures were made, each containing a unique subset of 12 to 13 components from the full 115 component mixture. Each mixture was analyzed on the LTM-GC-TOFMS under the same conditions as the full mixture (data omitted for brevity). An in-house library of mass spectra and retention times was created to aid in identifying overlapped peaks from the full 115 component mixture.

GC-TOFMS data was collected using an Agilent 6890A GC (Agilent Technologies, Palo Alto, CA) with a LECO Pegasus III TOFMS (LECO, St. Joseph, MI). An Agilent Series I Low Thermal Mass (LTM) column module was attached to the existing GC door. A 10 m x 100 µm i.d. column with a 0.4 µm DB-5 film (5% phenyl / 95% dimethyl polysiloxane) was used. Two segments of 100 µm i.d. deactivated fused silica capillary were used as a transfer line between the inlet and the head of the LTM module, and between the outlet of the LTM to the mass spectrometer, respectively. Ultra high purity helium was used as the carrier gas operated at a column flow rate of 2 ml/min. (Grade 5, 99.999%, Praxair, Seattle, WA, USA). The flow rate required the use of an aftermarket high-pressure inlet operated at 1034 kPa (150 psig). The inlet was operated at 300 °C in split mode at a 300:1 split ratio. An auto-injector equipped with a 500 nl (0.5 µl) micro-syringe (Hamilton, Reno, NV) injected 50 nl (0.05 µl) of the neat sample into

the inlet. The oven was held at 280 °C to prevent analytes from separating in the transfer lines prior to the analytical column as well as keeping the peaks narrow as they exited the column prior to detection. The LTM column was held at 50 °C for 30 s (void time) then ramped at 250 °C/min to a final temperature of 300 °C where it was held for 60 s for a total separation time of 150 s. The TOFMS collected *m/z* 33-250 at a collection rate of 500 Hz, which corresponds to a 2 ms time interval per spectrum collected. The ion source was 250 °C and the electron impact voltage was -70 eV.

Matlab R2012b (The Mathworks, Inc., Natick, MA, USA) was used to process the raw GC-TOFMS data and to create the method algorithm and a GUI (Graphical User Interface). Processing involved three steps to produce clusters with relatively narrow distributions in the two dimensions, W_b and t_R. First, the raw GC-TOFMS data (signal versus time vector for each *m/z*) were independently baseline corrected. Second, a Fast Fourier Transform (FFT) smoothing technique was used per each *m/z*, similar to the method previously described [50]. Use of the FFT smoothing facilitated a significant reduction in the noise in the chromatographic data which resulted in a further reduction in cluster dimension translating into a significant increase in the resolving power of the method. In the last step, the resulting smoothed data is subjected to peak finding and peak W_b measurements of each detected *m/z* above a user selected signal threshold, which is functionally a signal-to-noise ratio, *S/N*, threshold as the noise is relatively constant, and finally plotting to produce the cluster plot. PLS Toolbox version 7.8.2 (Eigenvector Research, Inc., Wenatchee, WA, USA) was used for performing MCR-ALS deconvolution. All *m/z*, including those under the initial signal threshold, were included in the MCR-ALS deconvolution. A non-negativity constraint was applied in the concentration and spectral profiles and a

unimodality constraint was applied for the concentration profiles. An in-house written function to import the data from the instrumental '.peg' file to the Matlab workspace was used [51].

3. Results and Discussion

The 115 component mixture analyzed by LTM-GC-TOFMS provided a data set that both highlights the fast, high peak capacity nature of the separation as well as allowing for the study of the 2D *m/z* cluster method in a fast GC separation environment. Figure 5.1A is the total ion current (TIC) chromatogram of a 50 nl aliquot (300:1 split) of the 115 component mixture (Table 1). The mixture was suitably complex requiring a traditional temperature program range (50 °C to 300 °C) to adequately resolve a significant majority of the components. The W_b ranged from 300 to 500 ms, with the majority of the peaks having W_b of ~ 350 ms. The separation window is ~120 s producing a n_c of 340 at unit resolution. The fast temperature program used, 250 °C/min, as well as the analyte on-column focusing effect provided by the LTM is critical in performing the separation rapidly with narrow peaks [42]. The highest boiling point (BP) compound in the mixture, 1-hexadecanol (BP 344 °C) eluted at 140 s. The two regions in the inscribed boxes will be focused on to describe relevant portions of implementing the method in subsequent sections.

Figure 5.1B is a zoom of the region from 44 s to 50 s from Figure 5.1A. This 6 s window shows the TIC of what appears to be 7 peaks. To put the 2D *m/z* cluster method into context with traditional 2D plots of GC-MS data, an image plot of the region from Figure 5.1B is shown in Figure 5.1C. This type of plot utilizes the multivariate aspect of MS detection and can aid the user in visualizing the mass spectral dimension in conjunction with the GC separation dimension in a single plot. The locations on the plot with dark color reflect the signal intensity of peaks at the respective *m/z* plotted against separation run time. Visualizing the data as in Figure 5.1C can be helpful in identifying areas of chromatographic overlap but is difficult to objectively

determine the rank of the overlapped peak(s). For example, the peak at t_R = 49.5s (right most peak in Figures 5.1B & 5.1C) appears to have significant overlap, but the correct rank is undeterminable by this type of plot. The 2D *m/z* cluster method, however, is able to determine the rank of the overlapped peaks. Analysis of the right most peak in Figures 5.1B and 5.1C in context of the 2D *m/z* cluster method will be provided in a subsequent section.

As previously reported [44], the spectral collection rate is an important parameter to consider when using the 2D *m/z* cluster method. Traditionally, with GC-MS instrumentation, W_b are generally between 2 s and 6 s with spectral collection rates of 5 to 20 Hz more commonly applied. Initially, the 2D *m/z* cluster method was developed using a 100 Hz spectral collection rate with 1 s W_b peaks. Fast data collection rates are commonly used to minimize extra column band broadening due to detection [52, 53], to permit data transformation such as alignment [54-56], and to aid in peak deconvolution [44, 57-59]. The previous report demonstrated that undersampling (at 20 Hz, which provided ~20 spectra across the peak) was insufficient to provide ample chemical selectivity in the W_b dimension. The spectral collection frequency implemented in this study was the maximum capable of the LECO Pegasus III TOFMS, at 500 Hz (*m/z* 33-250). In this study with LTM-GC-TOFMS, the W_b ranged from 300 ms to 500 ms, thus 150 to 250 spectra per peak were collected providing adequate data resolution and hence, selectivity, in the W_b dimension of the cluster plot. Additionally, the high spectral collection rate can aid in measuring the t_R of peaks very accurately, further facilitating the method.

The basic principles of the 2D *m/z* cluster method as applied with LTM-GC-TOFMS are now presented using a representative chromatographically resolved analyte, 1-butanol in Figure 5.2A. The superimposed ion chromatogram shows that the signal vectors of each *m/z* appear as nearly continuous functions, resulting from the extremely rapid data collection rate in

conjunction with the FFT smoothing technique. There is no digitization of the data, no angular artifacts due to undersampling, nor any apparent aliasing. The t_R is determined from the apex of each peak while the W_b is measured at 13% of the max height (4σ width) for each respective *m/z*. The signal threshold was 40 units, under which no peak maxima were measured. Figure 5.2B shows the resulting cluster plot of the data from Figure 5.2A where each point (colored box) is the W_b plotted versus the t_R per *m/z* peak. The color indicates the accumulative frequency that the *m/z* peaks within the analyte had an identical (t_R, W_b) coordinate relative to one another. In this case, there are no points that have identical (t_R, W_b) coordinates as indicated by all colored points being black. The rapid data collection rate of 500 Hz enables the t_R of each *m/z* to be determined with 2 ms precision. The fast data collection rate provides a greater precision in the t_R and W_b measurements compared to a slower collection rate, however, it is more unlikely that *m/z* will initially have identical (t_R, W_b) coordinate points.

The strength of the method relies on a sufficient data sampling rate to unambiguously determine the location of pure or overlapped analytes. The clusters represent the original chromatographic data but with additional selectivity. If the points representing the peak are not sufficiently overlapped (i.e. no colored points, as in Figure 5.2B), it becomes difficult to discern between pure and overlapped analytes. In order to achieve an optimal balance between retention time and peak width accuracy in relation to appropriate visualization of the data, where each pure analyte is represented by a small cluster with overlapped *m/z* points, the initial clustered data must be binned. The GC-TOFMS data was purposefully oversampled initially so there would not be any digitization of the clusters, (i.e. be undersampled) to obtain accuracy in the t_R and W_b dimensions. The data must be binned sufficiently such that a well-defined cluster of *m/z* is obtained. Since GC peaks are measured at their 4σ width which contains 95% of the area

(assuming a Gaussian peak shape), the appropriate binning factor would ideally sample 95% of the unbinned data in each dimension, ideally in 3 bins (similar to modulating a GC × GC peak at a modulation ratio $M_R = 2$).

For general application of the method to objectively determine the distribution of pure analyte clusters (in the t_R and W_b dimensions) and to determine the extent of any required binning, the following processes was performed. From the separation in Figure 5.1A, 10 fully resolved chromatographic peaks (each with 3 injection replicates) were analyzed to make a total of 30 pure *m/z* cluster plots containing 783 sufficiently independent *m/z* responses. The analytes used are noted in Table 1. To determine the cluster distribution in the t_R dimension, the clusters were aligned such that the most populated index (the t_R with the largest number of *m/z*) was aligned between each cluster. The 30 aligned cluster plots were then summed to form the distribution on the left in Figure 5.3A. Likewise, for the cluster distribution in the W_b dimension, the process was repeated by aligning the clusters such that the most populated index (in this case the W_b with the largest number of *m/z*) was aligned between each cluster. The data was then summed to form the distribution on the left of Figure 5.3B.

For binning the data, the t_R dimension was binned by a factor of two, such that each time interval became 4 ms, up from the initial 2 ms. The plot on the right of Figure 5.3A shows the binned t_R data, which now requires three 4 ms bins (12 ms) to gather 95% of the pure *m/z* in the t_R dimension. For the narrowest peak in the separation of 350 ms, the 'width' of the chromatographic "peak" is a reduced by a factor of ~ 30, from 350 ms to 12 ms. Thus, in 2D *m/z* cluster space, the peak capacity of the original LTM-GC-TOFMS separation is increased ~ 30-fold, from n_c of 340 to ~ 10,000. In the previous implementation of the method, the width of the

clusters was 30 ms wide, therefore herein we achieved a 3-fold improvement over the previous study [44].

The W_b dimension was binned by a factor of 15 resulting in 30 ms intervals. The results, depicted on the right in Figure 5.3B, shows that the W_b distribution required a larger bin size. The additional scatter in the W_b dimension is not due to any alterations of peak shape due to baseline correction or the FFT smoothing technique. The W_b is a more selective indicator for differing peak widths. Nearby peaks, even those separated at 4σ width, can still cause minute changes in the W_b which is detectable by the 2D *m/z* cluster method. This makes the method extremely sensitive for detecting outlying *m/z* based on their W_b. Based on the distributions from Figures 5.3A and 5.3B, a box consisting of 3 binned points (12 ms) in the t_R dimension and 3 binned points (90 ms) in the W_b dimension was used to define and determine the pure *m/z* of clusters.

Figure 5.4A shows the binned data for the 1-butanol cluster (compare to Figure 5.2B prior to binning), which has a width in the t_R axis of 12 ms (three 4 ms bins). When the data is processed in this way, there is a *S/N* increase which makes the location of the analyte more readily apparent. The color scheme for overlapped points is as follows: 1 *m/z* – light grey; 2 *m/z* – dark grey; 3 or more *m/z* – black. For example, after binning, the black square represents an accumulation of 3 mass channels with identical W_b = 450 ms and t_R = 48.704 s. The remaining cluster plots presented herein will be of the binned data. The appearance of points with darker shading within 2D *m/z* clusters provides confidence that pure *m/z* are present. Whereas when clusters of *m/z* are scattered (wide variance in t_R and W_b and not lightly shaded) suggests that adjacent analyte peak(s) may be altering the W_b and/or t_R, indicative of poorly resolved analytes.

Figure 5.4B, from the inscribed region in Figure 5.1B, demonstrates the method for LTM-GC-TOFMS data described thus far. The TIC (black line) is superimposed with the cluster plot of the same region. The cluster on the right (H) is the same cluster from Figure 5.4A. However, the grouping on the left appears to be two unresolved analytes marked F and G. However, in cluster space the analytes are well resolved. The points between the clusters F and G are the shared *m/z* between the two analytes. The binned 3 point by 3 point box which dictates pure *m/z* is shown by the dashed black box. There are three analytes present in the window, but only two peaks detected in the TIC. Traditional peak finding methods may only find two peaks, which would lead to improper peak identification and quantification. The analytes F, G, and H correspond to compounds 1, 1, 1-trichloroethane, 1-chlorobutane, and 1-butanol, respectively. Analytes F and G are at a chromatographic $R_s = 0.3$, which is well above the limit-of-resolution (LOR) of the 2D *m/z* cluster method, which is determined to be approximately 10 times lower, at $R_s \sim 0.03$ consistent with our previous report [44].

One of the primary uses of the 2D *m/z* cluster method is to provide an accurate assessment of the number of analytes in overlapped peaks (i.e. the rank) which consequently aids in accurately determining the number of analytes in an entire sample. Many software packages can significantly overestimate (or underestimate) the actual number of analytes present. This may be due to not detecting analytes at sufficiently low resolution or *S/N*, splitting peaks into multiple entries (when constructing peak tables), or not deconvoluting peaks adequately. To highlight these phenomena, the region of the chromatogram from Figure 5.1B is shown in Figure 5.5A. Again, rather than the TIC, each individual ion chromatogram is superimposed to better visualize the data. It is clear that many of the peaks have multiple co-eluting analytes that are not readily seen in the TIC. In addition, the analytes that are co-eluting are overlapped such that rank

determination is still ambiguous simply from visual inspection, similar to Figure 5.1C. It is at this stage in the data analysis that the 2D *m/z* cluster method would be applied.

Figure 5.5B is the resulting cluster plot from processing the data from the region in Figure 5.5A. It can be seen that many of the peaks are overlapped, which is represented by locations on the cluster plot with inflated W_b. However, due to the narrow distribution of the clusters in the t_R dimension (~12 ms) the resolution between analytes is greatly increased (compared to the standard chromatogram) such that the pure *m/z* for each analyte can be visualized. The rank of the overlapped peaks (similar to Figure 5.4B) can be determined by analyzing the clusters of pure *m/z* in relation to the size of the clusters of pure *m/z* from the distributions determined earlier (Figures 5.3A & 5.3B). Analytes A and B are overlapped in the TIC producing only one peak maxima, which is adjacent, but partially resolved to analyte C. Analytes A and B are separated at a $R_s = 0.25$ but produce only one peak in the TIC. The rank of the peak with A and B would thus be two. Analytes D and E, while slightly overlapping, appear to be adequately resolved ($R_s = 0.77$) to provide a single peak apex for each analyte in the TIC, so the rank of each peak would be 1.

Two additional regions in Figure 5.5B are highlighted to show their significant peak overlap. The first region, focusing on peaks F and G (at 48 s) is the same region from the left in Figure 5.4B. Peaks F and G would be a rank of two, while peak H is a chromatographically pure analyte with a rank of 1. The region on the far-right of Figure 5.5B (peaks I-L) will be analyzed in more depth in Figure 5.7A (with the rank determined to be four, using the 2D *m/z* cluster method). By combining the information gained from the plot in Figure 5.5B with Figure 5.5A, the superimposed ion chromatogram (and TIC) becomes more informative. Figure 5.5C is the TIC of the same region as Figures 5.5A & 5. 5B (with the superimposed ion chromatogram

below) but with the rank indicated, i.e. number of analytes in each peak. Based on the TIC alone, the number of actual analytes in this region could not confidently be determined; a traditional peak finding algorithm using the TIC would detect 7 peaks, which is only ~ 60% of the actual analytes; based on the 2D *m/z* cluster method there are 12 analytes present. Thus in this sample window, the method provides an unambiguous determination of the number of analytes per peak.

Incorporating the cluster plot into peak rank determination also aids in the determination of sample rank (i.e. number of analytes in the sample). Figure 5.6A is a complex region from the LTM-GC-TOFMS separation noted in Figure 5.1A where many peaks appear overlapped and convoluted. The separation window is 25 s with W_b of pure analytes of ~350 ms producing a corresponding n_c at unit resolution of 71. A traditional peak finding algorithm operating on the TIC identified 42 peaks. The instrument software was used to identify peaks and it detected 65 analytes (ChromaTOF version 3.32). The number of peaks determined by the 2D *m/z* cluster method was 52, which is in agreement with using retention time and mass spectral matching from the 9 separate mixtures (Experimental Section).

Figure 5.6B is the resulting cluster plot of the region from Figure 5.6A where each analyte cluster appears as a vertical line due to the scale difference between the cluster size and the separation window. The separation window encompasses 25 s (25,000 ms) while the dimension of the clusters in the t_R dimension are ~12 ms (see Figure 5.3A), which makes them appear extremely narrow but in reality still appear as clusters when viewed on a smaller time scale. The height of the clusters, 90 ms, was determined from the distribution in Figure 5.3B. The analytes are color coded based on their rank. A peak width rank 1 appears as a black line while peak(s) with rank greater than one appear red. Unit rank peaks are defined as analyte peaks that are chromatographically resolved enough to produce a single cluster per peak (e.g. analyte H

in Fig. 5.4B). Red clusters of rank greater than one represent overlapped analyte peaks that are no longer chromatographically pure and may only exhibit one peak maxima for a pair (or more) of analytes. However, with the 2D *m/z* cluster method, they are clearly resolved (e.g. analytes F and G in Figure 5.4B).

In this example in Figure 5.6B, the peak at t_R = 76.3 s was of unknown rank. The unknown rank TIC peak is at the LOR of the 2D *m/z* cluster method where the two or more analyte clusters are too unresolved to be distinguishable as separate clusters, which would be at $R_s \leq 0.03$.The peak was theorized not to be of single rank as evidenced by two observable characteristics: the width of the cluster in the t_R dimension was 20 ms which was wider than that of a pure cluster (12 ms), and the number of *m/z* in the cluster, 47, was disproportionately large for the any analyte in the sample, most analytes having ~20 to 30 *m/z* defining a cluster. Initially trying to match the peak to the mass spectral library resulted in mesitylene at a match value of 845. In general application of the method, this peak would be below the LOR of the method. However, selective application of the method provided feasible results in the deconvolution. The results of the selective application were t-butylbenzene (MV = 937) and isopropyl benzene (MV = 935). Mesitylene was identified elsewhere in the chromatogram at a significantly higher match value.

A critical parameter in peak deconvolution for many chemometric methods is having requisite knowledge of the number of analytes, (or rank, i.e. number of factors) in an overlapped peak. Using an inappropriate number of factors in deconvolution will lead to poor fit percentage, significant residuals, improper identification, and poor quantitative results. MCR-ALS is an excellent chemometric method for chromatographic peak deconvolution [45-49], however objective and straightforward determination of the rank would benefit by coupling with the 2D

m/z cluster method. The basic principles associated with doing so will be briefly explained and demonstrated here. For bilinear GC-TOFMS data, the data matrix, *D*, can be decomposed into concentration profiles (i.e., chromatographic peaks), *C*, and mass spectral profiles, *S*, with error (or residual) matrix, *E*.

$$D = C * S^T + E \quad (1)$$

The ALS algorithm reconstructs the data matrix from the concentration and spectral profiles, while minimizing the error (or residual) matrix. The model is said to converge when subsequent iterations of the processes fall below a specified residual value. By initializing the model with an initial estimation of the number of components, components concentration profiles, and/or mass spectra of any known compounds will aid in the model converging to a useful answer, i.e. a model that accurately represents the chemical constituents (concentration, spectra, rank, etc.) of the sample. A non-negativity constraint was imposed for both *C* and *S*. A unimodality constraint was also imposed for *C*, meaning each analyte can only contain one peak apex. For classical least squares (CLS), which was implemented in a previous study [44], either *C* or *S* must be known explicitly to solve for the other parameter. However, with MCR-ALS, there is no stringent requirement of knowing either. The ALS algorithm will alternate in solving for *C* and *S* until the model converges. However, providing initial guesses of *C* and *S*, possible useful constraints, and the rank of the peak will significantly aid in the model successfully converging. The main benefit of using MCR-ALS over CLS is that if certain information is omitted (i.e. missing peaks, spectra), the model can still fit the remaining data to a separate factor, whereas in CLS the missing data would be either modeled into one of the predetermined factors, or placed into the residuals and omitted.

As was discussed and demonstrated, one of the benefits of applying the 2D *m/z* cluster method is unambiguous detection of multiple analytes within a single chromatographic TIC peak. In the discussion of Figure 5.5, it was noted that the TIC peak at ~50 s contains 4 analytes (i.e. has a rank of 4). Figure 5.7A depicts the corresponding cluster plots of the 3 injection replicates of the same single TIC peak. The first 3 panels show the individual cluster plots for each replicate. Each plot looks relatively similar to the others with the same underlying structure. There are slight differences in W_b and t_R for a small number of *m/z* (due to noise and slight t_R misalignment between injection) between the three plots. However, each cluster plot has 4 clearly defined clusters located toward the bottom of each plot (narrower W_b) and an overarching scattering of points higher up on the y-axis. The clusters with narrow W_b represent the pure *m/z* for each analyte whereas the outlying points (i.e. points with higher peak W_b) represent *m/z* that are shared between multiple analytes within the peak and produce a net resultant *m/z* profile that has a wider W_b than a pure *m/z* channel. The fourth panel is the resulting plot of the first 3 panels which have been temporally aligned and summed together. The color map is the same as in previous figures: one *m/z* – light grey; two *m/z* – dark grey; three or more *m/z* – black. By aligning and summing the data, less ambiguous clusters are produced, which represent the 4 analytes. The red circles represent the pure *m/z* and location of each analyte. Cluster plots could, in principle, be used as a metric or marker used in conjunction with GC alignment software. Typically, in chromatographic alignment, a reference target chromatogram (or set of peaks) is chosen and the other chromatograms in the set are aligned to the reference target. The differences in t_R for a given set of peaks across multiple injections could be tracked and utilized to enhance alignment. This peak mapping could be utilized by alignment algorithms to check the adequateness of alignment and to further refine alignment.

The cluster plots for each injection replicate in Figure 5.7A were used to forward data to the MCR-ALS deconvolution. The number of factors (rank) was evidenced by the fact there are 4 clear clusters present in each cluster plot. The simplicity of the method has benefits over having to use extra chemometric methods for factor selection, such as principal component analysis (PCA) or evolving factor analysis (EFA). Specially, the initial guesses for *C* were provided by pure elution profiles of each pure cluster. The pure *m/z* vectors within each cluster were independently summed and averaged to produce 4 pure elution profiles, one for each analyte. The elution profiles are already 'aligned' to the data, meaning the pure elution profiles came from the same data set as the overlapped data. There is no need to run standards to identify overlapped peaks; in cases where peak overlap is so significant, the deviations in t_R between standards can be more than the difference in t_R between overlapped peaks. The 4 pure elution analyte profiles were forwarded to the MCR-ALS algorithm. It was noted that using the pure elution profiles as the initial guess or using them as hard constraints provided a nearly identical result, indicating that the model converged to the same answer. Figure 5.7B are the reconstructed TIC peaks for each factor for each injection replicate. A small amount of variance was observed due to slight deviations between each model, which is possible due to injection volume variation and slight retention time misalignment between samples. Also, variations in contributions between factors (within the limits of minimizing the residuals) may also produce slight changes in signal intensity between replicates. Multiplicative ambiguity can manifest itself in the results of the deconvolution with differing weighting factors for the intensity of the *C* and S profiles between each model. However, since spectral matching normalizes to the base peak, the ambiguity in signal intensity in the spectral profiles is not affected. Also, when the data is

reconstructed (as in Figure 5.7B) by taking the outer product of the *C* and *S* vectors and summing, the data is no longer multiplicatively ambiguous.

Figure 5.7C shows the average spectra and match values for each of the 4 factors in the MCR-ALS deconvolution among the 3 injection replicates. The reverse match value (RMV) was used instead of the traditional forward match value (MV). The reverse match value omits fragments from the sample (i.e. unknown) spectra that are not in the target library spectra. In many deconvolution methods, minor contributions from other factors may be misappropriated into other components. The RMV provides a more robust and defensible result than using all *m/z* that may not be appropriately present. The standard deviation of each match is given to show the reproducibility of the matching, which can be attributed to successful deconvolution. The spectra appear extremely pure, signified by the high match value. A slight misfit in the model can be seen with a small amount of signal at *m/z* 117, 119, and 121 in the neo-pentyl alcohol spectrum, which is likely being attributed from the significant signal intensity from the carbon tetrachloride. Additional knowledge of the system and applying more sophisticated constraining parameters may give higher match values and more accurate quantitation, however for this report it was shown to perform adequately using the conditions applied.

A previous report by van Stokkum, Mullen, and Mihaleva [45] demonstrated that the LOR of MCR-ALS for deconvoluting GC-MS peaks was at a $R_s \sim 0.2$, below which the deconvolution proved unsatisfactory. There reported LOR was determined by considering the match value of two peaks of varying degrees of overlap prior to deconvolution. They noted that by providing the "perfect starting values for the elution profiles" as the initial guess allowed the MCR-ALS model to reach the minimum error (i.e. converge) very quickly. The reason the 2D *m/z* cluster method works so well with MCR-ALS is because of the ability to provide the pure

elution profiles without *a priori* knowledge of the system. The excellent spectral quality of the deconvolution can be attributed to the rapid spectral collection rate used (500 Hz), which defines the peak profiles very well and any minute changes in W_b and t_R between *m/z* can be used in the MCR-ALS model to discriminate between compounds.

5. Conclusion

This report validates the implementation of the 2D *m/z* cluster method for processing and visualizing GC-TOFMS data for use with fast, high speed gas chromatography using LTM-GC coupled to TOFMS. The method, initially developed using standard GC-TOFMS operating conditions (30 m x 250 µm i.d. column, 7 min separation, 1.1 s W_b peaks), was validated in this report to work with a significantly faster separation (10 m x 100 µm i.d. column, 2 min separation) and with narrow analyte W_b (~ 350 ms). Significant algorithmic changes were made to successfully deal with the additional challenges the instrumentation introduced. A rapid data collection rate allows for the accurate detection and measurement of peaks to facilitate deconvolution (using MCR-ALS) of severely overlapped peaks with peak apices separated only by a few milliseconds. The 2D *m/z* cluster method shows promise in conjunction with current software for appropriate factor selection for deconvolution, accurate knowledge of numbers of analytes in a sample, as well as being a possible metric or facilitator in chromatographic peak alignment. The method presented could be used in conjunction with other tools and methods, i.e. peak table approaches, for analyzing complex GC-MS data sets. The method also demonstrated significant gains in effective peak capacity, from 340 at unit resolution to nearly 10,000 in 2D cluster space, which is an improvement of a factor of 3 compared to the previous result.

5.5 List of Works Cited

[1] V.R. Reid, R.E. Synovec, High-speed gas chromatography: The importance of instrumentation optimization and the elimination of extra-column band broadening, *Talanta* 76 (2008) 703–717.
[2] P.Q. Tranchida, L. Mondello, Current-day employment of the micro-bore open-tubular capillary column in the gas chromatography field, *Journal of Chromatography A* 1261 (2012) 23–36.
[3] J. Luong, R. Gras, R. Mustacich, H. Cortes, Low Thermal Mass Gas Chromatography: Principles and Applications, *Journal of Chromatographic Science* 44 (2006) 253–261.
[4] A.B. Fialkov, M. Morag, A. Amirav, A low thermal mass fast gas chromatograph and its implementation in fast gas chromatography mass spectrometry with supersonic molecular beams, *Journal of Chromatography A* 1218 (2011) 9375–9383.
[5] J. Luong, R. Gras, M. Hawryluk, R.A. Shellie, H.J. Cortes, Multidimensional gas chromatography using microfluidic switching and low thermal mass gas chromatography for the characterization of targeted volatile organic compounds, *Journal of Chromatography A* 1288 (2013) 105–110.
[6] F. Xu, W. Guan, G. Yao, Y. Guan, Fast temperature programming on a stainless-steel narrow-bore capillary column by direct resistive heating for fast gas chromatography, *Journal of Chromatography A* 1186 (2008) 183–188.
[7] Agilent LTM Column Module, http://www.chem.agilent.com/en-US/products-services/Columns-Sample-Preparation/GC-GC-MS-Columns/5975T-LTM-Column-Module/Pages/default.aspx.
[8] M.E. Hail, R.A. Yost, Compact gas chromatograph probe for gas chromatography/mass spectrometry utilizing resistively heated aluminum-clad capillary columns, *Analytical Chemistry* 61 (1989) 2410–2416.
[9] N. Roques, J. Crandall, Trans-configurable modular chromatographic assembly, US Patent #8336366 (2009).
[10] S.D. Stearns, H. Cai, J.A. Koehn, M. Brisbin, C. Cowles, C. Bishop, et al., A direct resistively heated gas chromatography column with heating and sensing on the same nickel element, *Journal of Chromatography A* 1217 (2010) 4629–4638.
[11] K. Maštovská, S.J. Lehotay, Practical approaches to fast gas chromatography–mass spectrometry, *Journal of Chromatography A* 1000 (2003) 153–180.
[12] A. Wang, H.D. Tolley, M.L. Lee, Gas chromatography using resistive heating technology, *Journal of Chromatography A* 1261 (2012) 46–57.
[13] J.A. Contreras, A. Wang, A.L. Rockwood, H.D. Tolley, M.L. Lee, Dynamic thermal gradient gas chromatography, *Journal of Chromatography A* 1302 (2013) 143–151.
[14] J.A. Contreras, A.L. Rockwood, H.D. Tolley, M.L. Lee, Peak sweeping and gating using thermal gradient gas chromatography, *Journal of Chromatography A* 1278 (2013) 160–165.
[15] X. Sun, D. Li, A.T. Woolley, P.B. Farnsworth, H.D. Tolley, K.F. Warnick, et al., Bilinear electric field gradient focusing, *Journal of Chromatography A* 1216 (2009) 6532–6538.
[16] H.D. Tolley, S.E. Tolley, A. Wang, M.L. Lee, Moving thermal gradients in gas chromatography, *Journal of Chromatography A* 1374 (2014) 189–198.
[17] V. Jain, John Phillips, Fast temperature programming on fused silica open tubular capillary columns by direct resistive heating., 33 (1995) 55–59.

[18] E.U. Ehrmann, H.P. Dharmasena, K. Carney, E.B. Overton, Novel Column Heater for Fast Capillary Gas Chromatography, *Journal of Chromatographic Science* 34 (1996) 533–539.
[19] E.B. Overton, K.R. Carney, New horizons in gas chromatography: Field applications of microminiaturized gas chromatographic techniques, *Trends in Analytical Chemistry* 13 (1994) 252–257.
[20] X. Yan, K.R. Carney, E.B. Overton, Application of Purge-and-Trap Method to Fast and Convenient Field Analysis of Water and Soil Samples, *Journal of Chromatographic Science* 30 (1992) 491–496.
[21] F. David, K. Jacq, P. Sandra, A. Baker, M.S. Klee, Analysis of potential genotoxic impurities in pharmaceuticals by two-dimensional gas chromatography with Deans switching and independent column temperature control using a low-thermal-mass oven module, Anal. *BioAnalytical Chemistry* 396 (2009) 1291–1300.
[22] E. Dumont, B. Tienpont, N. Higashi, K. Mitsui, N. Ochiai, H. Kanda, et al., Heart-cutting two-dimensional gas chromatography in combination with isotope ratio mass spectrometry for the characterization of the wax fraction in plant material, *Journal of Chromatography A* 1317 (2013) 230–238.
[23] J. Luong, R. Gras, R.A. Shellie, H.J. Cortes, Applications of planar microfluidic devices and gas chromatography for complex problem solving, *Journal of Separation Science* 36 (2013) 182–191.
[24] G. Gaspar, R. Annino, C. Vidal-Madjar, G. Guiochon, Influence of instrumental contributions on the apparent column efficiency in high speed gas chromatography, *Analytical Chemistry* 50 (1978) 1512–1518.
[25] H. Wollnik, R. Becker, H. Götz, A. Kraft, H. Jung, C.-C. Chen, et al., A high-speed gas chromatograph coupled to a time-of-flight mass analyzer, *International Journal of Mass Spectrometry and Ion Processes*. 130 (1994) L7–L11.
[26] A.J. Borgerding, C.W. Wilkerson, A Comparison of Cryofocusing Injectors for Gas Sampling and Analysis in Fast GC, *Analytical Chemistry* 68 (1996) 2874–2878.
[27] B.A. Ewels, R.D. Sacks, Electrically-heated cold trap inlet system for high-speed gas chromatography, *Analytical Chemistry* 57 (1985) 2774–2779.
[28] G.M. Gross, B.J. Prazen, J.W. Grate, R.E. Synovec, High-Speed Gas Chromatography Using Synchronized Dual-Valve Injection, *Analytical Chemistry* 76 (2004) 3517–3524.
[29] V.R. Reid, A.D. McBrady, R.E. Synovec, Investigation of high-speed gas chromatography using synchronized dual-valve injection and resistively heated temperature programming, *Journal of Chromatography A* 1148 (2007) 236–243.
[30] M.A. Klemp, M.L. Akard, R.D. Sacks, Cryofocusing inlet with reverse flow sample collection for gas chromatography, *Analytical Chemistry* 65 (1993) 2516–2521.
[31] J.L. Hope, K.J. Johnson, M.A. Cavelti, B.J. Prazen, J.W. Grate, R.E. Synovec, High-speed gas chromatographic separations with diaphragm valve-based injection and chemometric analysis as a gas chromatographic “sensor,” Anal. Chim. Acta. 490 (2003) 223–230.
[32] A. Van Es, J. Janssen, C. Cramers, J. Rijks, Sample enrichment in high speed narrow bore capillary gas chromatography, *Journal of High Resolution Chromatography* 11 (1988) 852–857.

[33] R.B. Wilson, B.D. Fitz, B.C. Mannion, T. Lai, R.K. Olund, J.C. Hoggard, et al., High-speed cryo-focusing injection for gas chromatography: Reduction of injection band broadening with concentration enrichment, *Talanta* 97 (2012) 9–15.
[34] R.B. Wilson, J.C. Hoggard, R.E. Synovec, High throughput analysis of atmospheric volatile organic compounds by thermal injection – isothermal gas chromatography – time-of-flight mass spectrometry, *Talanta* 103 (2013) 95–102.
[35] M.M. van Deursen, J. Beens, H.-G. Janssen, P.A. Leclercq, C.A. Cramers, Evaluation of time-of-flight mass spectrometric detection for fast gas chromatography, *Journal of Chromatography A* 878 (2000) 205–213.
[36] P. Ausloos, C.L. Clifton, S.G. Lias, A.I. Mikaya, S.E. Stein, D.V. Tchekhovskoi, et al., The critical evaluation of a comprehensive mass spectral library, *Journal of the American Society of Mass Spectrometry* 10 (1999) 287–299.
[37] S.E. Stein, An integrated method for spectrum extraction and compound identification from gas chromatography/mass spectrometry data, *Journal of the American Society of Mass Spectrometry* 10 (1999) 770–781.
[38] S.E. Stein, D.R. Scott, Optimization and testing of mass spectral library search algorithms for compound identification, *Journal of the American Society of Mass Spectrometry* 5 (1994) 859–866.
[39] C.A. Bruckner, B.J. Prazen, R.E. Synovec, Comprehensive Two-Dimensional High-Speed Gas Chromatography with Chemometric Analysis, *Analytical Chemistry* 70 (1998) 2796–2804.
[40] R.G. Dromey, M.J. Stefik, T.C. Rindfleisch, A.M. Duffield, Extraction of mass spectra free of background and neighboring component contributions from gas chromatography mass spectrometry data, *Analytical Chemistry* 48 (1976) 1368–1375.
[41] A. Lorber, L.E. Wangen, B.R. Kowalski, A theoretical foundation for the PLS algorithm, *Journal of Chemometrics* 1 (1987) 19–31.
[42] B.D. Fitz, B.C. Mannion, K. To, T. Hoac, R.E. Synovec, Evaluation of injection methods for fast, high peak capacity separations with low thermal mass gas chromatography, *Journal of Chromatography A* 1392 (2015) 82–90.
[43] J.M. Davis, J.C. Giddings, Statistical theory of component overlap in multicomponent chromatograms, *Analytical Chemistry* 55 (1983) 418–424.
[44] B.D. Fitz, B.C. Reaser, D.K. Pinkerton, J.C. Hoggard, K.J. Skogerboe, R.E. Synovec, Enhancing Gas Chromatography–Time of Flight Mass Spectrometry Data Analysis Using Two-Dimensional Mass Channel Cluster Plots, *Analytical Chemistry* 86 (2014) 3973–3979.
[45] R. Tauler, Multivariate curve resolution applied to second order data, *Chemometrics and Intelligent Laboratory* Systems 30 (1995) 133–146.
[46] R. Gargallo, R. Tauler, F. Cuesta-Sánchez, D.L. Massart, Validation of alternating least-squares multivariate curve resolution for chromatographic resolution and quantitation, *Trends Analytical Chemistry* 15 (1996) 279–286.
[47] A.K. Smilde, R. Tauler, J. Saurina, R. Bro, Calibration methods for complex second-order data, *Analytica Chimica Acta* 398 (1999) 237–251.
[48] J. Saurina, C. Leal, R. Compañó, M. Granados, M.D. Prat, R. Tauler, Estimation of figures of merit using univariate statistics for quantitative second-order multivariate curve resolution, *Analytica Chimica Acta* 432 (2001) 241–251.

[49] R.E. Synovec, E.S. Yeung, Comparison of an integration procedure to Fourier transform and data averaging procedures in chromatographic data analysis, *Analytical Chemistry* 58 (1986) 2093–2095.
[50] K.M. Pierce, B. Kehimkar, L.C. Marney, J.C. Hoggard, R.E. Synovec, Review of chemometric analysis techniques for comprehensive two dimensional separations data, *Journal of Chromatography A* 1255 (2012) 3–11.
[51] N.E. Watson, M.M. VanWingerden, K.M. Pierce, B.W. Wright, R.E. Synovec, Classification of high-speed gas chromatography–mass spectrometry data by principal component analysis coupled with piecewise alignment and feature selection, *Journal of Chromatography A* 1129 (2006) 111–118.
[52] S.N. Chesler, S.P. Cram, Effect of peak sensing and random noise on the precision and accuracy of statistical moment analyses from digital chromatographic data, *Analytical Chemistry* 43 (1971) 1922–1933.
[53] G. Guiochon, M.J. Sepaniak, Exchange of comments on data acquisition for chromatographic peaks, *Analytical Chemistry* 63 (1991) 73–73.
[54] J.S. Nadeau, R.B. Wilson, J.C. Hoggard, B.W. Wright, R.E. Synovec, Study of the interdependency of the data sampling ratio with retention time alignment and principal component analysis for gas chromatography, *Journal of Chromatography A* 1218 (2011) 9091–9101.
[55] J.S. Nadeau, B.W. Wright, R.E. Synovec, Chemometric analysis of gas chromatography–mass spectrometry data using fast retention time alignment via a total ion current shift function, *Talanta*. 81 (2010) 120–128.
[56] K.M. Pierce, J.L. Hope, K.J. Johnson, B.W. Wright, R.E. Synovec, Classification of gasoline data obtained by gas chromatography using a piecewise alignment algorithm combined with feature selection and principal component analysis, *Journal of Chromatography A* 1096 (2005) 101–110.
[57] Callis, J.B. Super Resolution in Chromatography by Numerical Deconvolution, in: Ultrahigh Resolution Chromatography. 1984.
[58] B.N. Colby, Spectral deconvolution for overlapping GC/MS components, *Journal of the American Society of Mass Spectrometry* 3 (1992) 558–562.
[59] X. Wei, X. Shi, S. Kim, J.S. Patrick, J. Binkley, M. Kong, et al., Data Dependent Peak Model Based Spectrum Deconvolution for Analysis of High Resolution LC-MS Data, *Analytical Chemistry* (2014).

5.6 Tables

Table 5.1 List of compounds in the 115 component mixture sorted by boiling point. * Indicates analyte used in creating *m/z* distributions in Figure 5.3A-5.3B.

Chemical	Mass (g)	BP (°C)	Vendor
pentane	0.2245	36	J.T. Baker
cyclopentane	0.2017	50	Sigma-Aldrich
ethyl formate	0.2183	54	Sigma-Aldrich
2-methylpentane	0.2065	60	Aldrich
1-chloroform	0.2082	61	Fischer
1-hexene	0.2093	63	Sigma-Aldrich
1-bromoheptane	0.2027	68	Sigma-Aldrich
hexane	0.2054	69	Sigma-Aldrich
1-hexyne	0.2112	71	Aldrich
methylcyclopentane	0.204	72	Fluka
1,1,1-trichloroethane	0.2127	75	Aldrich
carbon tetrachloride	0.1999	77	Aldrich
1-chlorobutane	0.208	78	Aldrich
2-butanone	0.2056	80	Sigma-Aldrich
benzene	0.2222	80	Fischer
1-bromooctane	0.2009	81	Sigma-Aldrich
cyclohexane	0.213	81	Sigma-Aldrich
2-methyl-2-propanol	0.2062	82	Aldrich
1,2-dichloroethane	0.2101	83	Aldrich
isopropyl alcohol	0.2982	83	EMD
1,6-dichlorohexane	0.2007	90	Aldrich
1-heptene	0.2066	94	Aldrich
1-propanol	0.2245	97	Sigma-Aldrich
heptane	0.2085	98	Sigma-Aldrich
2,2,4-trimethylpentane	0.2078	99	Sigma-Aldrich
methylcyclohexane	0.2134	101	Sigma-Aldrich

tert-amyl alcohol	0.2092	102	Aldrich
2-pentanone	0.2135	102	Sigma-Aldrich
isobutyl alcohol	0.2082	108	Baker
*1-heptyne	0.2005	109	Aldrich
* toluene	0.2122	111	Sigma-Aldrich
neopentyl alcohol	0.206	114	Aldrich
* 2,3,4-trimethylpentane	0.2092	114	Aldrich
2-butanol	0.2023	117	Sigma-Aldrich
* 1-butanol	0.2028	117	Aldrich
2-pentanol	0.2025	119	Aldrich
octane	0.2128	126	Sigma-Aldrich
3-hexanone	0.2117	128	Sigma-Aldrich
2-hexanone	0.2072	128	Aldrich
m-xylene	0.2007	128	Aldrich
* cis-1,2-dimethylcyclohexane	0.2086	130	Sigma-Aldrich
chlorobenzene	0.2041	131	Alfa-Aesar
1-chlorohexane	0.2222	134	Sigma-Aldrich
ethylbenzene	0.2142	136	Sigma-Aldrich
1-pentanol	0.2071	137	Sigma-Aldrich
3-heptanone	0.2032	141	Sigma-Aldrich
o-xylene	0.2098	145	Aldrich
cyclooctane	0.2108	150	Sigma-Aldrich
nonane	0.2179	151	Sigma-Aldrich
1-nonyne	0.2447	151	Aldrich
methly caproate	0.2062	151	Aldrich
2-heptanone	0.2131	152	Aldrich
anisole	0.2125	154	Aldrich
* bromobenzene	0.2154	155	Sigma-Aldrich
1-bromohexane	0.2361	158	Sigma-Aldrich
1-hexanol	0.1999	158	Sigma-Aldrich
* propylbenzene	0.2092	159	Sigma-Aldrich

2-heptanol	0.2101	160	Fluka
R-(-)-2,6-dimethyloctane	0.2124	160	Aldrich
cyclohexanol	0.2093	161	Aldrich
mesitylene	0.2075	163	Sigma-Aldrich
3-octanone	0.2115	167	Sigma-Aldrich
tert-butyl benzene	0.2057	167	Sigma-Aldrich
1,2,4-trimethylbenzene	0.2031	169	Aldrich
isobutylbenzene	0.2065	170	Sigma-Aldrich
sec-butyl benzene	0.2104	173	Sigma-Aldrich
* decane	0.2013	174	Sigma-Aldrich
5-decyne	0.2027	178	Aldrich
butylcyclohexane	0.2048	181	Sigma-Aldrich
* butylbenzene	0.2033	183	Sigma-Aldrich
1,2-propanediol	0.2069	188	Aldrich
p-xylene	0.2092	189	Aldrich
methyl caprylate	0.2289	193	Sigma-Aldrich
1-undecene	0.2118	194	Fluka
1-octanol	0.2763	194	Sigma-Aldrich
2-nonanone	0.2006	194	Sigma-Aldrich
undecane	0.2025	196	Sigma-Aldrich
benzyl alcohol	0.2036	205	Aldrich
1,3,5-trichlorobenzene	0.2013	208	Sigma-Aldrich
2-decanone	0.211	209	Sigma-Aldrich
1-octadecanol	0.2192	210	Aldrich
dodecene	0.207	214	Sigma
1-nonanol	0.2055	215	Sigma-Aldrich
dodecane	0.2093	216	Sigma-Aldrich
* naphthalene	0.2003	218	Sigma-Aldrich
1,2,3-trichlorobenzene	0.2364	218	Sigma-Aldrich
methyl salicylate	0.2035	220	Alfa-Aesar
methyl decanoate	0.2121	224	Eastman Chemicals

bicyclohexyl	0.2121	227	Sigma-Aldrich
1-decanol	0.2009	229	Sigma-Aldrich
1-geraniol	0.2076	230	Sigma-Aldrich
2-undecanone	0.2046	231	Sigma-Aldrich
ethyl salicylate	0.2066	234	Alfa-Aesar
tridecane	0.2063	235	Fluka
cyclohexylbenzene	0.2063	239	Sigma-Aldrich
2-dodecanone	0.2054	245	Sigma-Aldrich
1,2,4,5-tetrachlorobenzene	0.202	246	Aldrich
tetradecane	0.2243	254	Fluka
1-dodecanol	0.2096	256	Acros Organics
methyl laurate	0.2003	262	Sigma-Aldrich
pentadecane	0.2145	271	Alfa-Aesar
hexadecane	0.2163	287	Sigma-Aldrich
1-tetradecanol	0.2048	289	Sigma-Aldrich
2-pentadecanone	0.2053	293	Sigma-Aldrich
pristane	0.2061	296	Sigma-Aldrich
diethyl phthalate	0.2105	299	Aldrich
heptadecane	0.2085	302	ICN Biomedicals
benzophenone	0.2396	305	Sigma-Aldrich
octadecane	0.201	317	Fluka
nonadecane	0.205	330	Acros
phenanthrene	0.2023	340	Eastman
eicosane	0.202	343	Aldrich
1-hexadecanol	0.2034	344	Sigma-Aldrich
1-eicosanol	0.2002	372	Aldrich
adamantane	0.2116	sublimes	Sigma-Aldrich

5.7 Figures

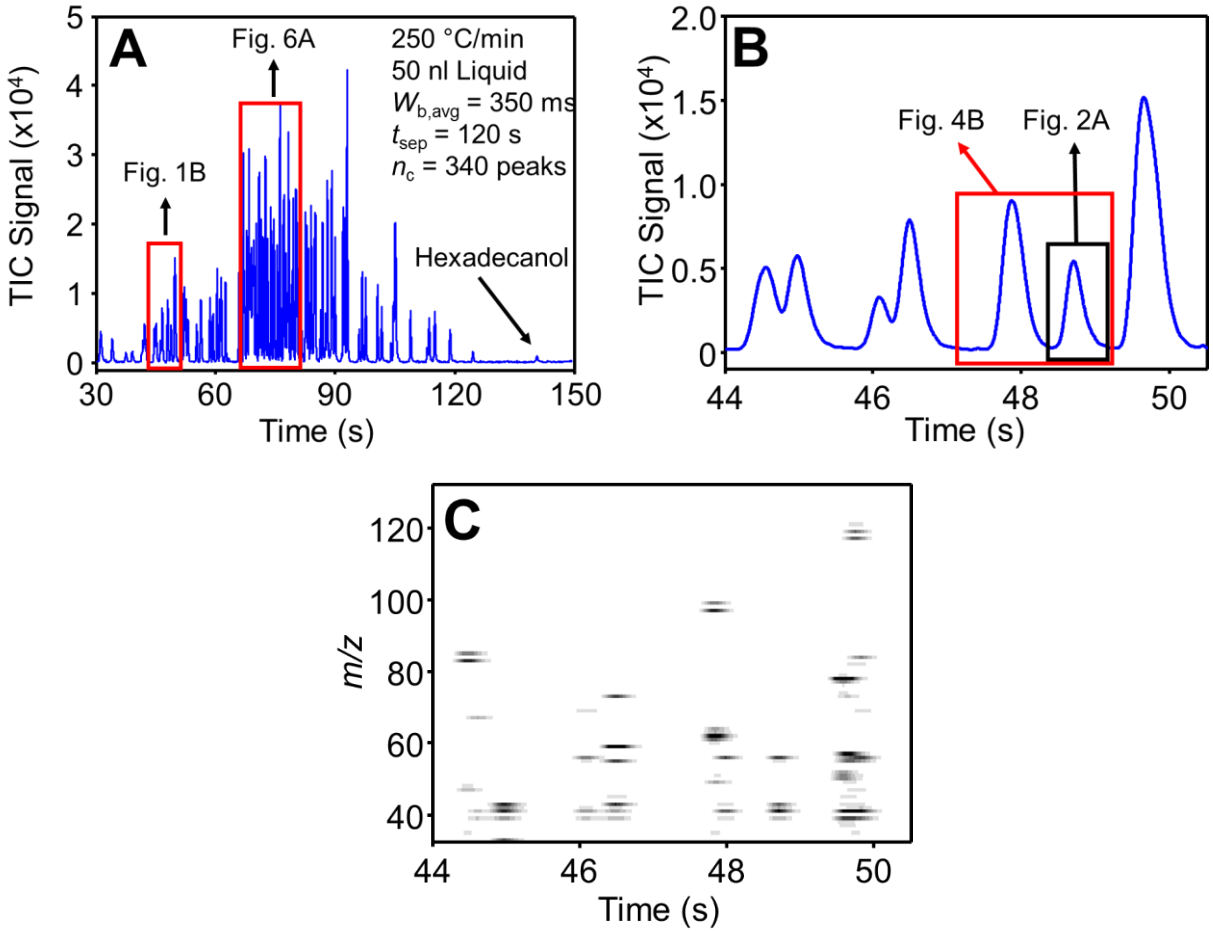

Figure 5.1 (A) Total ion current (TIC) chromatogram of the separation of the 115 component mixture by LTM-GC-TOFMS. (B) Region from (A) from 44-50 s focusing on what appears to be 7 peaks. (C) Traditional 2D GC-MS image plot of the region from (B) demonstrating multivariate nature of the data.

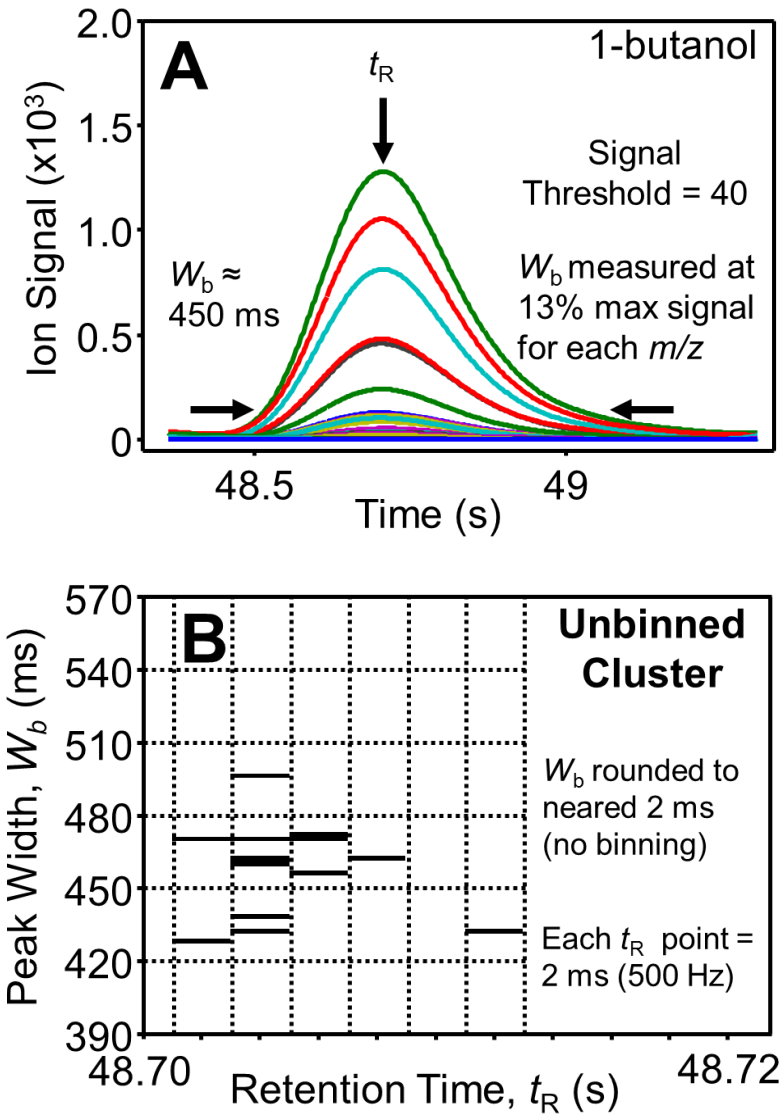

Figure 5.2 (A) 1-butanol peak with all *m/z* superimposed. Retention time, t_R, and peak width at base, W_b, measurements were made at indicated locations. (B) 2D *m/z* cluster plot of the data from (A). The W_b is plotted versus t_R for every peak above user defined signal threshold. Points in the plot with the same (t_R, W_b) coordinate are colored based upon the frequency of occurrence. The appearance of only black points indicates that no points are overlapped.

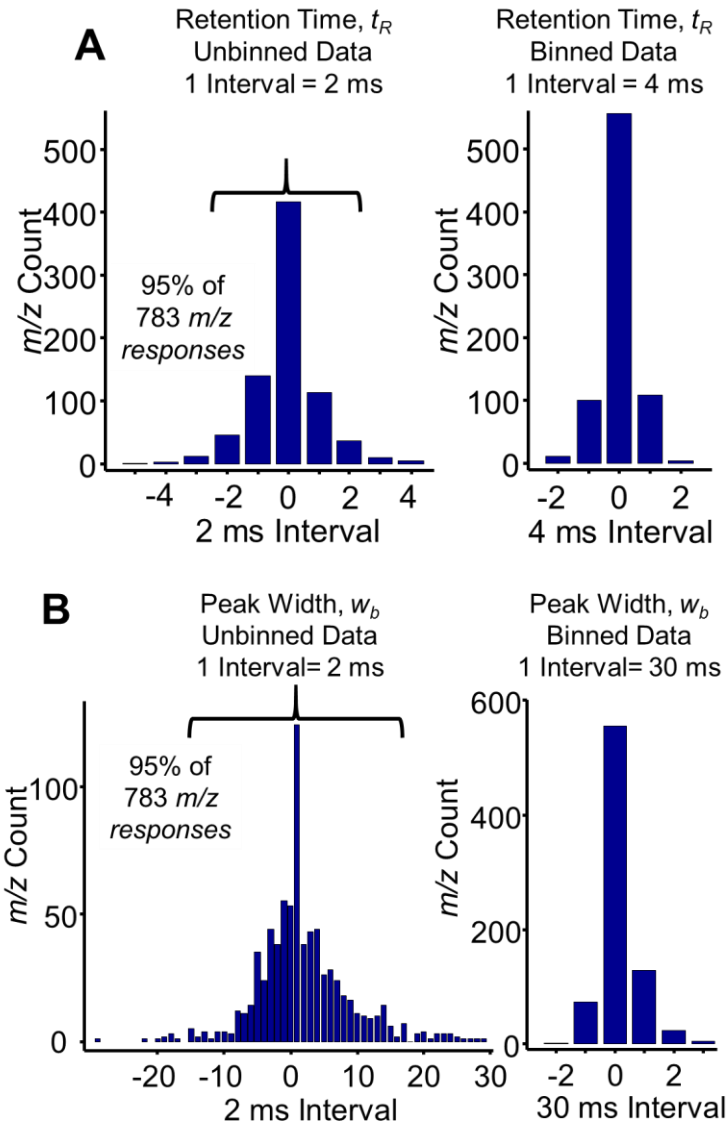

Figure 5.3 (A) Cumulative distributions for 30 pure *m/z* cluster plots (10 analytes with 3 injection replicates). Left: unbinned retention time (t_R) data. Right: Binned retention time (t_R) data by a factor of two. (B) Cumulative distributions for the same 30 pure *m/z* cluster plots from (A) but aligned in the width (W_b) dimension. Left: unbinned width data. Right: Binned width data by a factor of 15. See text for description of cluster alignment and binning.

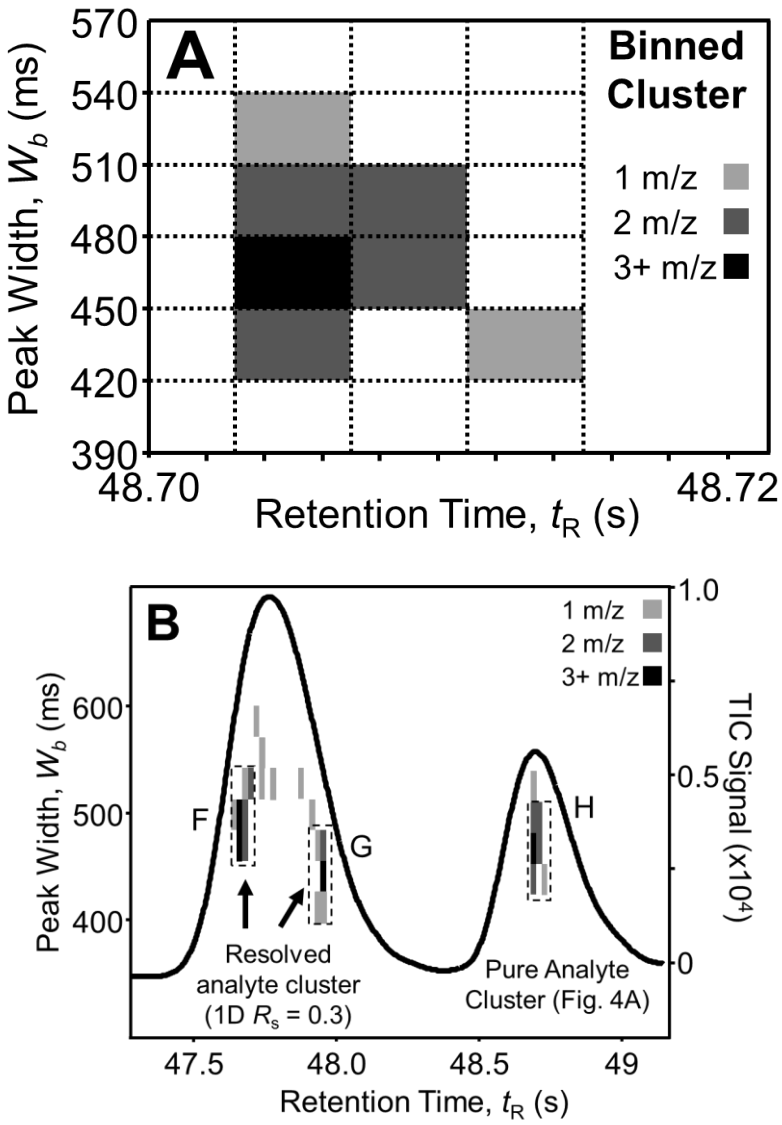

Figure 5.4 (A) 2D *m/z* cluster plot of the binned 1-butanol cluster. (B) 2D *m/z* cluster plot overlaid with the TIC from 47-49 s from the separation in Figure 5.1(B) demonstrating the 2D *m/z* cluster method. Legend: 1 *m/z* – light grey; 2 *m/z* – dark grey; 3 or more *m/z* – black.

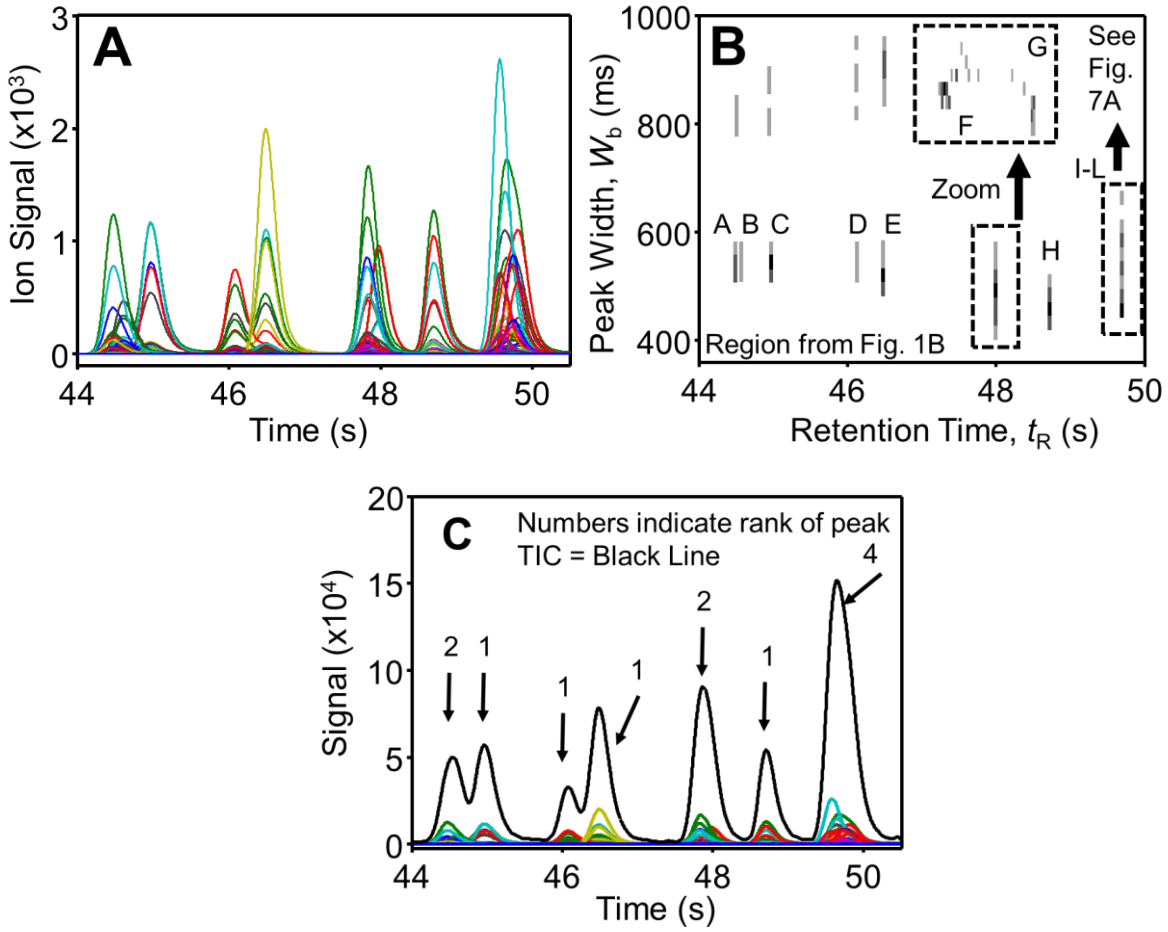

Figure 5.5 (A) Superimposed ion chromatogram (all *m/z*) from region in Figure 1(B) showing peak overlap and difficulty in obtaining accurate peak rank of overlapped analytes. (B) Cluster plot from (A). Peaks labeled A-L after identification using MCR-ALS: A-chloroform, B-1-hexyne, C-isobutanol, D-methylcyclopentane, E-t-amyl alcohol, F-1, 1, 1-trichloroethane, G-1-chlorobutane, H-1-butanol, I-benzene, J-neopentyl alcohol, K-cyclohexane, L-carbon tetrachloride. Overlapped analytes are indicated with locations in the 2D space with inflated W_b. (C) Superimposed ion chromatogram with TIC overlay indicating rank of each peak not visible from the TIC alone.

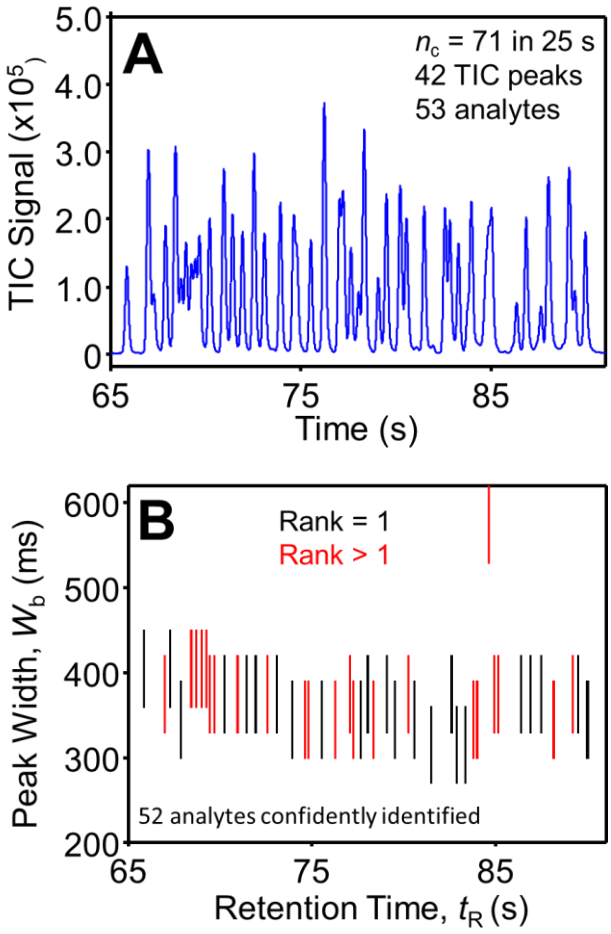

Figure 5.6 (A) (A) TIC of the region from 65-90 s from Figure 5.1(A). (B) Cluster plot from the region in (A) where each analyte is indicated by a vertical line 90 ms tall, from distribution in Figure 3(B) where clusters of rank 1 are black and clusters with rank greater than 1 are red

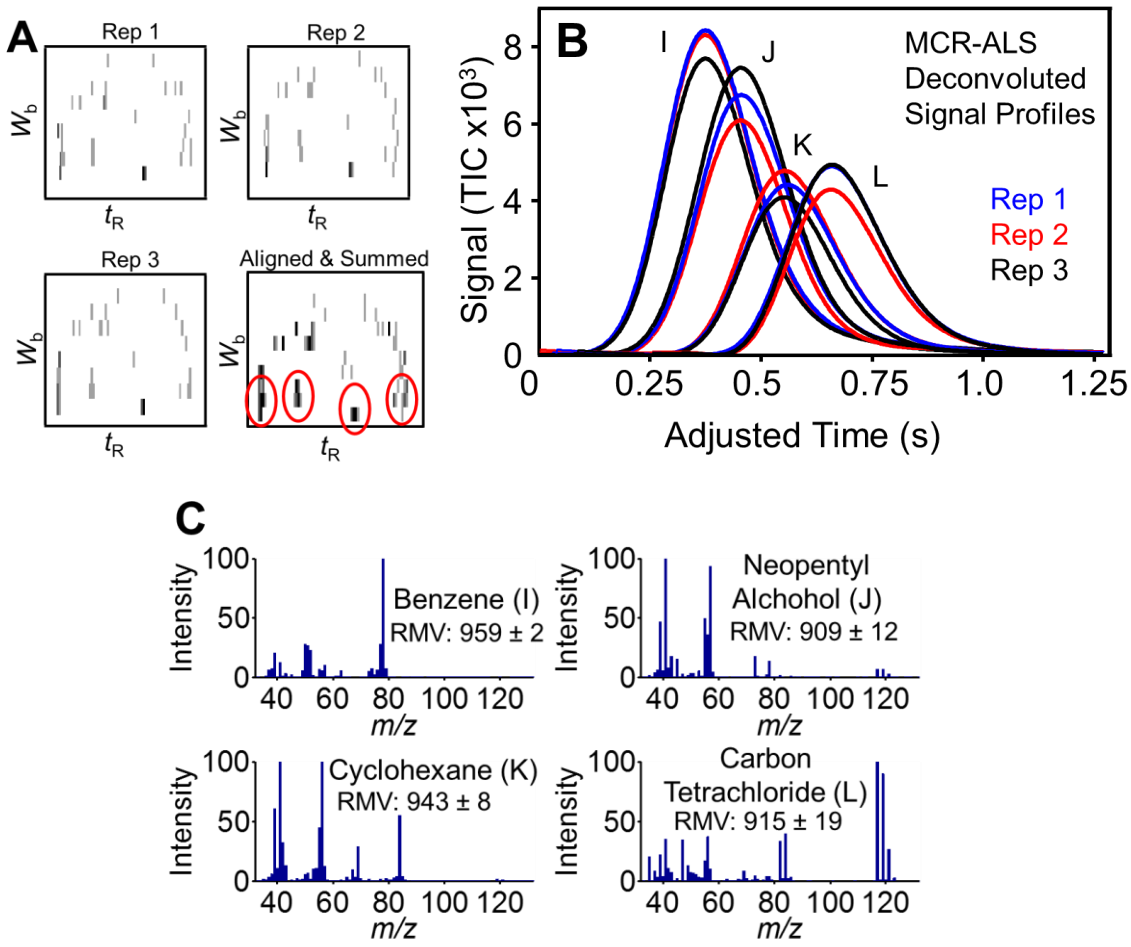

Figure 5.7 (A) Replicate (1-3) cluster plots from peak labeled I-L in Figure 5.5(A-C). The bottom right panel, 'Aligned & Summed' is the summations of the data from panels 1-3. The pure *m/z* for each analyte are located in the red circles. (B) MCR-ALS deconvolution profiles of the 4 analytes from Figure 6(A). (C) Deconvoluted mass spectra from the 4 analytes in (B) with match value for replicate analyses given.

Chapter 6. Conclusion

6.1 Summary of presented work

Gas chromatography is the workhorse of modern analytical chemistry for a wide variety of sample types that are analyzed in many scientific disciplines. As samples become increasingly complex and higher sample throughput is desired, new strategies for separating and analyzing the resulting data are required. The goal of the presented work was aimed at exploring ways to increase the peak capacity and peak capacity production of GC instruments to allow for more complex samples to be analyzed with sufficient resolution, to perform the analysis in a faster timeframe than is currently performed while maintaining separation figures of merit, and to evaluate the development of a novel chemometric approach to visualizing and processing GC-TOFMS data.

The first two chapters focused on the exploration of novel instrumental technologies to reduce the separation time of chromatographic analyses while maintaining similar figures of merit, namely peak capacity and peak capacity production. Providing rapid sample introduction through high-speed cryo-focusing injection, HSCFI, gave rise to peak capacity and peak capacity production values that were an order of magnitude higher compared to those produced with standard instrumentation. Chapter 2 utilized an LTM-GC to perform a traditional temperature program range (~50 - 250 °C) in 1 minute while achieving a peak capacity of nearly 300 for a liquid test sample, which is similar peak capacity in only ~7% of the time of a standard run. Chapter 3 focused on applying HSCFI to two-dimensional gas chromatography to achieve a theoretical maximum peak capacity production of 1,000 peaks/min for a total peak capacity of 6,000 in a 6 minute separation. This is an order of magnitude better than traditional instrumentation which produces ~100 peaks/minute for 60 minutes.

The last two chapters primarily focused on a novel chemometric data analysis algorithm, the mass cluster method, to produce mathematically higher peak capacities from the resulting GC-TOFMS data. The algorithm transformed GC-TOFMS data from a signal versus time format to a peak width versus time format. The data was plotted such that each peak was represented by a cluster of points resulting from the peak width and retention time measurements for each *m/z* for each peak in the sample. It was found that the peak width dimension, which had not been previously exploited, provided useful chemical information. In Chapter 4, the initial development of the algorithm was described and the peak capacity gains were significant, nearly a 100-fold increase compared to the standard signal versus time data format. A resolution of 0.03 was also found to be the limit of resolution using classical least squares deconvolution, which is an order of magnitude better than most chemometric deconvolution algorithms. In Chapter 5 the combination of instrumentation to produce high peak capacities (LTM-TOFMS) and the mass cluster method proved to be successful in increasing sample throughput and peak capacity. A peak capacity of 10,000 in 120s was produced for a peak capacity production of 5,000 peaks/min, which is significantly higher than traditional 1D GC-TOFMS can provide. The use of a different chemometric tool, multivariate curve resolution (MCR-ALS), was demonstrated to work in conjunction with the benefits of the mass cluster method.

6.2 Future directions of fast, high peak capacity GC and data analysis techniques

6.2.1 Future instrumental improvements

A possible initial direction for future research would be studying the use of LTM-TOFMS at faster heating rates. The LTM system used has a maximum heating rate of 1,800 °C/min, but was only studied at 250 °C/min. Results from Chapter 2 showed that thermal injection provided additional peak capacity improvements over standard auto-injection, A newly

developed diaphragm valve from Valco Instrument Co, Inc. (Houston, TX) has been made available which has a higher maximum operating temperature than previous valves. Regular diaphragm valves have a limit of ~ 175 °C. The temperature limit is due the rubber o-rings inside the valve body. The new valves have a special high-temperature perfluoroelastomer that can tolerate temperatures as high as 325 °C. These new valves would be useful for performing rapid sample introduction without the low-temperature limits of previous valves and also increased usability compared to the HSCFI apparatus. Using these high-temperature valves in conjunction with the LTM operating at 1,800 °C/min could provide even higher peak capacity production values than before. Figure 6.1 shows some initial results from a high-temperature valve injection onto the LTM-GC-FID. The peak widths range from ~100 ms on the narrow end to 140 ms on the wider end. The initial results show that the valve can provide narrower peaks than standard auto-injection (Chapter 2) with limited sampling bias.

6.2.2 Future improvements to data analysis techniques

There are several directions that could provide fruitful results from further development and studies of the two-dimensional mass cluster method. One of the points of discussion from Chapter 5 was to use the mass cluster method as a means of accurately measuring the true number of peaks in a sample. Traditional peak finding algorithms often only operate on the total ion chromatogram (TIC) and fail to find peaks with low resolution ($R_s < 0.4$). The mass cluster method was proven to have resolving power an order of magnitude lower than that, at $R_s = 0.03$. Statistical peak overlap theory, developed by Davis, is used to explain the amount of analyte saturation in chromatographic separations. The goal of the proposed work would be to study how the mass cluster method could be used in quantifying the increase of resolving power compared to traditional resolution. Figure 6.2A shows a simulated GC-TOFMS TIC chromatogram with a

saturation value of 50%, meaning 50% of the usable separation space is taken up by peaks. Figure 6.2B shows the resulting 2D *m/z* cluster plot of the data from Figure 6.2A. The cluster dimensions are similar to that in Chapter 4, i.e. 30 ms wide. The saturation value of the cluster plot is only 0.003, which is a 160 times lower than the simulated chromatogram. The cluster plot also identified 46 out of 50 possible analytes, whereas the TIC separation only determined 23 peaks.

Another direction of future research would be to apply the 2D *m/z* cluster method to a suitably complex sample that would benefit from the increased analyte resolution and deconvolution ability of the technique. Current research is studying the metabolomic flux of methylotrophic bacteria *M. Extorquens* AM1. The project is a semi-targeted metabolomic analysis of isotopically changing biomarkers. Figure 6.3A is the TIC chromatogram from a 1D GC-TOFMS separation. Using a traditional peak finding algorithm on the TIC, 101 peaks are detected. Figure 6.3B is the 2D *m/z* cluster plot of the data from Figure 6.3A. There are 50% more peaks detected, due to the increased resolving power of the method. Many of these peaks require deconvolution to obtain suitably pure spectra. The manuscript is currently under preparation for submission by Reaser, B.C. and Synovec, R.E.

A different avenue of future work would be to add additional functionality to the graphical user interface (GUI) that is used in conjunction with the aforementioned algorithm. The GUI allows for plotting of the 2D *m/z* cluster plots (from W_b and W_{HH} measurements), the TIC, the XIC (extracted ion chromatogram), and the full ion chromatogram (all *m/z*). It also allows the user to obtain a mass spectra at any point in the chromatogram (clicking any chromatographic point with a cursor) and allows for the deconvolution of peaks up to the rank of 4. The data (cluster plots, spectra, deconvolution profiles) can be saved to the Matlab workspace.

Future improvements would be to add MCR-ALS to the list of deconvolution tools (Chapter 5). Additionally, adding some automation to the determination of number of pure vs. overlapped clusters in the 2D *m/z* cluster plot would help streamline the usage. The GUI was developed in Matlab R2012b. Future releases of Matlab may alter some functionalities of the preexisting code, so creating an executable that could be run on multiple machines may be useful. Finally, adding extra support for alternative data structure (other than GC-TOFMS) would be useful for others users who may not have the exact instrumentation the software was developed for.

6.3 Figures

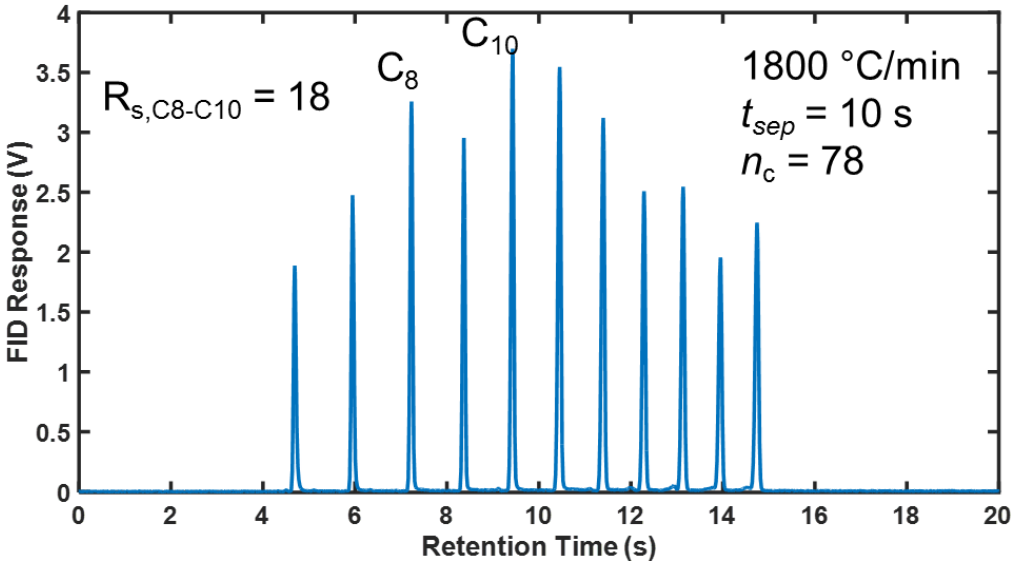

Figure 6.1 LTM-GC-FID separation of an 11 component hydrocarbon mixture (n-alkanes from hexane (C_6) to hexadecane (C_{16}) injected with a high temperature valve. The peak widths range from 101.5 ms to 141 ms.

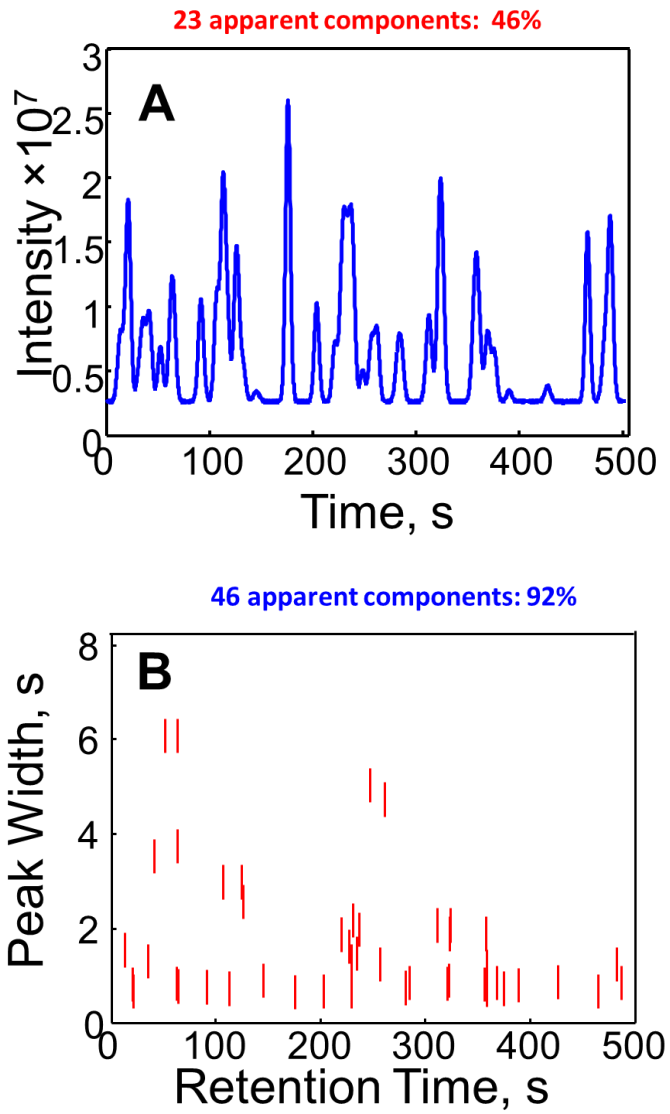

Figure 6.2 (A) Simulated GC-TOFMS TIC chromatogram of 50 components with a 50% saturation value (50% of the separation space is occupied with peaks). Only 46% of peaks were successfully identified with a traditional peak finder. (B) Two-dimensional mass cluster plot of (A). Clusters are 30 ms wide which provides a saturation value of only 0.003 (0.3% of space is occupied with peaks). 92 % of components were successfully identified.

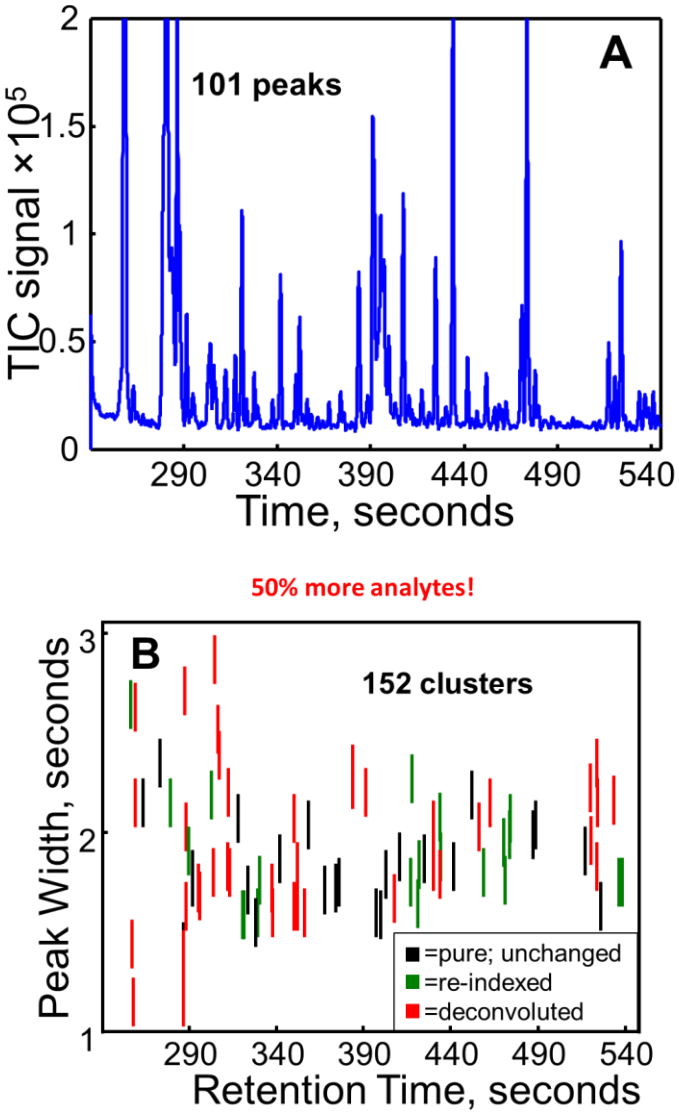

Figure 6.3 (A) TIC chromatogram of TMS derivatized *M. Extorquens* AM1 bacterial metabolite extract. 101 peaks are detected using a peak finding algorithm. (B) 2D *m/z* cluster plot of the data from (A). 50% more peaks are detected than conventional peak finding.

Bibliography

L.A. Adutwum, J.J. Harynuk, Unique Ion Filter: A Data Reduction Tool for GC/MS Data Preprocessing Prior to Chemometric Analysis, *Analytical Chemistry* 86 (2014) 7726–7733.

Agilent LTM Column Module, http://www.chem.agilent.com/en-US/products-services/Columns Sample-Preparation/GC-GC-MS-Columns/5975T-LTM-Column-Module/Pages/default.aspx.

E. Alm, R.J.O. Torgrip, K.M. Åberg, I. Schuppe-Koistinen, J. Lindberg, Time-resolved biomarker discovery in 1H-NMR data using generalized fuzzy Hough transform alignment and parallel factor analysis, *Analytical and Bioanalytical Chemistry* 396 (2010) 1681–1689.

J.L. Anderson, D.W. Armstrong, High-Stability Ionic Liquids. A New Class of Stationary Phases for Gas Chromatography, *Analytical Chemistry* 75 (2003) 4851–4858.

J.L. Anderson, D.W. Armstrong, Immobilized Ionic Liquids as High-Selectivity/High-Temperature/High-Stability Gas Chromatography Stationary Phases, *Analytical Chemistry* 77 (2005) 6453–6462.

J.L. Anderson, J. Ding, T. Welton, D.W. Armstrong, Characterizing Ionic Liquids on the Basis of Multiple Solvation Interactions, *Journal of the American Chemical Society*. 124 (2002) 14247–14254.

A. Ansari, J. Berendzen, S.F. Bowne, H. Frauenfelder, I.E. Iben, T.B. Sauke, et al., Protein states and proteinquakes, *Proceedings of the National Academy of Sciences* 82 (1985) 5000.

D.W. Armstrong, L. He, Y.-S. Liu, Examination of Ionic Liquids and Their Interaction with Molecules, When Used as Stationary Phases in Gas Chromatography, *Analytical Chemistry* 71 (1999) 3873–3876.

P. Ausloos, C.L. Clifton, S.G. Lias, A.I. Mikaya, S.E. Stein, D.V. Tchekhovskoi, et al., The critical evaluation of a comprehensive mass spectral library, *Journal of the American Society for Mass Spectrometry* 10 (1999) 287–299.

B.M.F. Ávila, B.G. Vaz, R. Pereira, A.O. Gomes, R.C.L. Pereira, Y.E. Corilo, et al., Comprehensive Chemical Composition of Gas Oil Cuts Using Two-Dimensional Gas Chromatography with Time-of-Flight Mass Spectrometry and Electrospray Ionization Coupled to Fourier Transform Ion Cyclotron Resonance Mass Spectrometry, *Energy Fuels* 26 (2012) 5069–5079

S.A. Batts, C.R. Shoemaker, Y. Raphael, Notch signaling and Hes labeling in the normal and drug-damaged organ of Corti, *Hearing Research* 249 (2009) 15–22.

K.R. Beebe, B.R. Kowalski, An Introduction to Multivariate Calibration and Analysis, *Analytical Chemistry* 59 (1987) 1007A–1017A.

Beebe, K. R.; Pell, R. J.; Seasholtz, M. B. *Chemometrics: A Practical Guide*; John Wiley & Sons, Inc., 1998.

J. Beltran, E. Serrano, F.J. López, A. Peruga, M. Valcarcel, S. Rosello, Comparison of two quantitative GC–MS methods for analysis of tomato aroma based on purge-and-trap and on solid-phase microextraction, *Analytical and Bioanalytical Chemistry* 385 (2006) 1255–1264.

V.G. Berezkin, I.V. Malyukova, D.S. Avoce, Use of equations for the description of

experimental dependence of the height equivalent to a theoretical plate on carrier gas velocity in capillary gas–liquid chromatography, *Journal of Chromatography A* 872 (2000) 111–118.
N.A. Bermingham, Math1: An Essential Gene for the Generation of Inner Ear Hair Cells, *Science* 284 (1999) 1837–1841.
O. Bermingham-McDonogh, E.C. Oesterle, J.S. Stone, C.R. Hume, H.M. Huynh, T. Hayashi, Expression of Prox1 during mouse cochlear development, *The Journal of Comparative Neurology* 496 (2006) 172–186.
A. Berthod, J.J. Kozak, J.L. Anderson, J. Ding, D.W. Armstrong, Ionic liquid-alkane association in dilute solutions, *Theoretical Chemistry Accounts* 117 (2006) 127–135.
C. Bicchi, C. Brunelli, C. Cordero, P. Rubiolo, M. Galli, A. Sironi, High-speed gas chromatography with direct resistively-heated column (ultra-fast module-GC)-separation measure (S) and other chromatographic parameters under different analysis conditions for samples of different complexities and volatilities, *Journal of Chromatography A* 1071 (2005) 3–12.
T.G. Bloemberg, J. Gerretzen, A. Lunshof, R. Wehrens, L.M.C. Buydens, Warping methods for spectroscopic and chromatographic signal alignment: A tutorial, *Analytica Chimica Acta* 781 (2013) 14–32.
L.M. Blumberg, F. David, M.S. Klee, P. Sandra, Comparison of one-dimensional and comprehensive two-dimensional separations by gas chromatography, *Journal of Chromatography A* 1188 (2008) 2–16.
A.J. Borgerding, C.W. Wilkerson, A Comparison of Cryo-focusing Injectors for Gas Sampling and Analysis in Fast GC, *Analytical Chemistry* 68 (1996) 2874–2878.
D. Bourgeois, B. Vallone, F. Schotte, A. Arcovito, A.E. Miele, G. Sciara, et al., Complex landscape of protein structural dynamics unveiled by nanosecond Laue crystallography, *Proceedings of the National Academy of Sciences* 100 (2003) 8704.
C. Brasseur, J. Dekeirsschieter, E.M.J. Schotsmans, S. de Koning, A.S. Wilson, E. Haubruge, et al., Comprehensive two-dimensional gas chromatography–time-of-flight mass spectrometry for the forensic study of cadaveric volatile organic compounds released in soil by buried decaying pig carcasses, *Journal of Chromatography A* 1255 (2012) 163–170.
R. Bro, S. de Jong, A Fast non-negativity constrained least squares algorithm, *Journal of Chemometrics* 11 (1997) 393–401.
R. Bro, PARAFAC. Tutorial and applications, *Chemometrics and Intelligent Laboratory Systems* 38 (1997) 149–171.
C.A. Bruckner, B.J. Prazen, R.E. Synovec, Comprehensive Two-Dimensional High-Speed Gas Chromatography with Chemometric Analysis, *Analytical Chemistry* 70 (1998) 2796–2804.
G.L. Burleson, B. Gonzalez, K. Simons, J.C.C. Yu, Forensic analysis of a single particle of partially burnt gunpowder by solid phase micro-extraction–gas chromatography-nitrogen phosphorus detector, *Journal of Chromatography A* 1216 (2009) 4679–4683.
J. Cafaro, G.S. Lee, J.S. Stone, Atoh1 expression defines activated progenitors and differentiating hair cells during avian hair cell regeneration, *Developmental Dynamics* 236 (2007) 156–170.
J.B. Callis, Super Resolution in Chromatography by Numerical Deconvolution, in: *Ultrahigh Resolution Chromatography*, 1984.

T.E. Carver, R.E. Brantley Jr, E.W. Singleton, R.M. Arduini, M.L. Quillin, G.N. Phillips Jr, et al., A novel site-directed mutant of myoglobin with an unusually high O2 affinity and low autooxidation rate. *Journal of Biological Chemistry* 267 (1992) 14443–14450.
A. Casilli, E. Decorzant, A. Jaquier, E. Delort, Multidimensional gas chromatography hyphenated to mass spectrometry and olfactometry for the volatile analysis of citrus hybrid peel extract, *Journal of Chromatography A* 1373 (2014) 169–178.
H.N. Chapman, M. Frank, S. Chung, R. London, R. Balhorn, M. Howells, et al., FY05 LDRD Final Report, A Revolution in Biological Imaging, United States. Department of Energy, 2006.
H.N. Chapman, P. Fromme, A. Barty, T.A. White, R.A. Kirian, A. Aquila, et al., Femtosecond X-ray protein nanocrystallography, *Nature* 470 (2011) 73–77.
N.H. Chen, D.F. Othmer, New Generalized Equation for Gas Diffusion Coefficient, *Journal of Chemical Engineering Data* 7 (1962) 37–41.
S.N. Chesler, S.P. Cram, Effect of peak sensing and random noise on the precision and accuracy of statistical moment analyses from digital chromatographic data, *Analytical Chemistry* 43 (1971) 1922–1933.
D.F. Chollet, E. Castella, L. Goumaz, G. Anderegg, Gas chromatography–mass spectrometry assay method for the therapeutic drug monitoring of the antiepileptic drug tiagabine, *Journal of Pharmaceutical and Biomedical Analysis* 21 (1999) 641–646.
B.N. Colby, Spectral deconvolution for overlapping GC/MS components, *Journal of the American Society for Mass Spectrometry* 3 (1992) 558–562.
G. Contarini, M. Povolo, Volatile Fraction of Milk: Comparison between Purge and Trap and Solid Phase Microextraction Techniques, *Journal of Agricultural and Food Chemistry* 50 (2002) 7350–7355.
J.A. Contreras, A.L. Rockwood, H.D. Tolley, M.L. Lee, Peak sweeping and gating using thermal gradient gas chromatography, *Journal of Chromatography A* 1278 (2013) 160–165.
J.A. Contreras, A. Wang, A.L. Rockwood, H.D. Tolley, M.L. Lee, Dynamic thermal gradient gas chromatography, *Journal of Chromatography A* 1302 (2013) 143–151.
M.A. Crumling, Y. Raphael, Manipulating gene expression in the mature inner ear, *Brain Research* 1091 (2006) 265–269.
L. Csenki, E. Alm, R.J.O. Torgrip, K.M. Åberg, L.I. Nord, I. Schuppe-Koistinen, et al., Proof of principle of a generalized fuzzy Hough transform approach to peak alignment of one-dimensional 1H NMR data, *Analytical and Bioanalytical Chemistry* 389 (2007) 875–885.
J. Dallüge, J. Beens, U.A.Th. Brinkman, Comprehensive two-dimensional gas chromatography: a powerful and versatile analytical tool, *Journal of Chromatography A* 1000 (2003) 69–108.
R. Danielsson, D. Bylund, K.E. Markides, Matched filtering with background suppression for improved quality of base peak chromatograms and mass spectra in liquid chromatography–mass spectrometry, *Analytica Chimica Acta* 454 (2002) 167–184.
M. Daszykowski, B. Walczak, D.L. Massart, Looking for natural patterns in data: Part 1. Density-based approach, *Chemometrics and Intelligent Laboratory Systems* 56 (2001) 83–92.
J.M. Davis, Justification of probability density function for resolution in statistical models of overlap, *Chromatographia* 44 (1997) 81–90.
J.M. Davis, P.W. Carr, Effective Saturation: A More Informative Metric for Comparing Peak

Separation in One- and Two-Dimensional Separations, *Analytical Chemistry* 81 (2009) 1198–1207.
J.M. Davis, J.C. Giddings, Statistical theory of component overlap in multicomponent chromatograms, *Analytical Chemistry* 55 (1983) 418–424.
J.M. Davis, J.C. Giddings, Statistical method for estimation of number of components from single complex chromatograms: application to experimental chromatograms, *Analytical Chemistry* 57 (1985) 2178–2182.
J.M. Davis, J.C. Giddings, Statistical method for estimation of number of components from single complex chromatograms: theory, computer-based testing, and analysis of errors, *Analytical Chemistry* 57 (1985) 2168–2177.
J.M. Davis, M. Pompe, C. Samuel, Justification of Statistical Overlap Theory in Programmed Temperature Gas Chromatography: Thermodynamic Origin of Random Distribution of Retention Times, *Analytical Chemistry* 72 (2000) 5700–5713.
J.M. Davis, D.R. Stoll, P.W. Carr, Effect of First-Dimension Undersampling on Effective Peak Capacity in Comprehensive Two-Dimensional Separations, *Analytical Chemistry* 80 (2008) 461–473.
J.M. Davis, Experimental affirmation of the statistical model of overlap, *Journal of Chromatography A* 449 (1988) 41–52.
J.M. Davis, Statistical Theory of Overlap for Variable Poisson Density: Relaxation of Constraint of Randomness, *Analytical Chemistry* 66 (1994) 735–746.
J.M. Davis, Extension of Statistical Overlap Theory to Poorly Resolved Separations, *Analytical Chemistry* 69 (1997) 3796–3805.
J.M. Davis, Prediction of numbers of singlets, doublets, and triplets in poorly resolved separations by statistical-overlap theory, *Journal of Chromatography A* 831 (1999) 37–49.
T.I. Dearing, J.S. Nadeau, B.G. Rohrback, L.S. Ramos, R.E. Synovec, Real-time target selection optimization to enhance alignment of gas chromatograms, *Talanta*. 83 (2011) 738–743.
H.-J. de Geus, J. de Boer, J.B. Phillips, E.B. Ledford, U.A.T. Brinkman, Increased Signal Amplitude due to Mass Conservation in a Thermal Desorption Modulator, *Journal of High Resolution Chromatography* 21 (1998) 411–413.
A.P. de la Mata, J.J. Harynuk, Limits of Detection and Quantification in Comprehensive Multidimensional Separations. 1. A Theoretical Look, *Analytical Chemistry* 84 (2012) 6646–6653.
C. Devos, N. Ochiai, K. Sasamoto, P. Sandra, F. David, Full evaporation dynamic headspace in combination with selectable one-dimensional/two-dimensional gas chromatography–mass spectrometry for the determination of suspected fragrance allergens in cosmetic products, *Journal of Chromatography A* 1255 (2012) 207–215.
A. dos Santos Pereira, S.A. Carbonell, F.R. de Aquino Neto, A.C.F. do Amaral, R.A. Barnes, High-temperature gas chromatography–mass spectrometry with glass capillary columns for the screening of natural products, *Journal of Chromatography A* 947 (2002) 255–265.
R.G. Dromey, M.J. Stefik, T.C. Rindfleisch, A.M. Duffield, Extraction of mass spectra free of background and neighboring component contributions from gas chromatography/mass spectrometry data, *Analytical Chemistry* 48 (1976) 1368–1375.
E.M.H. Duke, L.N. Johnson, Macromolecular crystallography at synchrotron radiation sources: current status and future developments, *Proceedings of the Royal Society A: Mathematical, Physical and Engineering Sciences* 466 (2010) 3421–3452.

E. Dumont, B. Tienpont, N. Higashi, K. Mitsui, N. Ochiai, H. Kanda, et al., Heart-cutting two-dimensional gas chromatography in combination with isotope ratio mass spectrometry for the characterization of the wax fraction in plant material, *Journal of Chromatography A* 1317 (2013) 230–238.
E.U. Ehrmann, H.P. Dharmasena, K. Carney, E.B. Overton, Novel Column Heater for Fast Capillary Gas Chromatography, *Journal of Chromatographic Science* 34 (1996) 533–539.
M. Ester, H.-P. Kriegel, J. Sander, X. Xu, DBSCAN: A density-based algorithm for discovering clusters in large spatial databases with noise., in: *KDD*, 1996: pp. 226–231.
B.A. Ewels, R.D. Sacks, Electrically-heated cold trap inlet system for high-speed gas chromatography, *Analytical Chemistry* 57 (1985) 2774–2779.
A. Felinger, A. Kilár, B. Boros, The myth of data acquisition rate, *Analytica Chimica Acta* 854 (2015) 178–182.
A.B. Fialkov, M. Morag, A. Amirav, A low thermal mass fast gas chromatograph and its implementation in fast gas chromatography mass spectrometry with supersonic molecular beams, *Journal of Chromatography A* 1218 (2011) 9375–9383.
M.R. Filgueira, C.B. Castells, P.W. Carr, A Simple, Robust Orthogonal Background Correction Method for Two-Dimensional Liquid Chromatography, *Analytical Chemistry* 84 (2012) 6747–6752.
B.D. Fitz, B.C. Mannion, K. To, T. Hoac, R.E. Synovec, Evaluation of injection methods for fast, high peak capacity separations with low thermal mass gas chromatography, *Journal of Chromatography A* 1392 (2015) 82–90.
B.D. Fitz, B.C. Reaser, D.K. Pinkerton, J.C. Hoggard, K.J. Skogerboe, R.E. Synovec, Enhancing Gas Chromatography–Time of Flight Mass Spectrometry Data Analysis Using Two-Dimensional Mass Channel Cluster Plots, *Analytical Chemistry* 86 (2014) 3973–3979.
B.D. Fitz, R.B. Wilson, B.A. Parsons, J.C. Hoggard, R.E. Synovec, Fast, high peak capacity separations in comprehensive two-dimensional gas chromatography with time-of-flight mass spectrometry, *Journal of Chromatography A* 1266 (2012) 116–123.
J.P. Foley, J.G. Dorsey, Equations for calculation of chromatographic figures of merit for ideal and skewed peaks, *Analytical Chemistry* 55 (1983) 730–737.
C.G. Fraga, Chemometric approach for the resolution and quantification of unresolved peaks in gas chromatography–selected-ion mass spectrometry data, *Journal of Chromatography A* 1019 (2003) 31–42.
C.G. Fraga, C.A. Bruckner, R.E. Synovec, Increasing the Number of Analyzable Peaks in Comprehensive Two-Dimensional Separations through Chemometrics, *Analytical Chemistry* 73 (2001) 675–683.
E. Fuller, P. Schettler,, J.C. Giddings, A new Method for prediction of binary gas-phase diffusion coefficients, *Industrial & Engineering Chemistry* 58 (1966) 18–27.
D. Gaddes, J. Westland, F.L. Dorman, S. Tadigadapa, Improved micromachined column design and fluidic interconnects for programmed high-temperature gas chromatography separations, *Journal of Chromatography A* 1349 (2014) 96–104.
R. Gargallo, R. Tauler, F. Cuesta-Sánchez, D.L. Massart, Validation of alternating least-squares multivariate curve resolution for chromatographic resolution and quantitation, *Trends in Analytical Chemistry* 15 (1996) 279–286.
G. Gaspar, R. Annino, C. Vidal-Madjar, G. Guiochon, Influence of instrumental contributions on

the apparent column efficiency in high speed gas chromatography, *Analytical Chemistry* 50 (1978) 1512–1518.
G. Gaspar, P. Arpino, G. Guiochon, Study in High Speed Gas Chromatography I. Injections of Narrow Sample Plugs, *Journal of Chromatographic Science* 15 (1977) 256–261.
J.A. Giannovario, R.J. Gondek, R.L. Grob, A cryogenic gas chromatograph, *Journal of Chromatography A* 89 (1974) 1–9.
M. Gilar, J. Fridrich, M.R. Schure, A. Jaworski, Comparison of Orthogonality Estimation Methods for the Two-Dimensional Separations of Peptides, *Analytical Chemistry* 84 (2012) 8722–8732.
G.D. Goodno, V. Astinov, R.J.D. Miller, Femtosecond Heterodyne-Detected Four-Wave-Mixing Studies of Deterministic Protein Motions. 2. Protein Response, *The Journal of Physical Chemistry A* 103 (1999) 10630–10643.
T. Graber, S. Anderson, H. Brewer, Y.S. Chen, H. Cho, N. Dashdorj, et al., BioCARS: a synchrotron resource for time-resolved X-ray science, *Journal of Synchrotron Radiation* 18 (2011) 658–670.
G.M. Gross, B.J. Prazen, J.W. Grate, R.E. Synovec, High-Speed Gas Chromatography Using Synchronized Dual-Valve Injection, *Analytical Chemistry* 76 (2004) 3517–3524.
G. Guiochon, M.J. Sepaniak, Exchange of comments on data acquisition for chromatographic peaks, *Analytical Chemistry* 63 (1991) 73–73.
M.E. Hail, R.A. Yost, Compact gas chromatograph probe for gas chromatography/mass spectrometry utilizing resistively heated aluminum-clad capillary columns, *Analytical Chemistry* 61 (1989) 2410–2416.
L.W. Hantao, A. Najafi, C. Zhang, F. Augusto, J.L. Anderson, Tuning the Selectivity of Ionic Liquid Stationary Phases for Enhanced Separation of Nonpolar Analytes in Kerosene Using Multidimensional Gas Chromatography, *Analytical Chemistry* 86 (2014) 3717–3721.
P.M. Harvey, R.A. Shellie, Data Reduction in Comprehensive Two-Dimensional Gas Chromatography for Rapid and Repeatable Automated Data Analysis, *Analytical Chemistry* 84 (2012) 6501–6507.
J. Harynuk, T. Górecki, J. de Zeeuw, Overloading of the second-dimension column in comprehensive two-dimensional gas chromatography, *Journal of Chromatography A* 1071 (2005) 21–27.
J. Harynuk, T. Górecki, New liquid nitrogen cryogenic modulator for comprehensive two-dimensional gas chromatography, *Journal of Chromatography A* 1019 (2003) 53–63.
J. Harynuk, P.J. Marriott, Fast GC×GC with Short Primary Columns, *Analytical Chemistry* 78 (2006) 2028–2034.
J. Harynuk, A.H. Kwong, P.J. Marriott, Modulation-induced error in comprehensive two-dimensional gas chromatographic separations, *Journal of Chromatography A* 1200 (2008) 17–27.
K. Hiller, J. Hangebrauk, C. Jäger, J. Spura, K. Schreiber, D. Schomburg, MetaboliteDetector: Comprehensive Analysis Tool for Targeted and Nontargeted GC/MS Based Metabolome Analysis, *Analytical Chemistry* 81 (2009) 3429–3439.
K. Hiller, C.M. Metallo, J.K. Kelleher, G. Stephanopoulos, Nontargeted Elucidation of Metabolic Pathways Using Stable-Isotope Tracers and Mass Spectrometry, *Analytical Chemistry* 82 (2010) 6621–6628.
A. Hoffman, Flavor and fragrance analysis of consumer products – dynamic headspace

compared to some traditional analysis approaches, Gerstel Application Note, (2014).
J.C. Hoggard, J.H. Wahl, R.E. Synovec, G.M. Mong, C.G. Fraga, Impurity Profiling of a Chemical Weapon Precursor for Possible Forensic Signatures by Comprehensive Two-Dimensional Gas Chromatography/Mass Spectrometry and Chemometrics, *Analytical Chemistry* 82 (2010) 689–698.
J.C. Hoggard, W.C. Siegler, R.E. Synovec, Toward automated peak resolution in complete GC × GC–TOFMS chromatograms by PARAFAC, *Journal of Chemometrics* 23 (2009) 421–431.
J.L. Hope, K.J. Johnson, M.A. Cavelti, B.J. Prazen, J.W. Grate, R.E. Synovec, High-speed gas chromatographic separations with diaphragm valve-based injection and chemometric analysis as a gas chromatographic "sensor," *Analytica Chimica Acta* 490 (2003) 223–230.
C.R. Hume, M. Kirkegaard, E.C. Oesterle, ErbB Expression: The Mouse Inner Ear and Maturation of the Mitogenic Response to Heregulin, *Journal of the Association for Research in Otolaryngology* 4 (2003) 422–443.
G. Hummer, F. Schotte, P.A. Anfinrud, Unveiling functional protein motions with picosecond x-ray crystallography and molecular dynamics simulations, *Proceedings of the National Academy of Sciences*. 101 (2004) 15330.
E.M. Humston, K.M. Dombek, J.C. Hoggard, E.T. Young, R.E. Synovec, Time-Dependent Profiling of Metabolites from Snf1 Mutant and Wild Type Yeast Cells, *Analytical Chemistry* 80 (2008) 8002–8011.
E.M. Humston, J.D. Knowles, A. McShea, R.E. Synovec, Quantitative assessment of moisture damage for cacao bean quality using two-dimensional gas chromatography combined with time-of-flight mass spectrometry and chemometrics, *Journal of Chromatography A* 1217 (2010) 1963–1970.
M. Izumikawa, S.A. Batts, T. Miyazawa, D.L. Swiderski, Y. Raphael, Response of the flat cochlear epithelium to forced expression of Atoh1, *Hearing Research* 240 (2008) 52–56.
M. Izumikawa, R. Minoda, K. Kawamoto, K.A. Abrashkin, D.L. Swiderski, D.F. Dolan, et al., Auditory hair cell replacement and hearing improvement by Atoh1 gene therapy in deaf mammals, *Nature Medicine* 11 (2005) 271–276.
V. Jain, J. Phillips, Fast temperature programming on fused silica open tubular capillary columns by direct resistive heating, *Journal of Chromatographic Science* 33 (1995) 55–59.
K.J. Johnson, B.W. Wright, K.H. Jarman, R.E. Synovec, High-speed peak matching algorithm for retention time alignment of gas chromatographic data for chemometric analysis, *Journal of Chromatography A* 996 (2003) 141–155.
A. de Juan, J. Jaumot, R. Tauler, Multivariate Curve Resolution (MCR). Solving the mixture analysis problem, *Analytical Methods* 6 (2014) 4964–4976.
M. Junge, S. Bieri, H. Huegel, P.J. Marriott, Fast Comprehensive Two-Dimensional Gas Chromatography with Cryogenic Modulation, *Analytical Chemistry* 79 (2007) 4448–4454.
B. Kehimkar, J.C. Hoggard, L.C. Marney, M.C. Billingsley, C.G. Fraga, T.J. Bruno, et al., Correlation of rocket propulsion fuel properties with chemical composition using comprehensive two-dimensional gas chromatography with time-of-flight mass spectrometry followed by partial least squares regression analysis, *Journal of Chromatography A* 1327 (2014) 132–140.

K.A. Kouremenos, M. Johansson, P.J. Marriott, Advances in gas chromatographic methods for the identification of biomarkers in cancer, *Journal of Cancer* 3 (2012) 404-420
W. Khummueng, P.J. Marriott, The Nomenclature of Comprehensive Two-Dimensional Gas Chromatography: Defining the Modulation Ratio (MR), *LC-GC Europe* 22(1) (2009) 38-45
W. Khummueng, J. Harynuk, P.J. Marriott, Modulation Ratio in Comprehensive Two-dimensional Gas Chromatography, *Analytical Chemistry* 78 (2006) 4578–4587.
M.S. Klee, J. Cochran, M. Merrick, L.M. Blumberg, Evaluation of conditions of comprehensive two-dimensional gas chromatography that yield a near-theoretical maximum in peak capacity gain, *Journal of Chromatography A* 1383 (2015) 151–159.
M.A. Klemp, M.L. Akard, R.D. Sacks, Cryofocusing inlet with reverse flow sample collection for gas chromatography, *Analytical Chemistry* 65 (1993) 2516–2521.
T.J. Klisch, Y. Xi, A. Flora, L. Wang, W. Li, H.Y. Zoghbi, In vivo Atoh1 targetome reveals how a proneural transcription factor regulates cerebellar development, *Proceedings of the National Academy of Sciences* 108 (2011) 3288–3293.
A. Knorr, A. Monge, M. Stueber, A. Stratmann, D. Arndt, E. Martin, et al., Computer-Assisted Structure Identification (CASI)—An Automated Platform for High-Throughput Identification of Small Molecules by Two-Dimensional Gas Chromatography Coupled to Mass Spectrometry, *Analytical Chemistry* 85 (2013) 11216–11224.
L.A. Lanning, R.D. Sacks, R.F. Mouradian, S.P. Levine, J.A. Foulke, Electrically heated cold trap inlet system for computer-controlled high-speed gas chromatography, *Analytical Chemistry* 60 (1988) 1994–1996.
A. Lara-Gonzalo, J.E. Sánchez-Uría, E. Segovia-García, A. Sanz-Medel, Critical comparison of automated purge and trap and solid-phase microextraction for routine determination of volatile organic compounds in drinking waters by GC–MS, *Talanta*. 74 (2008) 1455–1462.
M.L. Lee, F.J. Yang, K.D. Bartle, Open Tubular Column Gas Chromatography, Wiley, New York, 1984.
M. Libardoni, C. Fix, J.H. Waite, R. Sacks, Design and performance evaluation of a two-stage resistively-heated thermal modulator for GC × GC, *Analytical Methods* 2 (2010) 936–943.
Z. Liu, J.B. Phillips, Comprehensive Two-Dimensional Gas Chromatography using an On-Column Thermal Modulator Interface, *Journal of Chromatographic Science* 29 (1991) 227–231.
Z. Liu, J.B. Phillips, Sensitivity and detection limit enhancement of gas chromatographic detection by thermal modulation, *Journal of Microcolumn Separations* 6 (1994) 229–235.
Z. Liu, J.B. Phillips, High-speed gas chromatography using an on-column thermal desorption modulator, *Journal of Microcolumn Separations* 1 (1989) 249–256.
A.M.D. Livera, M. Sysi-Aho, L. Jacob, J.A. Gagnon-Bartsch, S. Castillo, J.A. Simpson, et al. Statistical Methods for Handling Unwanted Variation in Metabolomics Data, *Analytical Chemistry* (2015).
G.L. Long, J.D. Winefordner, Limit of Detection IUPAC, *Analytical Chemistry* 55 (1983).
A. Lorber, L.E. Wangen, B.R. Kowalski, A theoretical foundation for the PLS algorithm, *Journal of Chemometrics* 1 (1987) 19–31.
H. Lu, Y. Liang, W.B. Dunn, H. Shen, D.B. Kell, Comparative evaluation of software for

deconvolution of metabolomics data based on GC-TOF-MS, *Trends in Analytical Chemistry* 27 (2008) 215–227.
J. Luong, R. Gras, M. Hawryluk, R.A. Shellie, H.J. Cortes, Multidimensional gas chromatography using microfluidic switching and low thermal mass gas chromatography for the characterization of targeted volatile organic compounds, *Journal of Chromatography A* 1288 (2013) 105–110.
J. Luong, R. Gras, R. Mustacich, H. Cortes, Low Thermal Mass Gas Chromatography: Principles and Applications, *Journal of Chromatographic Science* 44 (2006) 253–261.
J. Luong, R. Gras, R.A. Shellie, H.J. Cortes, Applications of planar microfluidic devices and gas chromatography for complex problem solving, *Journal of Separation Science* 36 (2013) 182–191.
N.E. Madala, F. Tugizimana, P.A. Steenkamp, L.A. Piater, I.A. Dubery, The Short and Long of it: Shorter Chromatographic Analysis Suffice for Sample Classification During UHPLC-MS-Based Metabolic Fingerprinting, *Chromatographia* 76 (2012) 279–285.
L. Mahé, M. Courtiade, C. Dartiguelongue, J. Ponthus, V. Souchon, D. Thiébaut, Overcoming the high-temperature two-dimensional gas chromatography limits to elute heavy compounds, *Journal of Chromatography A* 1229 (2012) 298–301.
S. Mallia, E. Fernández-García, J. Olivier Bosset, Comparison of purge and trap and solid phase microextraction techniques for studying the volatile aroma compounds of three European PDO hard cheeses, *International Dairy Journal* 15 (2005) 741–758.
D. Mann, N. Putaansuu, Studies of the dehydration/calcination of gypsum wall board, *Fire and Arson Investigator* (2010) 38–44.
C. Manzano, E. Hoh, S.L.M. Simonich, Improved Separation of Complex Polycyclic Aromatic Hydrocarbon Mixtures Using Novel Column Combinations in GC × GC/ToF-MS, *Environmental Science and Technology* 46 (2012) 7677–7684.
L.C. Marney, W. Christopher Siegler, B.A. Parsons, J.C. Hoggard, B.W. Wright, R.E. Synovec, Tile-based Fisher-ratio software for improved feature selection analysis of comprehensive two-dimensional gas chromatography–time-of-flight mass spectrometry data, *Talanta*. 115 (2013) 887–895.
L.C. Marney, S.C. Kolwicz Jr., R. Tian, R.E. Synovec, Sample preparation methodology for mouse heart metabolomics using comprehensive two-dimensional gas chromatography coupled with time-of-flight mass spectrometry, Talanta. 108 (2013) 123–130. doi:10.1016/j.talanta.2013.03.005.
K. Maštovská, S.J. Lehotay, Practical approaches to fast gas chromatography–mass spectrometry, *Journal of Chromatography A* 1000 (2003) 153–180.
C. Meinert, U.J. Meierhenrich, A New Dimension in Separation Science: Comprehensive Two-Dimensional Gas Chromatography, *Angewandte Chemie International Edition*. (2012)
R. Minoda, M. Izumikawa, K. Kawamoto, Y. Raphael, Strategies for replacing lost cochlear hair cells, *Neuroreport* 15 (2004) 1089.
R. Minoda, M. Izumikawa, K. Kawamoto, H. Zhang, Y. Raphael, Manipulating cell cycle regulation in the mature cochlea, *Hearing Research* 232 (2007) 44–51.
B. Mitrevski, P.J. Marriott, Novel Hybrid Comprehensive 2D – Multidimensional Gas Chromatography for Precise, High-Resolution Characterization of Multicomponent Samples, *Analytical Chemistry* 84 (2012) 4837–4843.
K. Moffat, Time-Resolved Biochemical Crystallography: A Mechanistic Perspective, *Chemical Reviews* 101 (2001) 1569–1582.

R.E. Mohler, K.M. Dombek, J.C. Hoggard, E.T. Young, R.E. Synovec, Comprehensive Two-Dimensional Gas Chromatography Time-of-Flight Mass Spectrometry Analysis of Metabolites in Fermenting and Respiring Yeast Cells, *Analytical Chemistry* 78 (2006) 2700–2709.
L. Mondello, P.Q. Tranchida, A. Casilli, O. Favoino, P. Dugo, G. Dugo, Fast GC analysis with a 50 μm ID column: theory, practical aspects, and application to a highly complex sample, *Journal of Separation Science* 27 (2004) 1149–1156.
L. Mondello, P.Q. Tranchida, P. Dugo, G. Dugo, Comprehensive two-dimensional gas chromatography-mass spectrometry: A review, *Mass Spectrometry Reviews* 27 (2008) 101–124.
A. Mostafa, M. Edwards, T. Górecki, Optimization aspects of comprehensive two-dimensional gas chromatography, *Journal of Chromatography A* 1255 (2012) 38–55.
A. Mostafa, T. Górecki, P.Q. Tranchida, L. Mondello, History, Evolution, and Optimization Aspects of Comprehensive Two-Dimensional Gas Chromatography, in: L. Mondello (Ed.), *Comprehensive Chromatography in Combination with Mass Spectrometry*, John Wiley & Sons, Inc., 2011: pp. 93–144.
R.E. Murphy, M.R. Schure, J.P. Foley, Effect of Sampling Rate on Resolution in Comprehensive Two-Dimensional Liquid Chromatography, *Analytical Chemistry* 70 (1998) 1585–1594.
J.A. Murray, Qualitative and quantitative approaches in comprehensive two-dimensional gas chromatography, *Journal of Chromatography A* 1261 (2012) 58–68.
R.V. Mustacich, J.F. Everson, U.S. Patent 6,217,829 (2001)
R.V. Mustacich, J.P. Richards, U.S. Patent 6,209,386 (2001)
J.S. Nadeau, R.B. Wilson, J.C. Hoggard, B.W. Wright, R.E. Synovec, Study of the interdependency of the data sampling ratio with retention time alignment and principal component analysis for gas chromatography, *Journal of Chromatography A* 1218 (2011) 9091–9101.
J.S. Nadeau, B.W. Wright, R.E. Synovec, Chemometric analysis of gas chromatography–mass spectrometry data using fast retention time alignment via a total ion current shift function, *Talanta*. 81 (2010) 120–128.
J.S. Nadeau, R.B. Wilson, B.D. Fitz, J. Reed, R.E. Synovec. Utilizing a Constant Peak Width Transform for Isothermal Gas Chromatography. *Journal of Chromatography A* 1218 (2011) 3718–3724.
T.S. Nair, K.E. Kozma, N.L. Hoefling, P.K. Kommareddi, Y. Ueda, T.W. Gong, et al., Identification and characterization of choline transporter-like protein 2, an inner ear glycoprotein of 68 and 72 kDa that is the target of antibody-induced hearing loss, *The Journal of Neuroscience* 24 (2004) 1772–1779.
Y. Nakada, T.L. Hunsaker, R.M. Henke, J.E. Johnson, Distinct domains within Mash1 and Math1 are required for function in neuronal differentiation versus neuronal cell-type specification, *Development* 131 (2004) 1319–1330.
E.C. Oesterle, S. Campbell, R.R. Taylor, A. Forge, C.R. Hume, Sox2 and Jagged1 Expression in Normal and Drug-Damaged Adult Mouse Inner Ear, *Journal of the Association for Research in Otolaryngology* 9 (2007) 65–89.
E.B. Overton, K.R. Carney, New horizons in gas chromatography: Field applications of microminiaturized gas chromatographic techniques, *Trends in Analytical Chemistry* 13 (1994) 252–257.
O. Panic, C. McNeish, A.H. Goldstein, B.J. Williams, D.R. Worton, S.V. Hering, et al.,

Development of a new consumable-free thermal modulator for comprehensive two-dimensional gas chromatography, *Journal of Chromatography A* (2011).
D.G. Patterson Jr., S.M. Welch, W.E. Turner, A. Sjödin, J.-F. Focant, Cryogenic zone compression for the measurement of dioxins in human serum by isotope dilution at the attogram level using modulated gas chromatography coupled to high resolution magnetic sector mass spectrometry, *Journal of Chromatography A* 1218 (2011) 3274–3281.
A. Paulina de la Mata, K.D. Nizio, J.J. Harynuk, Integration parameters and their effects on quantitative results with two-step peak summation quantitation in comprehensive two-dimensional gas chromatography, *Journal of Chromatography A* 1255 (2012) 190–195.
M. Pavolo, V. Pelizzola, G. contarini, Directly resistively heated-column gas chromatography for the evaluation for cow milk fat purity, *European Journal of Lipid Science and Technology* 110 (2008) 1050–1057.
R.J. Pell, X. Chen, Multivariate curve resolution for understanding complex reactions: MCR for understanding complex reactions, *Journal of Chemometrics* 28 (2014) 411–419.
R.J. Pell, M.B. Seasholtz, K.R. Beebe, M.V. Koch, Process analytical chemistry and chemometrics, Bruce Kowalski's legacy at The Dow Chemical Company: Bruce Kowalski's legacy at Dow Chemical, *Journal of Chemometrics* 28 (2014) 321–331.
C.M. Perou, T. Sørlie, M.B. Eisen, M. van de Rijn, S.S. Jeffrey, C.A. Rees, et al., Molecular portraits of human breast tumors, *Nature*. 406 (2000) 747–752.
P. Persson, S. Lunell, A. Szöke, B. Ziaja, J. Hajdu, Shake-up and shake-off excitations with associated electron losses in X-ray studies of proteins, *Protein Science* 10 (2001) 2480–2484.
A. Peters, M. Klemp, L. Puig, C. Rankin, R. Sacks, Instrumentation and strategies for high-speed gas chromatography, *Analyst* 116 (1991) 1313–1320.
J.B. Phillips, J. Beens, Comprehensive two-dimensional gas chromatography: a hyphenated method with strong coupling between the two dimensions, *Journal of Chromatography A* 856 (1999) 331–347.
K.M. Pierce, J.L. Hope, K.J. Johnson, B.W. Wright, R.E. Synovec, Classification of gasoline data obtained by gas chromatography using a piecewise alignment algorithm combined with feature selection and principal component analysis, *Journal of Chromatography A* 1096 (2005) 101–110.
K.M. Pierce, J.C. Hoggard, Chromatographic data analysis. Part 3.3.4: handling hyphenated data in chromatography, *Analytical Methods* 6 (2014) 645–653.
K.M. Pierce, B. Kehimkar, L.C. Marney, J.C. Hoggard, R.E. Synovec, Review of chemometric analysis techniques for comprehensive two dimensional separations data, *Journal of Chromatography A* 1255 (2012) 3–11.
D.K. Pinkerton, B.A. Parsons, T.J. Anderson, R.E. Synovec, Trilinearity deviation ratio: A new metric for chemometric analysis of comprehensive two-dimensional gas chromatography time-of-flight mass spectrometry data, *Analytica Chimica Acta* 871 (2015) 66–76.
B.J. Prazen, R.E. Synovec, B.R. Kowalski, Standardization of Second-Order Chromatographic/Spectroscopic Data for Optimum Chemical Analysis, *Analytical Chemistry* 70 (1998) 218–225.
A.R. Raghani, High-speed gas chromatographic analysis of solvents in pharmaceuticals using solid phase microextraction, *Journal of Pharmaceutical and Biomedical Analysis* 29 (2002) 507–518.
C. Ragonese, D. Sciarrone, P.Q. Tranchida, P. Dugo, G. Dugo, L. Mondello, Evaluation of a

medium-polarity ionic liquid stationary phase in the analysis of flavour and fragrance compounds, *Analytical Chemistry* 83 (2011) 7947-7954.
C. Ragonese, P.Q. Tranchida, D. Sciarrone, L. Mondello, Conventional and fast gas chromatography analysis of biodiesel blends using an ionic liquid stationary phase, *Journal of Chromatography A* 1216 (2009) 8992–8997.
M. Rambla-Alegre, B. Tienpont, K. Mitsui, E. Masugi, Y. Yoshimura, H. Nagata, et al., Coupling gas chromatography and electronic nose detection for detailed cigarette smoke aroma characterization, *Journal of Chromatography A* 1365 (2014) 191–203.
Y. Raphael, Y.-H. Kim, Y. Osumi, M. Izumikawa, Non-sensory cells in the deafened organ of Corti: approaches for repair, *The International Journal of Developmental Biology* 51 (2007) 649–654.
S.E. Reichenbach, X. Tian, A.A. Boateng, C.A. Mullen, C. Cordero, Q. Tao, Reliable Peak Selection for Multisample Analysis with Comprehensive Two-Dimensional Chromatography, *Analytical Chemistry* 85 (2013) 4974–4981.
V.R. Reid, J.A. Crank, D.W. Armstrong, R.E. Synovec, Characterization and utilization of a novel triflate ionic liquid stationary phase for use in comprehensive two-dimensional gas chromatography, *Journal of Separation Science* 31 (2008) 3429–3436.
V.R. Reid, A.D. McBrady, R.E. Synovec, Investigation of high-speed gas chromatography using synchronized dual-valve injection and resistively heated temperature programming, *Journal of Chromatography A* 1148 (2007) 236–243.
V.R. Reid, R.E. Synovec, High-speed gas chromatography: The importance of instrumentation optimization and the elimination of extra-column band broadening, *Talanta*. 76 (2008) 703–717.
S. Risticevic, Y. Chen, L. Kudlejova, R. Vatinno, B. Baltensperger, J.R. Stuff, et al., Protocol for the development of automated high-throughput SPME–GC methods for the analysis of volatile and semivolatile constituents in wine samples, *Nature Protocols* 5 (2010) 162–176.
N. Roques, J. Crandall, Trans-configurable modular chromatographic assembly, US Patent 8336366, 2009
F.J. Santos, M.T. Galceran, Modern developments in gas chromatography–mass spectrometry-based environmental analysis, *Journal of Chromatography A* 1000 (2003) 125–151.
J. Saurina, C. Leal, R. Compañó, M. Granados, M.D. Prat, R. Tauler, Estimation of figures of merit using univariate statistics for quantitative second-order multivariate curve resolution, *Analytica Chimica Acta* 432 (2001) 241–251.
F. Schotte, Watching a Protein as it Functions with 150-ps Time-Resolved X-ray Crystallography, *Science* 300 (2003) 1944–1947.
J.V. Seeley, F. Kramp, C.J. Hicks, Comprehensive Two-Dimensional Gas Chromatography via Differential Flow Modulation, *Analytical Chemistry* 72 (2000) 4346–4352.
J.V. Seeley, S.K. Seeley, E.K. Libby, Z.S. Breitbach, D.W. Armstrong, Comprehensive two-dimensional gas chromatography using a high-temperature phosphonium ionic liquid column, *Analytical and Bioanalytical Chemistry* 390 (2007) 323–332.
J.V. Seeley, S.K. Seeley, Multidimensional Gas Chromatography: Fundamental Advances and New Applications, *Analytical Chemistry* 85 (2013) 557–578.
J.V. Seeley, N.J. Micyus, S.V. Bandurski, S.K. Seeley, J.D. McCurry, Microfluidic Deans Switch for Comprehensive Two-Dimensional Gas Chromatography, *Analytical Chemistry* 79 (2007) 1840–1847.

J.V. Seeley, Theoretical study of incomplete sampling of the first dimension in comprehensive two-dimensional chromatography, *Journal of Chromatography A* 962 (2002) 21–27.
G. Serrano, D. Paul, S.-J. Kim, K. Kurabayashi, E.T. Zellers, Comprehensive Two-Dimensional Gas Chromatographic Separations with a Microfabricated Thermal Modulator, *Analytical Chemistry* 84 (2012) 6973–6980.
S.B. Shibata, Y. Raphael, Future approaches for inner ear protection and repair, *Journal of Communication Disorders* 43 (2010) 295–310.
W.C. Siegler, B.D. Fitz, J.C. Hoggard, R.E. Synovec, Experimental Study of the Quantitative Precision for Valve-Based Comprehensive Two-Dimensional Gas Chromatography, *Analytical Chemistry* 83 (2011) 5190-5196.
A.E. Sinha, C.G. Fraga, B.J. Prazen, R.E. Synovec, Trilinear chemometric analysis of two dimensional comprehensive gas chromatography–time-of-flight mass spectrometry data, *Journal of Chromatography A.* 1027 (2004) 269–277.
A.E. Sinha, B.J. Prazen, C.G. Fraga, R.E. Synovec, Valve-based comprehensive two-dimensional gas chromatography with time-of-flight mass spectrometric detection: instrumentation and figures-of-merit, *Journal of Chromatography A* 1019 (2003) 79–87.
A.E. Sinha, K.J. Johnson, B.J. Prazen, S.V. Lucas, C.G. Fraga, R.E. Synovec, Comprehensive two-dimensional gas chromatography of volatile and semi-volatile components using a diaphragm valve-based instrument, *Journal of Chromatography A* 983 (2003) 195–204.
T. Skov, J.C. Hoggard, R. Bro, R.E. Synovec, Handling within run retention time shifts in two-dimensional chromatography data using shift correction and modeling, *Journal of Chromatography A* 1216 (2009) 4020–4029.
A.K. Smilde, R. Tauler, J. Saurina, R. Bro, Calibration methods for complex second-order data, *Analytica Chimica Acta* 398 (1999) 237–251.
M.S. Smyth, J.H.J. Martin, x Ray crystallography, *Molecular Pathology* 53 (2000) 8–14.
H. Snijders, H.-G. Janssen, C. Cramers, Optimization of temperature-programmed gas chromatographic separations I. Prediction of retention times and peak widths from retention indices, *Journal of Chromatography A* 718 (1995) 339–355.
H. Snijders, H.-G. Janssen, C. Cramers, Optimization of temperature-programmed gas chromatographic separations II. Off-line Simplex optimization and column selection, *Journal of Chromatography A* 756 (1996) 175–183.
S.D. Stearns, H. Cai, J.A. Koehn, M. Brisbin, C. Cowles, C. Bishop, et al., A direct resistively heated gas chromatography column with heating and sensing on the same nickel element, *Journal of Chromatography A* 1217 (2010) 4629–4638.
S.E. Stein, An integrated method for spectrum extraction and compound identification from gas chromatography/mass spectrometry data, *Journal of the American Society for Mass Spectrometry* 10 (1999) 770–781.
S.E. Stein, D.R. Scott, Optimization and testing of mass spectral library search algorithms for compound identification, *Journal of the American Society for Mass Spectrometry* 5 (1994) 859–866.
P. Sun, D.W. Armstrong, Ionic liquids in analytical chemistry, *Analytica Chimica Acta* 661 (2010) 1–16.
X. Sun, D. Li, A.T. Woolley, P.B. Farnsworth, H.D. Tolley, K.F. Warnick, et al., Bilinear electric field gradient focusing, *Journal of Chromatography A* 1216 (2009) 6532–6538.
P.A. Sutton, S.J. Rowland, High temperature gas chromatography–time-of-flight-mass

spectrometry (HTGC–ToF-MS) for high-boiling compounds, *Journal of Chromatography A* 1243 (2012) 69–80.
P.A. Sutton, M.J. Wilde, S.J. Martin, J. Cvačka, V. Vrkoslav, S.J. Rowland, Studies of long chain lipids in insects by high temperature gas chromatography and high temperature gas chromatography–mass spectrometry, *Journal of Chromatography A* 1297 (2013) 236–240.
R.E. Synovec, E.S. Yeung, Comparison of an integration procedure to Fourier transform and data averaging procedures in chromatographic data analysis, *Analytical Chemistry* 58 (1986) 2093–2095.
R. Tauler, Multivariate curve resolution applied to second order data, *Chemometrics and Intelligent Laboratory* Systems 30 (1995) 133–146.
R. Tautenhahn, G.J. Patti, D. Rinehart, G. Siuzdak, XCMS Online: A Web-Based Platform to Process Untargeted Metabolomic Data, *Analytical Chemistry* 84 (2012) 5035–5039.
E. Tengstrand, J. Lindberg, K.M. Åberg, TracMass 2—A Modular Suite of Tools for Processing Chromatography-Full Scan Mass Spectrometry Data, *Analytical Chemistry* 86 (2014) 3435–3442.
D.F. Thekkudan, S.C. Rutan, P.W. Carr, A study of the precision and accuracy of peak quantification in comprehensive two-dimensional liquid chromatography in time, *Journal of Chromatography A* 1217 (2010) 4313–4327.
B.R. Toledo, L.W. Hantao, T.D. Ho, F. Augusto, J.L. Anderson, A chemometric approach toward the detection and quantification of coffee adulteration by solid-phase microextraction using polymeric ionic liquid sorbent coatings, *Journal of Chromatography A* 1346 (2014) 1–7.
H.D. Tolley, S.E. Tolley, A. Wang, M.L. Lee, Moving thermal gradients in gas chromatography, *Journal of Chromatography A* 1374 (2014) 189–198.
P.Q. Tranchida, A. Casilli, P. Dugo, G. Dugo, L. Mondello, Generation of Improved Gas Linear Velocities in a Comprehensive Two-Dimensional Gas Chromatography System, *Analytical Chemistry* 79 (2007) 2266–2275.
P.Q. Tranchida, L. Mondello, Current-day employment of the micro-bore open-tubular capillary column in the gas chromatography field, *Journal of Chromatography A* 1261 (2012) 23–36.
P.Q. Tranchida, G. Purcaro, L. Conte, P. Dugo, G. Dugo, L. Mondello, Enhanced resolution comprehensive two-dimensional gas chromatography applied to the analysis of roasted coffee volatiles, *Journal of Chromatography A* 1216 (2009) 7301–7306.
P.Q. Tranchida, G. Purcaro, C. Fanali, P. Dugo, G. Dugo, L. Mondello, Optimized use of a 50 μm ID secondary column in comprehensive two-dimensional gas chromatography–mass spectrometry, *Journal of Chromatography A* 1217 (2010) 4160–4166.
E. Uliyanchenko, P.J.C.H. Cools, S. van der Wal, P.J. Schoenmakers, Comprehensive Two-Dimensional Ultrahigh-Pressure Liquid Chromatography for Separations of Polymers, *Analytical Chemistry* 84 (2012) 7802–7809.
M.M. van Deursen, J. Beens, C.A. Cramers, H.-G. Janssen, Possibilities and Limitations of Fast Temperature Programming as a Route towards Fast GC, *Journal of High Resolution Chromatography* 22 (1999) 509–513.
M.M. van Deursen, J. Beens, H.-G. Janssen, P.A. Leclercq, C.A. Cramers, Evaluation of time-of-flight mass spectrometric detection for fast gas chromatography, *Journal of Chromatography A* 878 (2000) 205–213.

A. Van Es, J. Janssen, C. Cramers, J. Rijks, Sample enrichment in high speed narrow bore capillary gas chromatography, *Journal of High Resolution Chromatography* 11 (1988) 852–857.
M. van Lieshout, M. van Deursen, R. Derks, H.-G. Janssen, C. Cramers, The Influence of Liner Dimensions on Injector Band Broadening in Split Injections in Fast Capillary Gas Chromatography, *Journal of High Resolution Chromatography* 22 (1999) 116–118.
R.L. Wade, S.P. Cram, Fluidic logic sampling and injection system for gas chromatography, *Analytical Chemistry* 44 (1972) 131–139.
A. Wang, H.D. Tolley, M.L. Lee, Gas chromatography using resistive heating technology, *Journal of Chromatography A* 1261 (2012) 46–57.
G.P. Wang, I. Chatterjee, S.A. Batts, H.T. Wong, T.W. Gong, S.S. Gong, et al., Notch signaling and Atoh1 expression during hair cell regeneration in the mouse utricle, *Hearing Research* 267 (2010) 61–70.
N.E. Watson, J.M. Davis, R.E. Synovec, Observations on "Orthogonality" in Comprehensive Two-Dimensional Separations, *Analytical Chemistry* 79 (2007) 7924–7927.
N.E. Watson, W.C. Siegler, J.C. Hoggard, R.E. Synovec, Comprehensive Three-Dimensional Gas Chromatography with Parallel Factor Analysis, *Analytical Chemistry* 79 (2007) 8270–8280.
N.E. Watson, M.M. VanWingerden, K.M. Pierce, B.W. Wright, R.E. Synovec, Classification of high-speed gas chromatography–mass spectrometry data by principal component analysis coupled with piecewise alignment and feature selection, *Journal of Chromatography A* 1129 (2006) 111–118.
A. Wegner, S.C. Sapcariu, D. Weindl, K. Hiller, Isotope Cluster-Based Compound Matching in Gas Chromatography/Mass Spectrometry for Non-Targeted Metabolomics, *Analytical Chemistry* 85 (2013) 4030–4037.
X. Wei, X. Shi, S. Kim, J.S. Patrick, J. Binkley, M. Kong, et al., Data Dependent Peak Model Based Spectrum Deconvolution for Analysis of High Resolution LC-MS Data, *Analytical Chemistry* (2014).
R. Weissenborn, T. Reinhardt, V. Hansen, G. Maret, T. Gisler, A broadband waveguide for protein crystallography under intense microwave fields, *Review of Scientific Instruments* 75 (2004) 5253.
R.B. Wilson, W.C. Siegler, J.C. Hoggard, J.S. Nadeau, R.E. Synovec, Achieving high peak capacity production for gas chromatography and comprehensive two-dimensional gas chromatography by minimizing off-column peak broadening, *Journal of Chromatography A* 1218 (2011) 2130-3139.
R.B. Wilson, B.D. Fitz, B.C. Mannion, T. Lai, R.K. Olund, J.C. Hoggard, R.E. Synovec High-speed cryo-focusing injection for gas chromatography: Reduction of injection band broadening with concentration enrichment, *Talanta*. 97 (2012) 9–15.
R.B. Wilson, J.C. Hoggard, R.E. Synovec, Fast, High Peak Capacity Separations in Gas Chromatography–Time-of-Flight Mass Spectrometry, *Analytical Chemistry* 84 (2012) 4167–4173.
R.B. Wilson, J.C. Hoggard, R.E. Synovec, High throughput analysis of atmospheric volatile organic compounds by thermal injection – isothermal gas chromatography – time-of-flight mass spectrometry, *Talanta*. 103 (2013) 95–102.
S.A. Wise, K.W. Phinney, L.C. Sander, M.M. Schantz, Role of chromatography in the

development of Standard Reference Materials for organic analysis, *Journal of Chromatography A* 1261 (2012) 3–22.
H. Wollnik, R. Becker, H. Götz, A. Kraft, H. Jung, C.-C. Chen, et al., A high-speed gas chromatograph coupled to a time-of-flight mass analyzer, *International Journal of Mass Spectrometry and Ion Processes* 130 (1994) L7–L11.
H.-L. Wu, Y. Li, R.-Q. Yu, Recent developments of chemical multiway calibration methodologies with second-order or higher-order advantages, *Journal of Chemometrics* 28 (2013) 476-489.
M. Wulff, A. Plech, L. Eybert, R. Randler, F. Schotte, P. Anfinrud, The realization of sub-nanosecond pump and probe experiments at the ESRF, *Faraday Discussions*. 122 (2003) 13–26.
F. Xu, W. Guan, G. Yao, Y. Guan, Fast temperature programming on a stainless-steel narrow-bore capillary column by direct resistive heating for fast gas chromatography, *Journal of Chromatography A* 1186 (2008) 183–188.
X. Yan, K.R. Carney, E.B. Overton, Application of Purge-and-Trap Method to Fast and Convenient Field Analysis of Water and Soil Samples, *Journal of Chromatographic Science* 30 (1992) 491–496.
S. Yang, J.C. Hoggard, M.E. Lidstrom, R.E. Synovec, Comprehensive discovery of 13C labeled metabolites in the bacterium Methylobacterium extorquens AM1 using gas chromatography–mass spectrometry, *Journal of Chromatography A* 1317 (2013) 175–185.
S. Yang, J.S. Nadeau, E.M. Humston-Fulmer, J.C. Hoggard, M.E. Lidstrom, R.E. Synovec, Gas chromatography–mass spectrometry with chemometric analysis for determining 12C and 13C labeled contributions in metabolomics and 13C flux analysis, *Journal of Chromatography A* 1240 (2012) 156–164.
X. Ye, A. Demidov, P.M. Champion, Measurements of the photodissociation quantum yields of MbNO and MbO2 and the vibrational relaxation of the six-coordinate heme species, *Journal of the American Chemical Society* 124 (2002) 5914–5924.
B. Yu, Y. Song, L. Han, H. Yu, Y. Liu, H. Liu, Optimizations of packed sorbent and inlet temperature for large volume-direct aqueous injection-gas chromatography to determine high boiling volatile organic compounds in water, *Journal of Chromatography A* 1356 (2014) 221–229.
J. de Zeeuw, J. Luong, Developments in stationary phase technology for gas chromatography, *Trends in Analytical Chemistry* 21 (2002) 594–607.
Z.-D. Zeng, H.M. Hugel, P.J. Marriott, A Modeling Approach for Orthogonality of Comprehensive Two-Dimensional Separations, *Analytical Chemistry* 85 (2013) 6356–6363.
Z. Zhu, J. Harynuk, T. Górecki, Effect of first-dimension column film thickness on comprehensive two-dimensional gas chromatographic separation, *Journal of Chromatography A* 1105 (2006) 17–24.

Curriculum Vitae

Education

Ph.D., Analytical Chemistry, University of Washington, Seattle, WA 2015
Advances in instrumentation and data analysis techniques for increasing peak capacity and peak capacity production in one and two-dimensional gas chromatography.
B.S., Chemistry (ACS Certified), University of Washington, Seattle, WA 2010

Research Experience & Summary

Graduate Research Assistant, University of Washington 2010-2015
Advisor: Professor Robert E. Synovec
Projects:

- Aided in developing and testing of a high-speed cryo-focusing injection (HSCFI) device to deliver ultra-narrow injection pulses to gas chromatographic (GC) systems.
- Applied HSCFI to a comprehensive two-dimensional gas chromatographic system coupled to a time-of-flight mass spectrometer (GC × GC - TOFMS) to achieve a peak capacity of 6,000 in only 6 minutes, which is 10 times faster than conventional 2D GC instrumentation.
- Applied HSCFI to a low-thermal-mass gas chromatograph (LTM-GC) to produce a peak capacity of 300 in a 1 minute temperature programmed separation, an increase in peak capacity production 3 times higher than conventional 1D instrumentation in 7% of the typical timeframe.
- Developed a novel data analysis algorithm and graphical user interface (GUI) for GC-TOFMS data to facilitate separation visualization and deconvolution of ultra-low resolutions (R_s) peaks. The algorithm also facilitates significant peak capacity increases by nearly 2 orders of magnitude from 400 to ~10,000 in 6 minutes.

Dr. Fitz is an analytical chemist with a theoretical and experimental background in chromatographic science with mass spectral detection (qMS, TOFMS) for the separation of complex mixtures in short timescales (1-10 minutes). He has an established technical publication record on improving technologies in the field of one and two-dimensional gas chromatography. His method development work involved developing new techniques for extracting chemical data from GC-TOFMS chromatograms. He is a knowledgeable analyst with working experience with the majority of analytical instrumentation used in the identification of unknown compounds. He has experience in the separation of various types of fuels (gasoline, diesel, rocket propellant). He has a strong background in the analysis of gas chromatographic and mass spectral data. He has excellent presentation and group work skills to effectively communicate complex data sets to experts and non-experts alike in order to facilitate informed decision making.

Teaching Experience

Graduate Teaching Assistant (Chemistry), University of Washington, Seattle, WA 2010–2015

- 300 Level: Quantitative Analysis Laboratory
    - Supervised undergraduates in quantitative techniques such as gravimetric analysis, spectroscopy, titrations, solid phase extraction, flow injection analysis, and chromatography.
- 200 Level: General Chemistry for non-Chemistry Majors
- 100 Level: General Chemistry for Science Majors

Undergraduate Research Supervisor, University of Washington, Seattle, WA 2012-2015

- Managed and trained 4 undergraduate students over the course of 3 years in GC theory, data analysis instrumentation, maintenance, troubleshooting, and sample preparation resulting in two publications in peer reviewed journals.

Awards

Amy Scott and Stephen C. Alley Endowed Fellowship in Chemistry 2012
Finalist, FSU National Undergraduate Research Competition 2009
Eagle Scout, Troop 360, Burien, WA, Boy Scouts of America 2005

Previous Employment

MDE, Inc. (Forensic Engineering Firm), Seattle, WA
Forensic Chemistry Laboratory Assistant 2007–2010
Administrative Assistant, Fire Investigation Assistant, Groundskeeper 2002–2010

Peer Reviewed Publications

10) Non-targeted ^{13}C-metabolic flux analysis of Methylobacterium extorquens AM1 using the two-dimensional mass cluster method and principal component analysis. Brooke C. Reaser, Song Yang, **Brian D. Fitz**, Brendon A. Parsons, Mary E. Lidstrom, and Robert E. Synovec. *Manuscript submitted to Journal of Chromatography A* (2015).

9) Implementation of two-dimensional mass cluster plots in fast, high peak capacity separations with low thermal mass gas chromatography time-of-flight mass spectrometry (LTM-GC-TOFMS). **Brian D. Fitz**, Robert E. Synovec, *Manuscript submitted to Analytica Chimica Acta* (2015).

8) Evaluation of injection methods for fast, high peak capacity separations with low thermal mass gas chromatography. **Brian D. Fitz**, Brandyn C. Mannion, Khang To, Trinh Hoac, Robert E. Synovec, *Journal of Chromatography A* 1392 (2015) 82-90.

7) Enhancing gas chromatography – time of flight mass spectrometry data analysis using two-dimensional mass channel cluster plots**. Brian D. Fitz**, Brooke C. Reaser, David K. Pinkerton, Jamin C. Hoggard, Kristen J. Skogerboe, Robert E. Synovec, *Analytical Chemistry* 86 (2014) 3973-3979.

6) Fast, high peak capacity separations in comprehensive two-dimensional gas chromatography with time-of-flight mass spectrometry. **Brian D. Fitz**, Ryan B. Wilson, Brendon A. Parsons, Jamin C. Hoggard, Robert E. Synovec, *Journal of Chromatography A* 1266 (2012), 116-123.

5) High-speed cryo-focusing injection for gas chromatography: Reduction of injection band broadening with concentration enrichment. Ryan B. Wilson, **Brian D. Fitz**, Brandyn C. Mannion, Tina Lai, Roy K. Olund, Jamin C. Hoggard, Robert E. Synovec, *Talanta* 97(2012) 9-15.

4) Experimental study of the quantitative precision for valve-based comprehensive two-dimensional gas chromatography. W. Christopher Siegler, **Brian D. Fitz**, Jamin C. Hoggard, Robert E. Synovec, *Analytical Chemistry* 83 (2011) 5190–5196.

3) Achieving high peak capacity production for gas chromatography and comprehensive two-dimensional gas chromatography by minimizing off-column peak broadening. Ryan B. Wilson, W. Christopher Siegler, Jamin C. Hoggard**, Brian D. Fitz**, Jeremy S. Nadeau, Robert E. Synovec, *Journal of Chromatography A* 1218 (2011) 3130-3139.

2) Utilizing a constant peak width transform for isothermal gas chromatography. Jeremy S. Nadeau, Ryan B. Wilson, **Brian D. Fitz**, Jason T. Reed, Robert E. Synovec, *Journal of Chromatography A* (1218) 2011 3718-3724.

1) Studies of the dehydration/calcination of gypsum wall board. Dale C. Mann, Noel D. Putaansuu. *Fire & Arson Investigator.* 2010, 38-44. (Acknowledged for work performed).

Oral Presentations

Chemistry 529 – Separation Techniques (Guest Lecturer). June 11, 2015, University of Washington, Seattle, WA. "Instrumentation to enable fast, high peak capacity separations in one-dimensional gas chromatography."

Center for Process Analysis and Control (CPAC) Spring Meeting. May 12, 2015, Seattle, WA. "Hyper-fast, high peak capacity separations using low thermal mass gas chromatography (LTM-GC) and chemometrics."

Center for Process Analysis and Control (CPAC) Summer Institute. July 22, 2014, Seattle, WA. "Improving GC–TOFMS Data Interpretation Using Two-Dimensional Mass Cluster Plots."

Canadian Research Conference (CSC 2014), Vancouver, BC. June 4 2014. "Advances in Instrumentation and Data Analysis Methods to Improve Peak Capacity in GC–TOFMS and GC×GC–TOFMS. "

Center for Process Analysis and Control (CPAC) Spring Meeting, May 13, 2014, Seattle, WA. "Advances in Process Gas Chromatography and Chemometrics."

Pacific Northwest National Labs (PNNL) August 14, 2013, Richland, WA. "Increasing Peak Capacity Production in Fast One and Two-Dimensional Gas Chromatography."